COMPARISON OF DIPPING AND SPRAYING METHODS IN LAYER-BY-LAYER DEPOSITION OF CHITOSAN AND SODIUM CASEINATE

A Thesis Submitted to
the Graduate School of Engineering and Sciences of
Izmır Institute of Technology
In Partial Fulfillment of the Requirements for the Degree of

MASTER OF SCIENCE

in Food Engineering

by
Sinem ÜNEY

August 2016
İZMİR

We approve the thesis of **Sinem ÜNEY**

Examining Committee Members:

Assist. Prof. Dr. Beste BAYRAMOĞLU
Department of Food Engineering, Izmir Institute of Technology

Prof. Dr. Ahmet YEMENİCİOĞLU
Department of Food Engineering, Izmir Institute of Technology

Assoc. Prof. Dr. Seda ERSUS BİLEK
Department of Food Engineering, Ege University

1/August/2016

Assist. Prof. Dr. Beste BAYRAMOĞLU
Supervisor,
Department of Food Engineering
Izmir Institute of Technology

Prof. Dr. Ahmet YEMENİCİOĞLU
Head of the Department of
Food Engineering

Prof. Dr. Bilge KARAÇALI
Dean of the Graduate School of
Engineering and Sciences

To My Family

ACKNOWLEDGEMENTS

Initially, I am thankful to my supervisor Assist. Prof. Dr. Beste BAYRAMOĞLU whose kind support, advises, guidance and encouragement aided me during research and writing of this thesis.

I would like to express my special gratitude to Prof. Dr. Ahmet YEMENİCİOĞLU, who is a member of my thesis committee, and Prof. Dr. Figen KOREL for valuable recommendations in my microbiological experiments. I also want to add my thankfulness to Assoc. Prof. Dr. Seda ERSUS BİLEK from Food Engineering Department at Ege University for her special kindness in my thesis committee and precious suggestions in my thesis defense.

I am thankful to Specialist Mine BAHÇECİ and Specialist Yekta GÜNAY OĞUZ for their kind assistance.

I wish to thank my friends, Başak AVCI, Esra TUNÇER, Gökçen KAHRAMAN, Derya BOYACI, Elif AKBAŞ and Keriman ARSERİM for their motivation and moral support during my studies.

TUBITAK (The Scientific & Technological Research Council of Turkey) is greatly acknowledged for supporting this project (114O696).

Lastly, I am thankful to Egemen ÇAM to his for being the most important supporter and I would like to dedicate this work to my family members, Alpay-Nazan-Alp ÜNEY for their great moral support and belief in me.

ABSTRACT

COMPARISON OF DIPPING AND SPRAYING METHODS IN LAYER-BY-LAYER DEPOSITION OF CHITOSAN AND SODIUM CASEINATE

In this thesis; it is aimed to develop a novel, ultra thin, homogeneous edible coating with adequate gas barrier properties by layered deposition of chitosan and sodium caseinate with dipping and spraying methods and compare the coating structures.

The parameters considered in this study are pH, adsorption times, number of layers and the types of the top layer. To determine the appropriate conditions, zeta potential and hydrodynamic diameter measurements of chitosan and sodium caseinate were done. After determining the appropriate concentrations and pH values, layer deposition has been initiated. Following the formation of multilayer coating by UV-Vis spectrophotometer, the most suitable combination was determined for the formation of multilayer coating. Multilayered coating characterization was done by Scanning Electron Microscopy (SEM), Atomic Force Microscopy (AFM) and Surface Plasmon Resonance which allows to observe coating formation in-situ. Moreover antimicrobial activity, water vapor permeability and oxygen permeability were also investigated.

It has been observed that the multilayer coating structures obtained by dipping and spraying methods have some differences. The formation of multilayer coating has been followed successfully with UV-Vis spectrophotometer; besides information about surface topography and coating thickness is obtained by Atomic Force Microscopy (AFM). The multilayered coatings have no significant effects on oxygen permeability and water vapor permeability; however it has contact antimicrobial effect.

ÖZET

KİTOSAN VE SODYUM KAZEİNATIN KATMANLI DEPOZİSYON İŞLEMİNDE DALDIRMA VE PÜSKÜRTME YÖNTEMLERİNİN KARŞILAŞTIRILMASI

Bu tezde kitosan ve sodyum kazeinat materyallerinin katmanlı depozisyon işlemi sonucunda, minimal işlem görmüş taze sebze ve meyveler için, yeni nesil çok ince, homojen, dayanıklı ve yeterli gaz bariyer özelliklerinde sahip kaplamaların daldırma ve püskürtme yöntemleri ile elde edilmesi ve kaplama yapılarının karşılaştırılması amaçlanmıştır.

Bu çalışmada ele alınan parametreler; pH değeri, adsorbsiyon süresi, katman sayısı ve üst katmanın çeşididir. Uygun deney koşullarını belirleyemek adına kitozan ve sodyum kazeinatın zeta potansiyeli ve hidrodinamik çap ölçümleri yapılmıştır. Bu aşamada belirlenen uygun konsantrasyon ve pH değerleri ile katmanlı depozisyon deneylerine geçilmiştir. UV-Vis spektrofotometre ile çok katmanlı kaplama oluşumu eğrisi takip edilerek, çok katmanlı kaplama oluşumu için en uygun kombinasyon belirlenmiştir. Taramalı Elektron Mikroskopisi (TEM) ile kaplama oluşumunun yerinde gözlemlenmesine olanak veren Yüzey Plazmon Rezonansı (YPR) ve Atomik Kuvvet Mikroskopisi (AKM) ile elde edilen kaplamaların karakterizasyonu yapılmıştır. Elde edilen kaplamaların su buharı ve oksijen geçirgenliği ile antimikrobiyal etkisinin olup olmadığı da araştırılmıştır.

Daldırma ve püskürtme yöntemleri ile elde edilen çok katmanlı kaplama yapıları arasında farklılık gözlemlenmiştir. UV-Vis spektrofotometre ile çok katmanlı kaplama oluşumu başarılı bir şekilde takip edilmiş, Atomik Kuvvet Mikroskopisi (AKM) ile kaplamaların yüzey topoğrafyası ve kalınlığı hakkında bilgiler edinilmiştir. Elde edilen kaplamaların su buharı ve oksijen geçirgenliği üzerinde belirgin bir etkisi bulunmamasına karşın, kaplamaların kontak antimikrobiyal etkisinin olduğu görülmüştür.

TABLE OF CONTENT

LIST OF FIGURES

Figure **Page**

LIST OF TABLES

CHAPTER 1

INTRODUCTION

1.1.Preservation of Fresh and Fresh-Cut Fruits and Vegetables

In recent years, the changes of lifestyles have been accompanied by an evolution of the structure of food consumption. Accordingly, the minimally processed fresh and fresh-cut fruits and vegetables were developed to respond to the consumers demand for healthy, fresh-like and easy to prepare products (Galgano et al., 2014).

Minimally processed fresh and fresh-cut fruits and vegetables are submitted to selection, cleaning, cutting, shredding, and packaging (Ramos et al.,2013). It is well known that processing of fresh and fresh-cut fruits and vegetables promotes faster deterioration, since fruits and vegetables are living tissues. They can be wounded and enzymatic browning, off-flavor, off-odor, texture breakdown, and microbial spoilage might develop. The reasons for this; microbial attacks on texture, product injuries that occur during mechanical process, increasing the rate of respiration and sweating which are reducing the shelf life of fresh fruits and vegetables. Consequently product browning, shrinkage caused by dehydration, softening, oxidation and decomposition of pigments, bleaching depends on the surface dehydration and bad taste with odor is seen as undesirable changes. Therefore, the shelf life of fresh and fresh-cut products tends to be very short if they are wounded (Sipahi et al.,2013).

Major losses in quality and quantity of fresh and fresh-cut fruits and vegetables occur between harvests. When the fruit is harvested, there is a change of the gaseous balance between the consumption of oxygen and the production of carbon dioxide which causes a poor product shelf life (Dhall, 2015).

Minimizing the deterioration can provide long-term shelf life. This can be achieved by modified atmosphere packaging. Also edible coatings can be applied as an alternative or supportive to modified atmosphere packaging to extend the shelf life of fresh and fresh-cut fruits and vegetables. Edible coatings and modified atmosphere packaging are promising techniques which reduce the deleterious effects with minimal processing and also improve the quality and safety (Rojas-Graü et al., 2009).

1.2. Modified Atmosphere Packaging (MAP)

Modified atmosphere packaging (MAP) is a technique used for the long-term shelf-life period of foods. This preservation technique is based on changing the atmosphere in the package. The desired atmosphere can be obtained using active or passive MAP.

Active MAP is based on the replacement of gases in the package. On the other hand, passive MAP depends on the use of a special packaging material which provides a desired atmosphere in a natural way due to the respiration rate of products and the diffusion of gases through the packaging material (Oliveira et al., 2015).

O_2, CO_2 and N_2 are the most common gases used in MAP. The choice of gas, which is used for packaging is related with the food product being packed (Sandhya, 2010). During product storage, O_2 is consumed and CO_2 is produced by respiration. Therefore, to extend the shelf life of foods the package atmosphere should include a low concentration of oxygen. In food packaging, nitrogen can be used to prevent pack collapse and used as filler gas to balance the volume decrease due to CO_2 absorption. Additionally, the noble gases such as helium, neon, argon, xenon have been used in MAP to preserve the quality of food product (Oliveira et al., 2015).

There are several polymeric films used as packaging materials for MAP. The most commonly used polymeric films are polypropylene (PP), low-density polyethylene (LDPE), linear low-density polyethylene (LLDPE), high-density polyethylene (HDPE), polyvinyl chloride (PVC), polyethylene terephthalate (PET), polyvinylidene chloride (PVDC), polystyrene and biodegradable polymers (Mangaraj et al., 2009). Choosing the appropriate packaging material is a critical parameter in the success of MAP. The atmospheric modification degree is dependent on several factors like gas permeability, product respiration rate, film thickness and package surface area (Caleb et al., 2013).

For minimally processed fresh fruits and vegetables, MAP maintains the shelf life more than 50% and it provides a high quality product. Closed packages can act as barriers to preserve contamination, so ripening may be delayed. MAP also improves product presentation and reduced economic losses (Ramos et al., 2013). Besides the advantages, MAP has limitations. Primary concern in MAP is temperature control, because the poor temperature can lead to the deterioration for packaged product (Sandhya, 2010). In atmosphere packaging, high levels of CO_2 dissolving to food could

cause package collapse, off-flavors and growth of pathogens. Another limitation is that packaging materials should have specific properties such as strength, selective gas permeability and being odorless and also packaging materials should be environmentally desirable (Ramos et al., 2013).

Therefore, in order to protect the freshness of semi-finished fruits and vegetables, helping method is recommended (Rojas-Graü et al., 2009). One of the most effective options is edible films and coatings.

1.3. Edible Coatings

Edible coatings are thin layers of edible materials that cover the surface of the food (Vargas et al., 2008). Edible coatings can provide an alternative or be supportive to MAP to extend the shelf life of fresh and fresh-cut fruits and vegetables (Rojas-Graü et al., 2009). Ideally, edible coatings should possess the following properties:

- Suitable sensory characteristics (i.e. being transparent, tasteless and odorless).
- Suitable barrier properties (i.e. being water resistant, having adequate water vapor permeability and selective permeability to gases and volatile compounds).
- Improvement of the appearance and mechanical properties
- Carrier of active agents (antioxidants, vitamins etc.).
- Economical.

There is a wide range of components that can be used in edible coating composition. Classifications of edible coatings are based on their structural material and target application. Proteins, lipids, polysaccharides or composites are the most common major coating materials (Galus & Kadzińska, 2015).

Selection of coating material is based on their sensory and barrier properties (Lin & Zhao, 2007). Cellulose, starch, pectin, chitosan, alginates, carrageenan and agar are examples for polysaccharides. Protein based edible coating can be either animal source (i.e. casein, whey protein, gelatin and egg albumin) or plant source (i.e. corn, soybean, wheat, peanut and rice). Fatty acids, acylglycerols, resins and waxes are the examples of lipids (Mellinas et al., 2015).

Edible coatings are applicable on whole and fresh-cut fruits and vegetables. Apple, orange, lemon, strawberry, tomato, cucumber are examples for whole fruits and

vegetables that are coated. As an example of fresh-cut fruits and vegetables, which can be coated, fresh-cut apple, fresh-cut pear, minimally processed carrot, fresh-cut lettuce are given (Dhall, 2015).

There are significant advantages of edible coatings such as maintaining the shelf life, improving food quality, helping the preservation of fruits and vegetables, reducing the use of synthetic packaging materials, providing oxygen barrier and moisture properties, reducing metabolism and oxidation rates, incorporating compounds such as antioxidants, antimicrobials or nutraceuticals and improving the appearance (Rials & Ods, 2000). The greatest benefit is that edible coatings can be consumed with food.

On the other hand, there are some problems associated with edible coatings. Sensory implications are one of the main challenges for edible coatings. Thick coating on the food surface might become an undesirable barrier. This can result in anaerobic respiration, which produces much more carbon dioxide, ethanol and acetaldehyde. This process gives off-flavor to the product. In addition, incorporation of compounds might lead to undesirable properties such as bitter taste, astringent or off-flavor. Consumers may reject the product because of these inappropriate properties. Furthermore, many edible-coating materials can cause allergic reactions. Wheat, milk, peanuts and fish are the most important allergens. (Dhall, 2015).

1.4.Motivation and Objectives of the Study

Shelf life extension obtained by modified atmosphere packaging may not be sufficient for some fresh-cut fruits and vegetables. Edible coatings are considered as an alternative or a supportive agent to modified atmosphere packaging to extend the shelf life. However, they may sometimes impose some undesirable sensory properties such as bitter taste, off-flavors, etc., on the food product on which they are applied. One alternative to minimize these unwanted effects could be to fabricate ultra-thin edible coatings with adequate gas barrier properties. However, it does not seem possible to fabricate nor apply such thin edible coatings on food products in a controlled manner with the conventional methods. It is obvious that there is a need for new techniques, which provide better control on the thickness and morphology of the coatings.

Layer-by-layer assembly, which is based on successive adsorption of two or more materials onto each other due to the physicochemical interactions in-between, is a promising technique to fabricate such ultrathin edible coatings.

The objectives of this study are; developing novel, ultra thin, homogeneous, edible coatings with adequate gas barrier properties for fresh-cut fruits and vegetables using LbL deposition, characterization of the LbL coatings with a multidisciplinary approach to investigate the structure-property relationship and comparison of dipping and spraying methods on LbL coatings.

1.5. Layer-By-Layer Assembly (LbL)

1.5.1. Background

Layer-by-layer assembly, which was introduced by Decher (1997), is a bottom-up nano-assembly technique for the fabrication of multilayer films and coatings. Multilayer films obtained by layer-by-layer assembly have been widely used to coat and functionalize the surface of materials in different studies such as drug delivery (Junthip et al., 2016), biosensors (Alessio et al., 2016), and coatings. The attempts to utilize layer-by-layer assembly in food research have mainly centered on stabilizing emulsions (McClements et al., 2009), (Decker et al., 2011), while edible coating studies are fairly recent.

The layer-by-layer assembly can be driven by physicochemical interactions such as electrostatic forces, hydrogen bonding, Van Der Waals forces or covalent bonding. However, the most common driving force used so far is the electrostatic interactions between oppositely charged polyelectrolytes. The deposition is achieved by the successive adsorption of oppositely charged polyelectrolytes on a charged surface. Each deposited layer leads to a charge overcompensation that has two important consequences: (i) the repulsion of equally charged molecules and thus self-regulation of the adsorption and; (ii) the formation of a new layer by the adsorption of oppositely charged molecules on the top of the previous layer (Acevedo-Fani et al., 2015).

The general process is as follows (Figure 1.1): Layer-by-layer assembly is started with a charged substrate. Firstly, the charged substrate is incubated in a polycation (if the substrate surface is negatively charged) or polyanion solution (if the substrate surface is positively charged) for an appropriate amount of time. Then, excess amount of adsorbed molecules is removed by rinsing with the buffer solution that has same pH value with the incubation solution. Thus, the adsorption of the first layer is achieved and the surface charge is changed (from positive to negative or negative to positive.) After that, the substrate covered with the first layer is immersed in the polycation or polyanion solution to absorb the second layer (of opposite charge) for a certain amount of time. Then, the substrate is rinsed with the buffer solution that has the same pH value with second incubation solution. This process is continued until the desired number of layers is obtained and the average thickness is calculated based on the number of layers (Jokar et al., 2012).

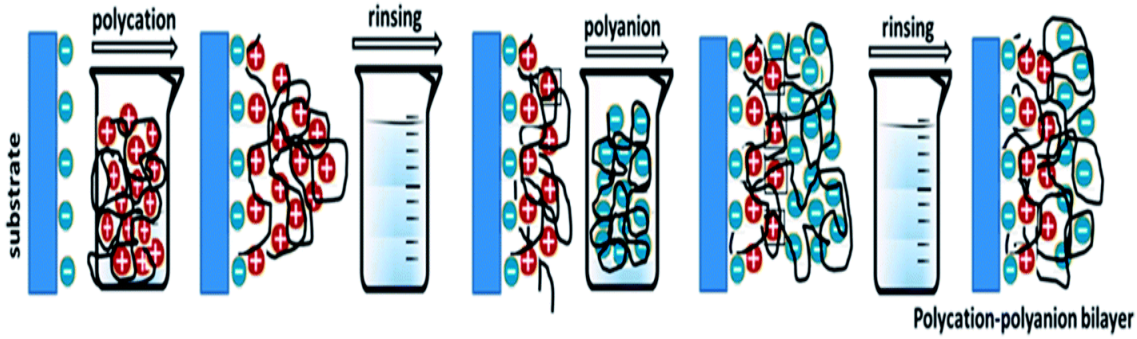

Figure 1.1. Schematic representation of layer- by- layer deposition of polycation and polyanion onto a solid substrate (Source: Joseph et al., 2014).

1.5.2. State of the Art of Layer-by-Layer Assembly Applications as Edible Coatings and on Modified Atmosphere Packaging Materials

Layer-by-Layer (LbL) technique has been used to produce ultrathin films at interfaces to increase the shelf stability of minimally processed fresh fruits and vegetables. These studies achieved by modification of the surface of modified atmosphere packaging materials. The attempts to utilize layer-by-layer assembly in food studies have mainly focused on stabilizing emulsions and coatings. However, edible-coating studies is quite new.

Medeiros et al. (2012) developed and characterized a nanomultilayer coating system, which composed of five nanolayers of pectin and chitosan and applied to 'Tommy Atkins' mangoes. This coating was characterized in terms of the water vapor, oxygen and carbon dioxide permeabilities. They compared mass loss, total soluble solids, and lower titratable acidity of uncoated and coated mangoes. Coated mangoes performed better than uncoated mangoes. They indicated that combination of chitosan and pectin layers were efficient on gas flow reduction and on the extension of the shelf life of mangoes.

Sipahi et al. (2013) studied the alginate based edible coating to increase the shelf life of fresh-cut watermelon. Sodium alginate (0.5, 1, 2 g/100 g), beta-cyclodextrin and

microencapsulated trans-cinnamaldehyde (natural antimicrobial agent), pectin, and calcium lactate were used as coating systems by using the layer-by-layer (LbL) technique. Coated samples were stored at 4° C for 15 days. Texture, color, weight loss, oBrix, pH, and growth of total coliforms, yeasts and molds, aerobics, and psychrotrophs were monitored every 3 days throughout storage. Coated samples' texture was well preserved and showed less weight loss compares the uncoated samples. They recommended 1g/100 g of alginate, 2 g /100 g of natural antimicrobial complex and 2 g / 100 g of pectin as a coating formulation to extend the shelf life and maintain the quality attributes of fresh-cut watermelon.

Mantilla et al. (2013) investigated the effect of antimicrobial edible coating on quality and shelf life of fresh-cut pineapple. Pineapples were coated with calcium chloride, alginate plus antimicrobial, calcium chloride and pectin respectively.
Coated pineapples were stored for 15 days at 4° C. Color, texture, pH, titratable acidity, moisture content, weight loss and vitamin C were evaluated every 3-4 days. They found that the antimicrobial coating well preserved the texture of fresh cut pineapple and also coating helped preserve color, odor and pH of the pineapple. The best coating formulation in terms of the preservation of quality attributes of fresh-cut pineapple is 1 g/100 g of alginate, 2 g/100 g of antimicrobial compound (transcinnamaldehyde) and 2 g/100 g of pectin.

Brasil et al. (2012) evaluated the polysaccharide based multilayered antimicrobial edible coating and its effects on quality of fresh cut papaya. To obtain the multilayered coating, they used chitosan, pectin and calcium chloride ($CaCl_2$) solutions. Uncoated and coated fruits were stored at 4 °C for 15 days. Coated fruits' shelf life extended up to 15 days at 4° C, however the shelf life of uncoated fruits was found less than 7 days. The multilayered antimicrobial edible coating improved the quality of fresh cut papaya. They indicated that the uncoated fruits lost quality properties quickly.

Laufer et al. (2013) investigated the oxygen barrier property of multilayered thin films composed of chitosan, carrageen and montmorillonite clay. They fabricated 10 trilayers of chitosan, carrageen and clay on PET films and this film reduced the oxygen permeability of PET. The quadlayer film, which was obtained by adding an extra layer of chitosan to the trilayer formulation, reduced the oxygen permeability of PET even further. The effectiveness of nanocoating at ambient conditions (22 °C and 55% RH) was demonstrated on bananas that were monitored as a function of time. They

concluded that fabrication of thin films with high oxygen barrier property depends on the nanostructure of films and these films provide a chance for renewable foil for food packaging.

Elsabee et al. (2008) examined the antifungal and antibacterial properties of corona treated polypropylene (PP) films, which were dipped into acidic solutions of chitosan and pectin, respectively. All strains in fungi and bacteria were used in this study as pure cultures. They indicated that the films coated with chitosan and derivatives showed higher antifungal and antimicrobial compared to the native and corona treated PP films. Increasing the amount of chitosan on the surface of corona treated PP films increased the antimicrobial activity. Using these films for tomato packaging kept it almost intact with no apparent rotting infection for 13 days. They found that the films did not suffer deterioration so that films could be used as packaging materials.

Souza et al. (2014) evaluated the effect of an alginate chitosan nanomultilayer coating obtained by layer- by-layer assembly method in the quality and shelf life of fresh-cut mangoes. LbL assembly process was repeated with the alternate deposition of a total of five nanolayers (Alg-Ch-Alg-Ch-Alg). Then samples stored at 8 °C and 93% RH. The changes in mass loss, titratable acidity, pH, ascorbic acid content, total soluble solids, browning rate, and microbial count were evaluated during storage. Based on the microbiological analyses, shelf life of fresh-cut mangoes could be extended up to 8 days at 8 °C when compared with uncoated fresh-cut mangoes. According to this result, they concluded that the nanomultilayer coatings could be considered as a safe and effective treatment for fresh-cut mangoes.

Thin films composed of polyethylenimine (PEI) and polyacrylic acid (PAA) deposited using layer-by-layer assembly technique were studied by Yang et al. (2012). They investigated the effect of various crosslinking methods on their oxygen and water vapor barrier of films. Films were crosslinked with glutaraldehyde (GA) or 1-[3-(dimethylamino) propyl]-3-ethylcarbodiimide methiodide (EDC) solution for 3, 30 or 300 min. Thermal crosslinking was performed by heating the film in an oven at 120, 150 or 180 °C for 1, 2, or 5 h. In order to examine the influence thickness growth following crosslinking, films were grown to 10 BL and then crosslinked with GA, EDC or heat. Growth of crosslinked films reduced film thickness with the extent of reduction ranging from 2 to 50%. Maximum barrier improvements occur at different GA and EDC concentrations. Thermally crosslinked films showed some improvement in

moisture barriers, but this required a high number of layers. They concluded that the crosslinker chemistry influences the barrier properties.

Pinheiro et al. (2012) investigated the interactions between κ-carrageenan and chitosan in nanolayered coatings. In order to prepare the nanolayered coating, aminolyzed PET pieces were used. The nanolayered coating was composed of an A/C PET support layer adsorbed with a polysaccharide multilayer constituted of 5 polysaccharide layers (three κ-carrageenan and two chitosan layers). Nanolayered coatings were characterized in terms of its surface (contact angle measurements) and gas barrier properties (water vapor and O2 permeabilities). The deposition of the κ-carrageenan layers induced a decrease in contact angle, whereas the deposition of chitosan led to the increase of contact angle. The results of κ-carrageenan and chitosan nanolayers exhibit good gas barrier properties. They concluded that the knowing the interactions that play role during the construction of this type of nanostructures could be used to produce edible, biodegradable multilayered nanostructures with improved mechanical and barrier properties for food applications.

1.5.3. Comparison of Dipping and Spraying Methods in LbL Assembly

Dipping and spraying methods are two methods of the Layer-by-Layer assembly. Compared to methods of dipping and spraying, spraying methods seems to be easily controlled than the dipping method. The possibility of contamination is lower for spraying method. In the literature different opinions are included about the effects on the structure of the LBL films of the two methods.

Denis - Rohr et al. (2015) used to coat polypropylene (PP) with n-halamine and polyacrylic acid (PAA) by using dipping and spraying methods. Films were characterized and compared in terms of surface morphology, surface chemistry and antimicrobial activity against *Listeria monocytogenes*. Both methods showed 99.99% reduction against the *L. monocytogenes* population. Regarding surface morphology films obtained by dipping method were found to be rougher than those obtained by spraying. They conclude that LbL assembly with spraying is a rapid and inexpensive fabrication method for rechargeable antimicrobial surfaces compared to the dipping method.

Aoki et al. (2012) investigated the possibility of Layer-by-Layer assembly of dipalmitoly phosphatidyl glycerol (DPPG) and polyallylamine hydrochloride (PAH) with dipping and spraying methods. They characterized the films using UV- Visible spectroscopy, AFM and FTIR. Multilayer films, which were obtained by spraying were thicker than the films obtained by dipping. Spraying time was 60 times shorter than dipping time, however spray-LbL films did not cover PAH layers completely. Besides, average height and surface roughness obtained for spray- LbL films were lower than those obtained for dip-LbL films.

Kolansinska et al. (2009) compared the properties of polyelectrolyte multilayer films, which were prepared using dipping and spraying. Polyallylamine hydrochloride (PAH) and polyethyleneimine were used as polycations and polysodium4-styrenesulfonate (h-PSS) and perdeuteurated PSS (d-PSS) were used as polyanions. Films prepared by spraying method were thinner and rougher than the films obtained by dipping. They concluded that the short time of preparation for spraying technique was a great advantage, however films were less stable compared to the films prepared by dipping technique.

Izquierdo et al. (2005) studied the deposition conditions for speeding up Layer-by-Layer Assembly. Poly (sodium 4-styrene- sulfonate) (PSS) and poly (allylamine hydro- chloride) (PAH) multilayer films were deposited on a poly- (ethylenimine) (PEI) precursor layer. Spraying time, polyelectrolyte concentration, and effect of film drying during multilayer construction was investigated. They found that the spray deposition allowed achieving regular multilayer growth even under conditions for which dipping fails to produce homogeneous films. Besides films prepared by dipping method are always thicker than films prepared by spraying method and in less time film formation obtained by spraying method.

1.6. Some Nanotechnology-Oriented Characterization Methods for Multilayered Nano-Coatings

1.6.1. Surface Plasmon Resonance (SPR)

Surface plasmon resonance (SPR) is an efficient method used for the surface characterization of organic or inorganic substances. SPR is used to determine thickness, porosity and refractive index of thin films and also the surface reactions can be observed in situ. SPR technique has many advantages for sensing technology due to its unique properties i.e. accurate results and non-destructive and label free measurements (Olaru et al., 2015).

In Figure 1.2, the principle of SPR at Kretschmann configuration is demonstrated. When a polarized light penetrates the metal interface over a wide range of incident angles; the evanescent wave will be generated under total internal reflection condition. When a light beam hits the metal surface with an incidence angle, which is above the critical angle, light beam is reflected from the surface completely. However, at a certain incidence angle the energy and momentum of polarized light that is sent to the surface matches the energy and momentum of surface plasmons. As a result of this matching, surface plasmon resonance phenomenon occurs. This situation causes the reflected light intensity fall to a minimum. The angle at which the reflectivity is minimum is called the SPR angle (Li et al., 2012).

SPR angle is sensitive to the sample contacting with the metal surface. SPR angle can change based on the changes in the environment or amount of accumulated biomolecules on the metal-dielectric interface. When an angular scan is taken, an intensity-angle curve (SPR curve) is obtained. When the substrates are connected to the metal-dielectric interface, SPR angle shift to the right. As a result of the adsorption of the substance in metal-dielectric interface, changes in SPR minimum angle is shown in Figure 1.3 (a) by curve 2. Shift in SPR angle based on the adsorption in metal-dielectric interface is observed as a function of time. In Figure 1.3. (b) depicts changes in SPR angle in real time. Fixed angle mode is important to follow the in situ deposition. By using fixed angle mode, equilibrium time of deposition can be determined.

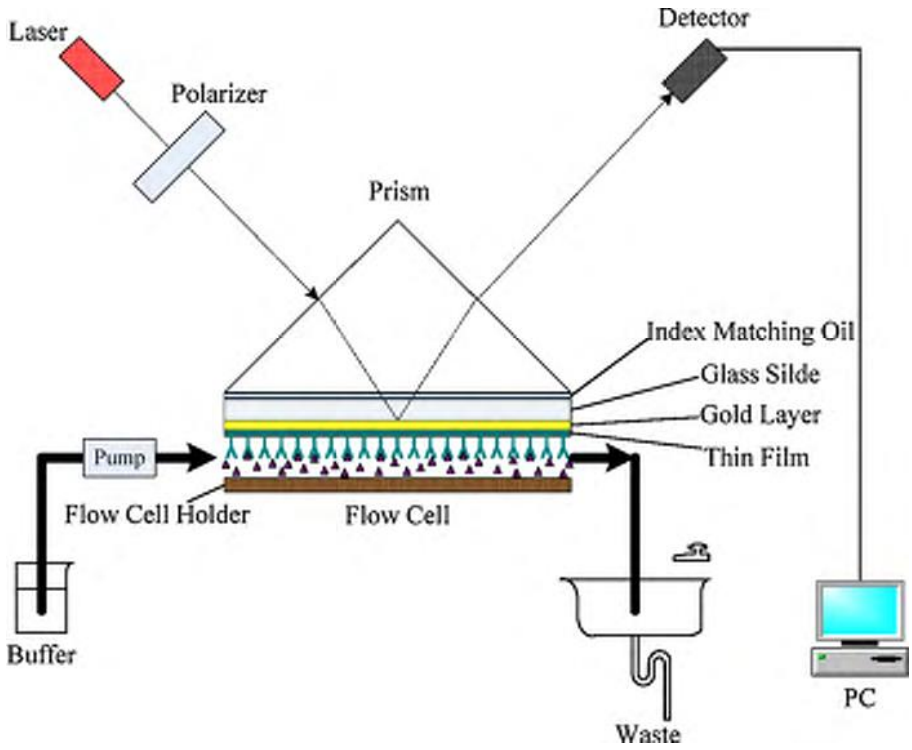

Figure 1.2. Schematic illustration of Kretschmann configuration (Source: Liang et al., 2010)

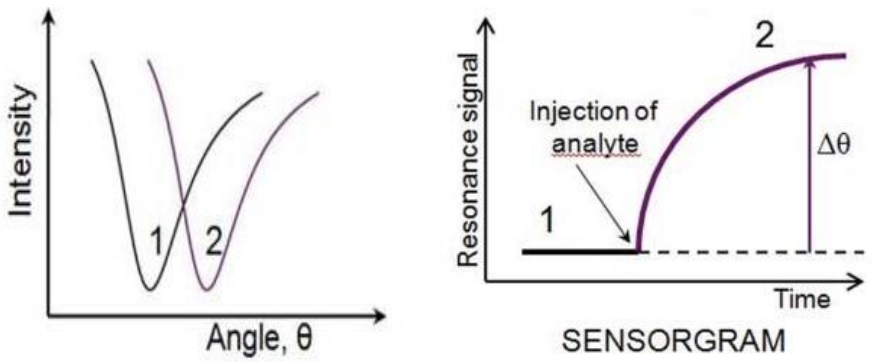

(a) (b)

Figure 1.3. Intensity- angle curve obtained from SPR angular scan (a) Based on substrate adsorption SPR angle shift to the right (1-2), Changes in SPR angle in real time (b) (Source: Olaru et al., 2015)

1.6.2. Atomic Force Microscopy (AFM)

Atomic force microscopy (AFM) is a scanning probe microscopy with high resolution. Principle of AFM is based on the laser beam deflection system where the laser is reflected from back of the AFM cantilever onto a detector (Morris et al., 2011).

AFM creates topographic images by scanning surface of samples with a sharp tip mounted to a cantilever. Cantilever is usually made from silicon (Si) or silicon nitride (Si_3N_4). When an AFM tip approaches to surface, forces between the tip and the surface leads to twisting of the cantilever based on Hooke's Law. To measure the cantilever deflection (lateral and/or vertical), a laser beam is focused on the free end of the cantilever and the position of reflected beam is determined by a position-sensitive photo detector. During measuring process, sample is attached to a piezoelectric scanner that provides a three-dimensional positioning. The surface topography map is obtained during scanning and computer generates the surface topography image of the sample (Figure 1.4) (D. Liu & Cheng, 2011).

There are different AFM imaging modes such as contact mode, peak-force tapping mode and tapping mode, which may be utilized in preference depending on the nature of the materials used and the imaging environment. Contact mode is the basic mode for all AFM techniques in which the probe tip is in constant contact with the sample surface, tapping mode enabled researchers to getting image for samples too fragile with high scan speeds. Peak force tapping mode allows the researcher to precisely control probe -sample interaction and provides high-resolution AFM images from the softest biological samples to very hard materials. Additionally, AFM allows to obtain images both in air and liquid medium (Funami, 2010).

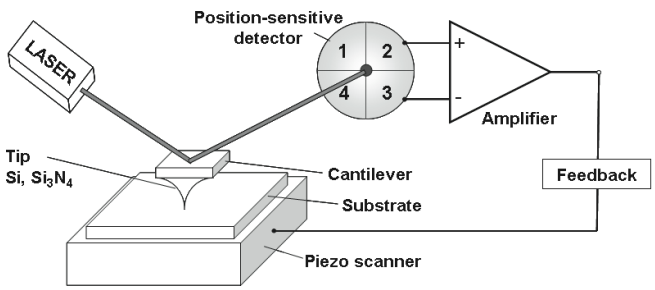

Figure 1.4. Basic and schematic principle of AFM
(Source: Funami, 2010).

CHAPTER 2

MATERIALS AND METHODS

2.1. Materials

Chitosan, derived from chitin (medium molecular weight, 81% deacetylated) was obtained from Sigma-Aldrich (448877 - St. Louis, MO, USA). Casein (sodium, salt bovine milk) was obtained from Sigma-Aldrich (C8654 - St. Louis, MO, USA). Quartz slides (50 x 25 x 1 mm) were purchased from Lightpath Optical (UK). Spray cans made of polyethylene purchased from İnterlab (I.062.11.250, diameter 30 mm; nozzle, 0.50 mm). Acetic acid, ethanol and glass slide cleaning liquid (Hellmanex III, Fluka, Germany) were purchased from Sigma (St. Louis, MO, USA). Corona treated PP films were kindly donated by Polinas Plastik Sanayi ve Ticaret A.Ş (Manisa). Surface plasmon resonance sensors coated with Au+ SiO_2 were obtained from Bionavis (Finland). Scanasyst-Fluid+ AFM probes were purchased from Bruker (Germany).

2.1.1. Cleaning Procedure of Quartz and Glass Slides

Quartz slides and glass substrates (for AFM analysis) should be properly cleaned before being handled in order to avoid alteration of the layer-by-layer assembly by any possible contamination. Artyukhin and Stroeve (2003)'s method was applied as the cleaning procedure. The substrates were exposed to ultrasonication at 55°C for 15 minutes in ultra pure water (18 mΩ, Milli-Q Ultrapure Water System, Millipore) 2 % (v/v) Hellmanex solution and pure ethanol, respectively. After each step, the substrates were rinsed with plenty of deionized water. At the end of the procedure, the substrates were dried with nitrogen gas and stored in a clean container until the deposition process.

2.1.2.Cleaning Procedure of Surface Plasmon Resonance Sensors

Au+SiO_2 coated sensors, as obtained already clean from the manufacturer were further treated by rinsing with plenty of ethanol followed by plenty of ultra pure water. Finally, they were dried with nitrogen before use.

2.2. Methods

2.2.1. Preparation of Chitosan and Sodium Caseinate Solutions at Different Concentrations and pH Values

Chitosan solutions (1%, 0.5% and 0.2% w/v) were prepared in acetic acid solution (1% v/v) with magnetic stirring (250 rpm) for 2 - 4 hours at room temperature. Sodium caseinate solutions (0.5% and 0.2% w/v) were prepared by dispersing sodium caseinate powder in ultra pure water with continuous stirring (250 rpm) for 2 – 4 hours at room temperature.

The pH values of the chitosan solutions were adjusted to 3, 3.5, 4, 4.5, 5, 5.5 using proper amounts of 5 M NaOH or HCI solutions. The pH values of the sodium caseinate solutions were adjusted to 5, 5.5, 6, 7, 8 using proper amounts of 1 M NaOH or HCI solutions.

2.2.2. Determination of the Critical Micelle Concentration of Sodium Caseinate

In this thesis, it is aimed to perform layer-by-layer assembly at concentrations at which both chitosan and sodium caseinate molecules behave as polyelectrolytes. As sodium caseinate is a surfactant, the molecules in the solution form micelles above the

critical micelle concentration (CMC). Therefore, in order to determine the correct sodium caseinate concentration range to work with, CMC of sodium caseinate was determined in the first place. For the determination of the CMC, conductometric method was used. In this method, conductivity data were collected starting from high casein concentration proceeding to low concentrations. Because the critical micelle concentration of ionic surfactants (such as sodium caseinate) depends on pH, determination of CMC was performed at each pH value of interest (5, 5.5, 6, 7, 8). A stock solution of 4% (w/v) sodium caseinate at the desired pH was prepared initially. The stock solution was diluted by 0.2% (v/v) at each measurement step until the lowest concentration of sodium caseinate (0.2% w/v) was obtained. As a result of the dilution process, 20 concentration points were obtained and conductivity values at these concentrations were measured. The measurements were carried out by the Hanna Instruments EC 215 conductivity meter (USA). All the measurements were carried out at 22°C ± 0.2. The temperature was controlled by a cooling water bath (J1154OS – Termal, Turkey). All experiments were conducted in duplicate and results were expressed as mS/cm^2. CMC was calculated from the slope of ratio of conductivity to concentration vs. square root of concentration as described in Section 3.2.1 using MATLAB release 8 (Mathworks Inc., U.S.A).

2.2.3. Determination of the Physical and Electrical Properties of the Polyelectrolyte Solutions

Zeta potential and particle size measurements of chitosan and sodium caseinate solutions at various pH and concentrations were performed in order to determine the appropriate LbL assembly conditions for each polyelectrolyte solution.

The prepared solutions were, first passed through a syringe filter (pore size 0.45 μm, CA, Isolab, Germany), and then transferred to a private cuvette. The measurements were carried out with Zetasizer Nano-ZS (UK) at room temperature in at least two replications (In case of high standard deviations, measurements were performed in four replications). 3 measurements were taken for each sample, so the results were calculated as the average of 6 (or 12) readings.

The zeta potential is calculated using the result of electrophoresis applied to the sample based on Henry equation (1).

$$U_E=2\varepsilon z f(Ka)/3\eta \quad (1)$$

where U_E is electrophoretic mobility; ε is dielectric coefficient; z is zeta potential; $f(Ka)$ is Henry function and η is the dynamic viscosity.

Particle size is determined with dynamic light scattering based on Brownian motion and calculated via Stokes-Einstein equation (2).

$$D= kT / 6\pi\eta R_h \quad (2)$$

where D is diffusion coefficient of the particles; k is Boltzmann constant (1.38×10^{-23} JK^{-1}); T is temperature; and R_h represents hydrodynamic radius of the particles.

2.2.4. Layer-By-Layer Assembly by Dipping

The substrates used for multilayered nano-coating assembly were quartz slides, glass slides, Au+SiO_2 coated SPR sensors and coronated PP films for UV-Vis, AFM, SPR and SEM analysis, respectively. In all cases, the surface of the substrate is negatively charged. LbL assembly of chitosan and sodium caseinate is performed as follows: Initially, the substrate, which was cleaned according to an appropriate method mentioned above, was submerged in the chitosan solution of desired pH in order to obtain the first layer. The substrates were incubated in the solution for 2, 10 and 20 minutes. After this step, the sample was rinsed in ultrapure water at the same pH of chitosan solution for 1 minute. Rinsing step was performed to remove the chitosan molecules that were not strongly bound to the substrate. Afterwards, the sample was dried with a gentle flow of nitrogen gas. Straightaway, the sample (chitosan coated substrate) was immersed in the sodium caseinate solution of desired pH for 2, 10 and 20 minutes to obtain the second layer. Here, the negatively charged sodium caseinate molecules were adsorbed onto the previously adsorbed positively charged chitosan layer by means of (mainly) electrostatic interactions. The process was followed by a rinsing step with ultrapure water at the pH of sodium caseinate solution for 1 minute. The deposition was continued alternatively until 12 layers were obtained.

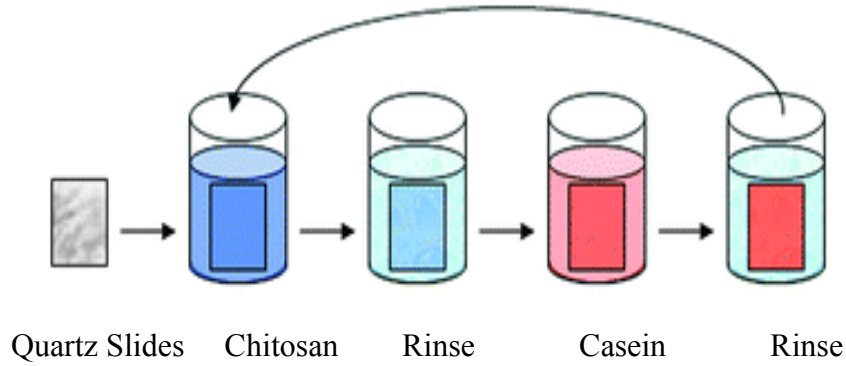

Figure 2.1. Schematic diagram of layer-by-layer assembly by dipping

2.2.5. Layer-By-Layer Assembly by Spraying

The spray bottles (30 mm in diameter) used for the LbL deposition by spraying experiments were made of polyethylene (Interlab, I.062.11.250) with a 0.55 mm spraying nozzle. Spraying angle to the substrate surface was 90°±5 and the spraying distance (distance between the nozzle and the substrate) was determined according to the method of Izquierdo et. al. (2005). According to this method, pure water was sprayed (once-for 1 sec) on a dark cardboard, which has low water absorbency, at different spraying distances. Then, the diameter of the homogeneously wetted area was determined for each spraying distance. Measurements were performed in 3 replications and average diameters were calculated. Visual inspection of the diameter of wet area versus spraying distance graph (Figure 3.8. in Chapter 3) suggested that the appropriate spraying distance should be chosen as 20 cm. The results are given and discussed in section 3.2.3.

The substrates used for LbL deposition by spraying were quartz slides, glass slides, and coronated PP films for UV-Vis, AFM, and SEM analysis, respectively. The general procedure that was followed in spraying experiments is given in Table 2.1. Here, t_1 and t_3 represent the amount of time the polyelectrolyte solution and the rinsing water is sprayed onto the surface of the substrate (or the number of sprayings based on the assumption that single spraying takes 1 sec), respectively, while t_2 represents the waiting time between the adsorption and the subsequent rinsing step and t_4 represents the drying time between the rinsing and the subsequent adsorption step. Note that the

drainage and evaporation of water on the substrate are continued during this waiting period. In order to examine the importance and impact of spraying and rinsing steps, different versions of the general procedure (varying in values of t_1, t_2, t_3 and t_4) are experimented. The modified versions and the corresponding results are given Section 3.2.3.

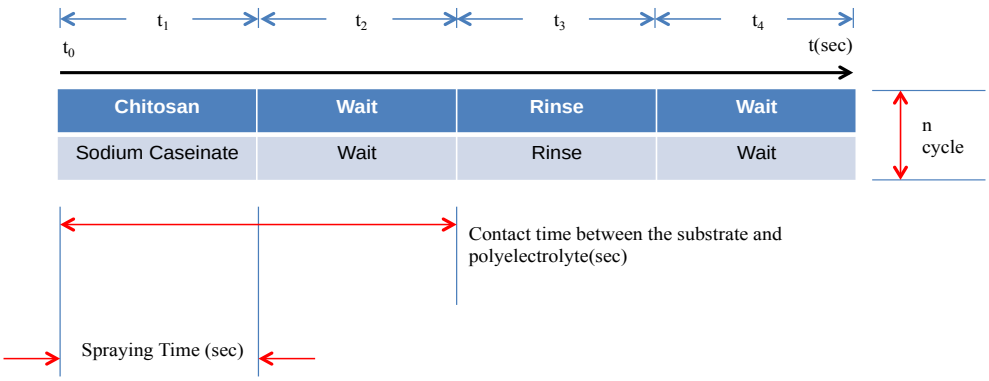

Table 2.1. Layer-by-layer assembly by spraying procedure.

2.2.6. Characterization Methods

2.2.6.1. UV-Visible Spectroscopy

This technique was used to monitor the film growth by following the absorption value at a certain wavelength. Measurements were carried out using Perkin Elmer Lambda 25 UV-Visible Spectrometer (USA). In order to determine the follow-up wavelength(s), 1% (w/v) sodium caseinate and chitosan solutions were prepared and the absorption spectra of each were examined separately in the range 190-400 nm (see Figure 3.8. in Section 3). The results suggested the choice of 280 nm as the follow-up wavelength. All measurements were carried out at room temperature and conducted at

least in duplicate. Each measurement was corrected by the reference (uncoated quartz slide) values.

2.2.6.2. Surface Plasmon Resonance (SPR)

SPR (Bionavis SPR-Navi 200) was used both in scan and fixed angle modes to monitor the film growth. The optic prism was used in Kretschmann configuration. A glass substrate coated with 50 nm Au+10 nmSiO_2 was used as an SPR sensor. The LbL coating was formed in the flow cell of the instrument to enable in-situ observation of the multilayer formation. Chitosan solution at appropriate concentration and pH was injected into the flow cell with the aid of a syringe and then adsorption was allowed for the appropriate amount of time. At the end of the process, the sensor was rinsed with deionized water of the same pH value as chitosan solution. After the rinsing step, SPR angular scan was taken and it was switched to the next deposition step. The procedure was repeated for the casein solution. The characterization of 10 layers, which were formed in this way, was performed with Winspall 3.02 (Germany).

All the solutions were filtered by a syringe filter (pore size 0.45 μm, CA, Isolab, Germany) followed by degassing by ultrasonification (Elmasonic, S40, Germany) for 15 min before being injected into the flow cell.

2.2.6.3. Atomic Force Microscopy (AFM)

Surface morphology and topology of the layers were monitored by using atomic force microscopy (AFM) (Digital Instruments – MMSPM Nanoscope IV, USA). Glass slides were cut into small pieces (1 cm x 1 cm) and used as a substrate for AFM analysis. AFM imaging was performed in both air and liquid environments. Air analyses were performed after each sample was completely dried in a desiccator, which was conditioned with silicon beads. The samples were affixed in special AFM tabs and Rtespa probe (silicon tip, resonant frequency 300kHz, spring constant 40 N/m) was used for scanning the surface. The analysis was conducted in peak force -tapping mode.

AFM imaging in liquid environment was conducted in contact mode with the use of Scanasyst-fluid (+) probe (silicon tip, resonant frequency 150kHz, spring

constant 0.7 N/m). The multilayer formation was achieved in the special liquid cell of the instrument, which allowed for *in situ* examination of the surface topology of the layers. Only the 1st, 2nd, 5th, 6th and 12th layers were analyzed.

The surface roughness of the layers was determined in terms of Rq (root mean square deviations of the average of height profile taken from the mean line, and Ra (arithmetic average of the absolute values of surface height deviations measured from the mean line). In Rq and Ra equations; Z represents number of height deviations and N refers to the total number of measurements that were taken from the image data plane.

$$Rq=\sqrt{\frac{\Sigma Zi^2}{N}} \tag{3}$$

$$Ra=\frac{1}{N}\sum_{j=1}^{N} Zj \tag{4}$$

The thicknesses of the layers were determined during imaging in air using the scratch method as follows: First, the sample surface was scratched slightly with sterile blades wrapped with parafilm (to prevent scratching of the glass substrate) and then the scan was taken. The depth of the scratch, which gives the thickness of layer, is determined from the height profile of a line along the scratch. The thickness measurements were repeated at 3 different parts of the scratch and the results were given as the average of these 3 measurements.

2.2.6.4. Scanning Electron Microscope (SEM)

The surface and cross-sectional morphology of the multilayered coatings were scanned using Philips XL 30S FEG (FEI Company, Eindhoven, Netherlands). Corona treated PP films were used as substrates for the LbL assembly in SEM analyses. Nanofilms prepared on PP films were coated with gold (0.05nm) in the presence of argon gas using a K550 X sputter coater (Quorum Technologies, London). This step was necessary to give electrical conductive properties to the substrate with nanofilms. Samples were analyzed with an acceleration voltage of 3 kV and a 1μm to 50μm working distance.

2.2.7. Oxygen Permeability Measurements

The oxygen permeability of the films was measured according to the ASTM D1434- 82 standard using gas permeation instrument, Lyssy L100-5000 (PBI Dansensor, Denmark) based on the manometric testing principle. In the manometric testing method, a pressure difference (driving force) across the sample is created by maintaining the test gas at atmospheric pressure in the upper chamber, while vacuum is applied in the lower measuring chamber. While the gas permeates through the sample, the pressure in the lower measuring chamber increases. The instrument measures the time required for the lower chamber pressure to increase from a predefined lower limit to a pre-defined upper limit. The measured time interval is then transformed into the gas permeability rate expressed in $ml/m^2/day$. Gas permeability of the PP film samples coated with chitosan and sodium caseinate were determined at constant temperature (23 ° C) and relative humidity (0% RH) conditions with 5–10 cm^3/min gas flow.

2.2.8. Water Vapor Permeability Measurements

The water vapor transmission rates of the films were measured with Mocon Permatran-W model 3/33 (USA) water vapor permeation measurement systems. Measurements were performed at 37.8 °C and 90% relative humidity with 100 cm^3/min nitrogen gas flow rate (ASTM F1249 standard).

To analyse water vapor barrier performance PP film samples coated with chitosan and sodium caseinate are mounted in a test cell. Test cells are divided into two chambers separated by the sample material. The inner chamber is filled with nitrogen (carrier gas) and the outer chamber with water vapor (test gas). Water molecules diffuse through the film to the inside chamber and are conveyed to the sensor by the carrier gas. The computer monitors the increase in water vapor concentration in the carrier gas and it reports that value on the screen as the water vapor transmission rate.

By using water vapor transmission rate, (WVTR), permeance and permeability can be calculated from the following formulas:

$$\text{Permeance} = \text{WTR} / S\,(R1 - R2)$$

$$\text{Permeability} = \text{Permeance} \times \text{Thickness}$$

Where:

ΔP = Vapor pressure difference in inches of mercury

R_1 = Relative humidity at the source expressed as a fraction (for 90% RH chamber R_1 = 0.90)

R_2 = Relative humidity of the vapor sink expressed as a fraction (R_2 = 0 for the 0% RH chamber (dry side))

S = Vapor pressure of water at the test temperature.

2.2.9. Antimicrobial Activity of Multilayered Films

Antimicrobial activity of multilayered coatings obtained by chitosan and sodium caseinate at pH 5.5 with both dipping and spraying methods was investigated against *Escherichia coli* (NRRL B-3008). The overnight cultures were incubated in plate count agar medium (PCA, Merck, Germany) at 37 °C. After the incubation, cell concentration was set to 0.5 McFarland unit (Biosan Company, Riga, Latvia) with 1% (v/v) peptone water and inoculated on plate count agar (PCA) medium. For antimicrobial tests, 24 disks (2 cm in diameter) from each type of film were prepared. 5^{th} (chitosan), 6^{th} (casein) and 11^{th} (chitosan) layers were examined to determine the antimicrobial activity of the coatings. Petri dishes were incubated at 37 °C for 72 hours.

2.2.10. Statistical Analysis

All data obtained were subject to statistical analysis with MINITAB® release 16 (Minitab Inc., State College, Pa., U.S.A.) Significant differences were analyzed using one-dimensional analysis of variance (ANOVA). Whenever significant differences between means were obtained, Tukey pairwise comparison test ($P<0.05$) was performed.

CHAPTER 3

RESULTS AND DISCUSSION

3.1. Preliminary Results

3.1.1. Critical Micelle Concentration (CMC) of Sodium Caseinate

Sodium caseinate molecules are surface-active agents. Thus, they are found in solution in the form of micellar structures above their CMC. As it was already mentioned, in this study, it is aimed to perform layer-by-layer assembly at concentrations at which both chitosan and sodium caseinate molecules behave as polyelectrolytes. Therefore, in order to determine the correct sodium caseinate concentration range to work with, CMC of sodium caseinate at each solution pH was determined in the first place. Conductometric method was used for this purpose.

In order to determine the CMC of sodium caseinate at each pH values concentration (C) - conductivity (K) curves were plotted. However, in these curves, there was not observing any significant breakage that indicates the CMC of sodium caseinate. This is a highly common situation for surfactants with low number of aggregation. Several methods have been proposed to overcome this problem in the literature (Tyowua et al., 2012). One such methodology is to calculate the ratio of conductivity to the concentration (K/C) and square root of concentrations ($C^{1/2}$) by using the obtained data and to plot the corresponding. In this way, a significant break can be observed in the transition of high concentrations to low concentrations. To determine the CMC, curves were plotted based on the conductivity/concentration ratio and square root of concentration values. Obtained graphs of each pH value were shown in Figure 3.1. As shown in graphs K/C values increased until reach medium concentration. In high concentrations, K/C values were reached highest values. Crossing point of the simple linear regression equation of values in high concentrations of sodium caseinate and simple linear regression equation with the values in low

concentrations gives the critical micelle concentration of sodium caseinate. The CMC values were calculated in this way were given in Table 3.1.

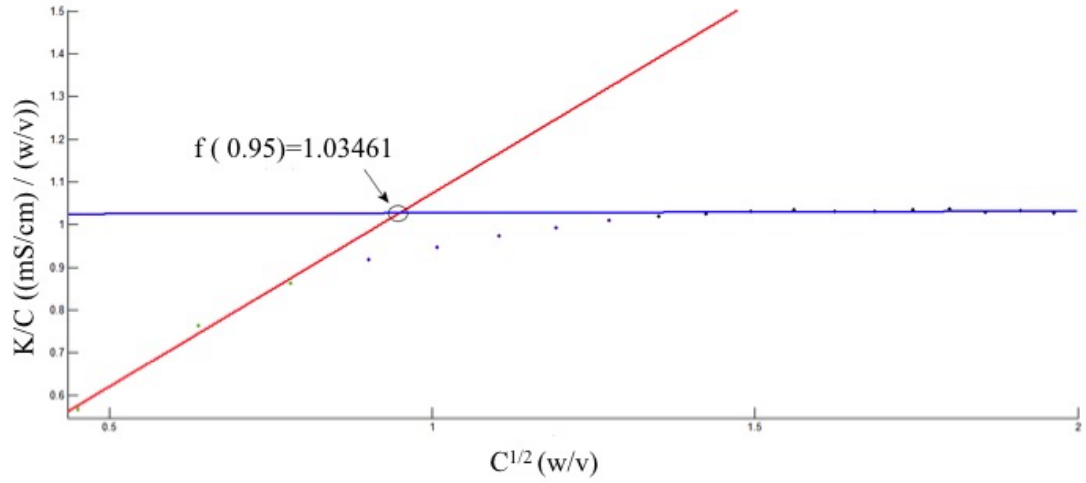

(a)

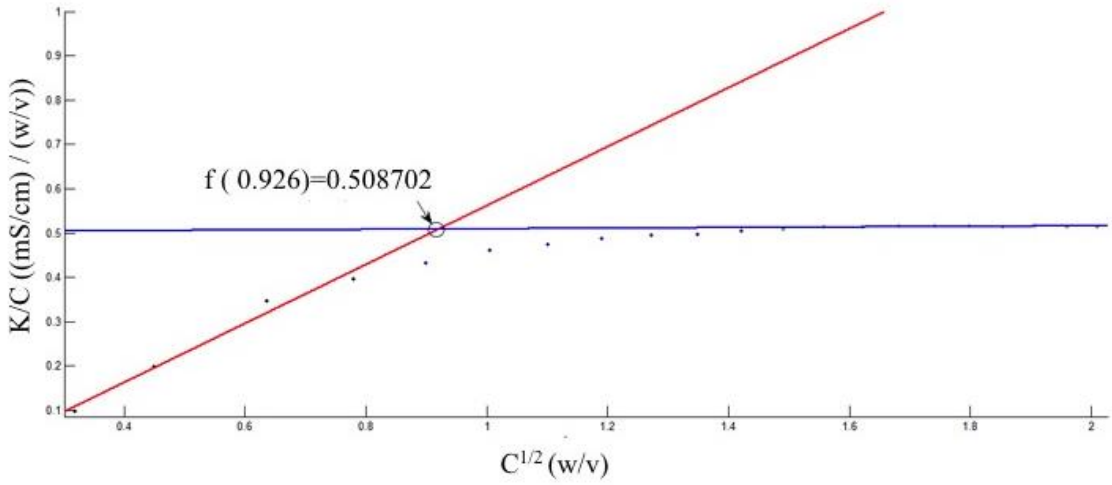

(b)

Figure 3.1. Determination of the critical micelle concentration (CMC) of sodium caseinate at different solution pH values via conductometric method (a) pH=5.5 (b) pH=6 (c) pH=7 (d) pH=8.

(Cont. on next page)

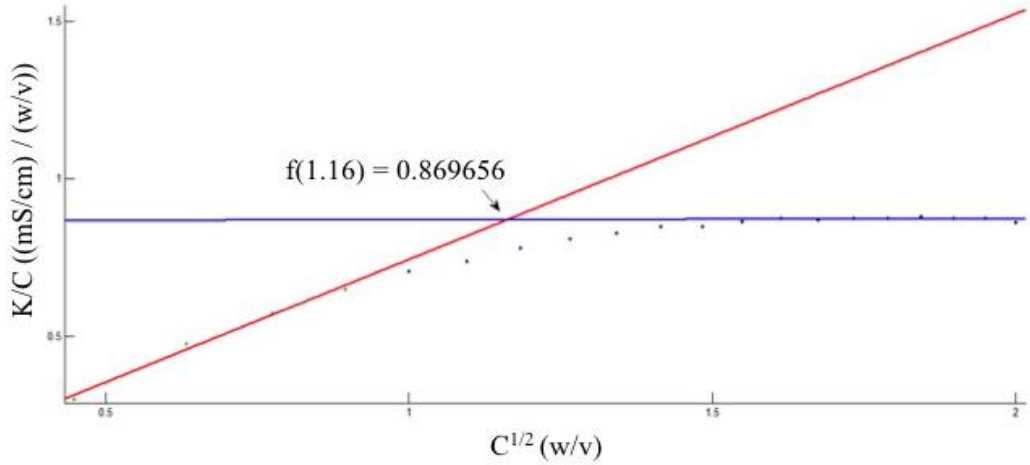

(c)

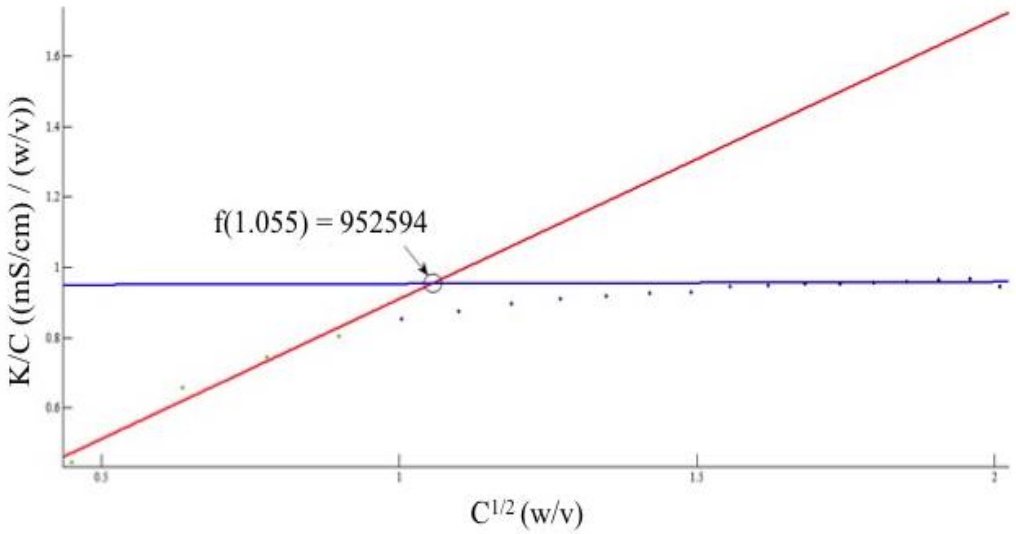

(d)

Figure 3.1. (cont.)

CMC values calculated in this way are given in Table 3.1. In order to ease the discussion of the results, the added ionic strength originating from pH adjustments with NaCl or NaOH solutions of appropriate molarity are also given. As it

is seen clearly, the CMC of sodium caseinate at pH 7 and 8 were found higher than at pH 5.5 and 6. It is considered that two factors are affecting this situation. Firstly, as the pH of the environment approaches the isoelectric point of casein (4.6), a decrease occurs in the net effective surface charge density of sodium caseinate. Secondly, an increase in the ionic strength by the HCl solution addition to reduce the pH of the environment and existence of stabilizer molecules inhibits the electrostatic interactions between the casein molecules. Thus, casein molecules can come together at lower concentrations and can create micelle structures.

The results indicate that the CMC of sodium caseinate is around 1% (w/v). This value is comparable to that of Jayasundera et.al.'s (2011) study in which the CMC of sodium caseinate was determined as 3% (w / w). The discrepancy is most probably due to the use of different sodium caseinate samples; i.e. difference in the level of impurities and amount of salt in the bulk powder.

In accordance with our results, the concentrations for sodium caseinate to work with in LbL experiments were chosen as 0.2% (w/v) and 0.5% (w/v).

Table 3.1 Critical micelle concentrations of sodium caseinate at different solution pHs. The added ionic strength originating from pH adjustments with NaCl or NaOH solutions of appropriate molarity are also given. Statistically significant differences were tested with one-way ANOVA and significant differences ($P < 0.05$) were determined by the Tukey test. CMC values with different superscript letters are significantly different.

pH	**CMC(w/v %)**	**Ionic Strength (mM)**
5.5	0.95 ± 0.03^{b}	13.80671 (HCl)
6	0.850 ± 0.008^{b}	10.88032 (HCl)
7	1.15 ± 0.05^{a}	-
8	1.11 ± 0.13^{a}	9.017937 (NaOH)

3.1.2. Zeta Potential and Particle Size Measurements of Chitosan and Sodium Caseinate

One of the main factors that determine the behavior of polyelectrolytes in polar solutions is the zeta potential value. There is a region that tightly bound to the surface of the particles consisting of opposite charge ions. Also apart from this region, the surface of particles consists of secondary ion layer that do not covered but moving along with particles (diffuse double layer or slip plane). Both the region and layer are called as electric double layer. Thus, the electrical potential of the end of electric double layer, which is outside the particles, is referred as zeta potential. In other words, the zeta potential indicates the net effective charge on the particle surface.

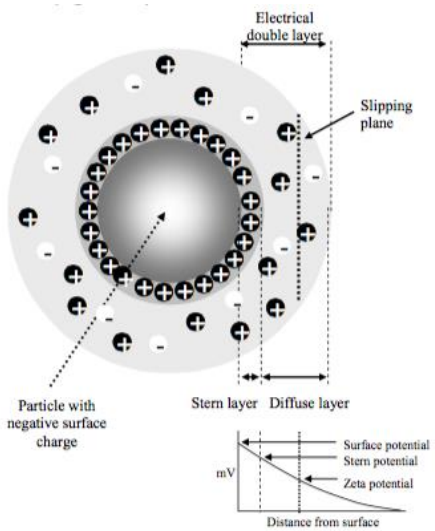

Figure 3.2. Negatively charged electrical double layer around the particles and the zeta potential (Source: Nanocomposix, 2012).

In this part, the zeta potential and the average hydrodynamic diameter of chitosan particles in dilute solutions of 0.2% and 0.5% (w/v) at 6 different pH values (3, 3.5, 4, 4.5, 5, 5.5), and sodium caseinate particles in solutions of 0.2% and 0.5% (w/v) at 4 different pH values (5, 5.5, 6, 7, 8) were determined. The results are given in Table 3.2. The changes in ionic strength due to addition of appropriate amounts of NaCl or NaOH solutions to reach the desired pH value are also given.

When the 0.2% (w/v) chitosan results are evaluated, it is observed that the general trend is a decrease in the zeta potential with an increase in the solution pH. This decrease is due to the fact that pKa value of chitosan is 6.5. When the pH increases, pKa

is being approached closer and thus, the degree of ionization of chitosan molecules decreases, which in turn decreases their zeta potential. Carneiro-Da-Cunha et al. (2011) reported that zeta potential of 0.2% (w/v) chitosan solution at pH 3.5 as +38.4 mV. In this study, at the same pH and concentration of the chitosan zeta potential value was found + 30.63 ± 9.9 mV. This indicates the accuracy of the results.

In 0.5% (w / v) chitosan solutions, changes in zeta potential values depending on the pH of the solution did not show a clear trend as it was seen in 0.2% (w / v) chitosan solutions. It is expected that when the pH of the environment decreases, zeta potential will increase. However, it was seen that there was an interruption at pH 3.5. This situation may be occurring based on the sharp changes in the types of ions in the environment (Table 3.2). Compared with Na + and OH-, large Cl- ions screens the surface charge of chitosan molecules and it may have caused a decrease in net effective surface potential.

Qi et al. (2004) studied the chitosan nanoparticles. They concluded that the zeta potential range of 0.5% (w/v) chitosan nanoparticles between pH 4.6 to 4.8 was from 30.8 to 68.9mV. In our study, at the same pH and concentration of the chitosan zeta potential value was found + 30.95 ± 2.42.This situation was indicated that the accuracy of the results.

When the zeta potential results for sodium caseinate in both concentrations are evaluated, it is clearly seen that the zeta potential decreases (its magnitude increases) when the solution pH increases. As mentioned in Section 3.1.1 this is expected as the isoelectric point of sodium caseinate is ~4.6.

Table 3.2. Zeta potential, particle size, polydispersity index and (added) ionic strength values of chitosan and sodium caseinate solutions with different concentrations at different pH values.

Concentration(w/v) - pH	**Zeta Pot. (mV) ± SD**	**Par. Size (nm) ± SD**	**PDI ± SD**	**Ionic Strength (mM)**
0.2% chitosan - 3	45.95 ± 15.25	2998.5 ± 901.6	0.81 ± 0.27	1.8 (HCl)
0.2% chitosan – 3.5	30.63 ± 9.90	2445.0 ± 86.3	0.74 ± 0.20	7.62 (HCl)
0.2% chitosan - 4	22.88 ± 5.63	940.3 ± 199.1	0.99 ± 0.02	22.8 (NaOH)
0.2% chitosan – 4.5	25.83 ± 1.98	301.1 ± 37.8	0.97 ± 0.05	63.8 (NaOH)
0.2% chitosan - 5	17.38 ± 1.67	165.5 ± 0.9	0.97 ± 0.02	102.7 (NaOH)
0.2% chitosan – 5.5	15.47 ± 1.08	116.8 ± 5.5	0.99 ± 0.01	139 (NaOH)
0.5% chitosan - 3	27.87 ± 10.56	8240.0 ± 182.4	0.65 ± 0.12	12.6 (HCl)
0.5% chitosan – 3.5	13.76 ± 3.03	3862.50 ± 2163.04	0.84 ± 0.22	2 (HCl)
0.5% chitosan - 4	43.63 ± 1.41	7318.0 ± 3343.2	0.61 ± 0.19	15.9 (NaOH)
0.5% chitosan – 4.5	30.95 ± 2.42	3931.5 ± 659.7	0.79 ± 0.07	52.9 (NaOH)
0.5% chitosan - 5	21.25 ± 5.21	3028.0 ± 2040.7	0.78 ± 0.31	85.9 (NaOH)
0.5% chitosan – 5.5	13.28 ± 7.10	1003.0 ± 411	1 ± 0	110 (NaOH)
0.2 sodium caseinate- 5.5	-12.95± 5.79	254.6 ± 90.7	0.29 ± 0.14	0.9 (HCl)
0.2% sodium caseinate - 6	-20.72 ± 4.13	157.4 ± 54.5	0.38 ± 0.19	0.5 (HCl)
0.2% sodium caseinate - 7	-22.18 ± 1.34	181.7 ± 68.8	0.37 ± 0.13	-
0.2% sodium caseinate - 8	-25.68± 1.16	160.9 ± 9.5	0.26 ± 0.01	0.4 (NaOH)
0.5% sodium caseinate – 5.5	-18.16 ± 2.53	158.5 ± 24.1	0.26 ± 0.07	2.4 (HCl)
0.5% sodium caseinate - 6	-20.28 ± 0.35	130.5 ± 3.5	0.295 ± 0.002	1.2 (HCl)
0.5% sodium caseinate - 7	-23.45± 1.96	168.7 ± 1.8	0.26 ± 0.01	-
0.5% sodium caseinate - 8	-21.17 ± 6.32	179.2 ± 2.2	0.27 ± 0.02	1 (NaOH)

During the LbL deposition process, other important parameters are the size and conformation of the polyelectrolytes in the solution. Average hydrodynamic diameter of the particles in the solution provides valuable information about these parameters. As mentioned before, the hydrodynamic diameter was measured by dynamic light scattering (DLS) based on the assumption of Brownian motion of the particles. One of the important data obtained by dynamic light scattering is the Z-average diameter, which is calculated based on the amount of light scattered by the particles in the solution. Another important information obtained by DLS is the polydispersity index (PDI), which represents the range of particle size distribution curve. In other words, PDI shows the homogeneity of the samples. Low PDI values indicate homogeneous solutions; i.e. containing particles of similar sizes. PDI value larger than 0.5 indicates a higher heterogeneity; i.e. particles in the solution are of variable sizes. DLS is a low-resolution technique and it can give meaningful results only for solutions of low polydispersity (Ball, S., 2015).

Evaluation of the PDI values in Table 3.2 indicates that chitosan solutions (regardless of the concentration and solution pH) are highly heterogeneous (PDI <0.7), while sodium caseinate solutions are moderately heterogeneous (PDI <0.4). This suggests that the Z-values obtained, especially, for chitosan may be misleading. This situation can be explained as follows: As mentioned before, Z-value is based on the amount of light scattered by the particles. In the solutions with biomolecule or polymer existence, the light scattering caused by a particle is proportional to the square of particle's molecular weight. Thus, a small cluster in the system may lead to an increase in the amount of light scattering and Z-average value. Therefore, the value of the Z-ave is considered to be significant for solution that has very low PDI (PDI <0.1) and gives misleading results for the solutions with high heterogeneity (PDI >0.1). In such a case, intensity-based particle distribution must be evaluated together with the number and volume distribution.

Nevertheless, we can confirm the accuracy of the Z-ave results by comparing with similar studies in the literature. It was reported that the particle size of original chitosan pH between 4.6 to 4.8 was distributed in a range of 2000-3500nm (Vaezifar et.al., 2013). Another example is the study of Carneiro-Da-cunha. et al. (2011) in which the Z-ave of chitosan in an aqueous solution of 0.6% (w/v) at pH 3.5 was found to be 2590 nm, which is comparable to our results for 0.5% (w/v) chitosan at pH 3.5.

When the intensity-, volume-, and number-based particle size distributions of 0.2% chitosan (pH=3) are evaluated (Figure 3.3), the following conclusions are made. Intensity based particle size distributions indicate large clusters, whereas the volume and number distributions are indicate small clusters. Especially when the particle number distribution was examined, it was understood that there was a small amount of large clusters. This situation seems to correct for solutions in other concentrations and pH values (see in Appendix A). Therefore, according to obtained results, the particles in the chitosan solutions were located both individually and small clusters.

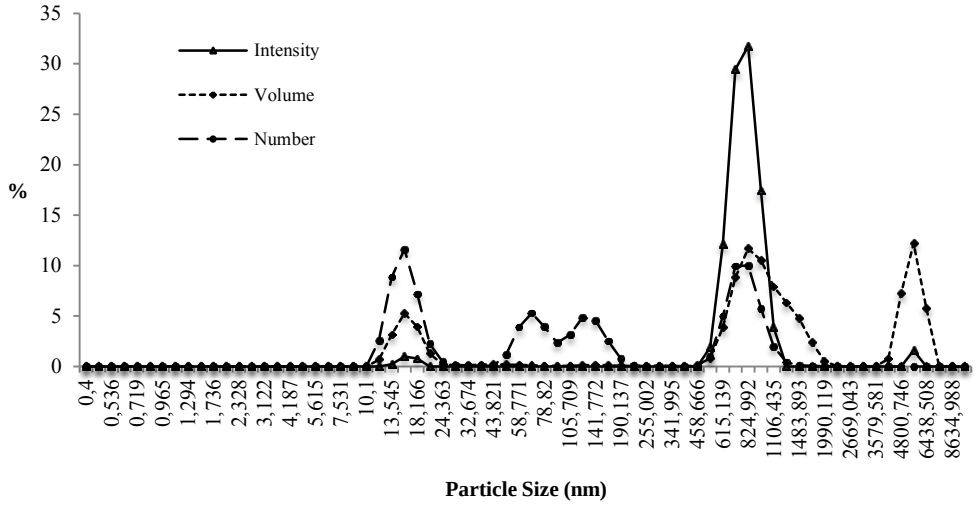

Figure 3.3. Intensity-, volume- and number-based average particle size distributions for 0.2% (w/v) chitosan at pH 3.

The fact that the PDI values of sodium caseinate are lower than 0.4 suggests that Z-ave results is more reliable. As it is observed in Figure 3.4, 0.2% (w/v) sodium caseinate solution at pH 5.5 is dominated by particles of about 80-100 nm. However when pH increases (pH= 6,7,8) smaller clusters (~60 nm and ~25 nm) and casein monomers (~10nm) start to appear. These results are in accordance with the literature.

Average hydrodynamic diameter of casein monomers are known to ~9 nm (Mezdour et al., 2006). Experimental studies that examined the structure of sodium caseinate molecules in solution indicate that sodium caseinate molecules at pH 7 are found sodium caseinate monomers (10 nm) and casein particles (10-20 nm) in mixture

(Qi , 2007; Loveday et al., 2010). Additionally, casein particles generate clusters in solution and radius of gyration of clusters was reported in the range of 22 nm to 48 nm (Loveday et al., 2010).

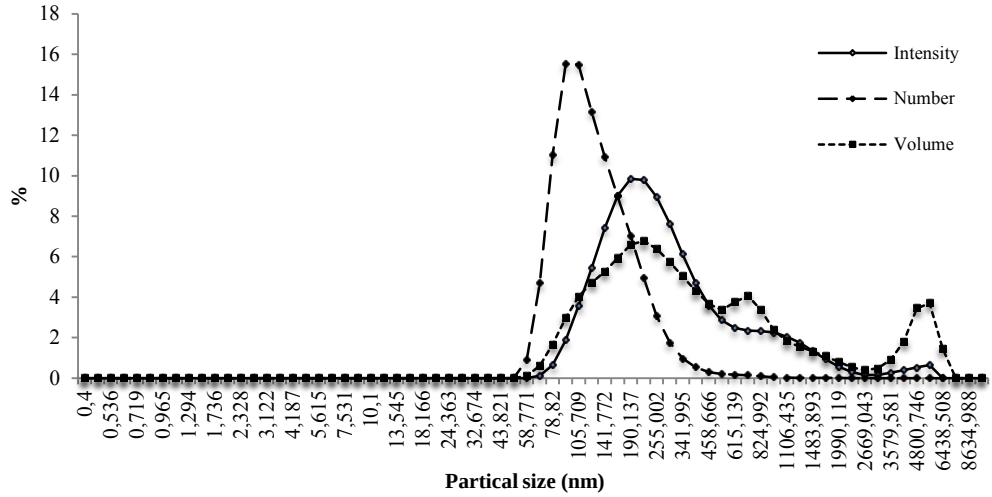

Figure 3.4. Intensity-, volume- and number-based average particle size distributions for 0.2% (w/v) sodium caseinate at pH 5.5.

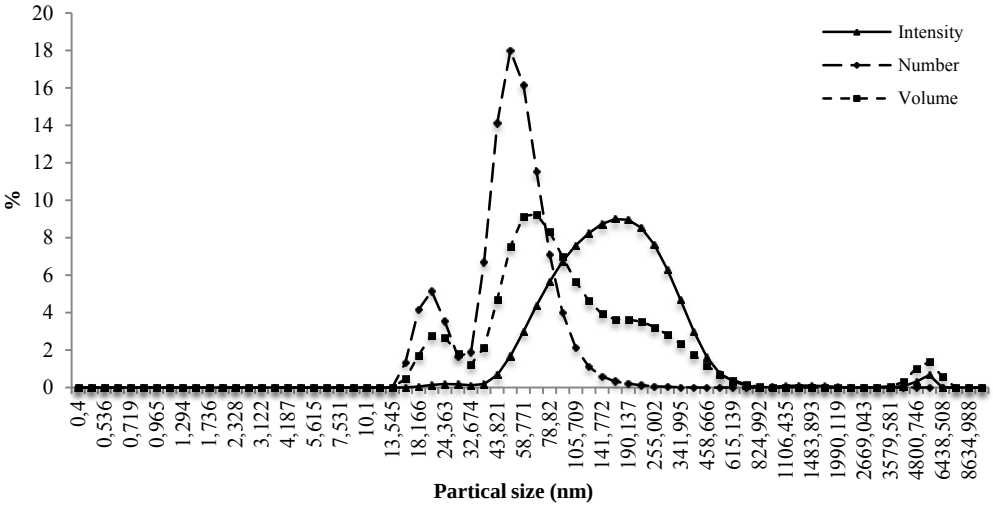

Figure 3.5. Intensity-, volume- and number-based average particle size distributions for 0.2% (w/v) sodium caseinate at pH 6.

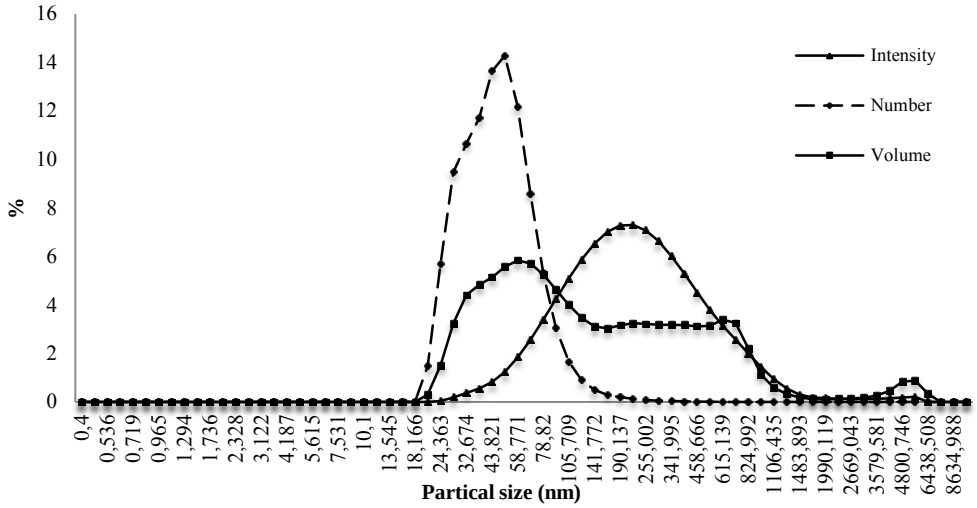

Figure 3.6. Intensity-, volume- and number-based average particle size distributions for 0.2% (w/v) sodium caseinate at pH 7.

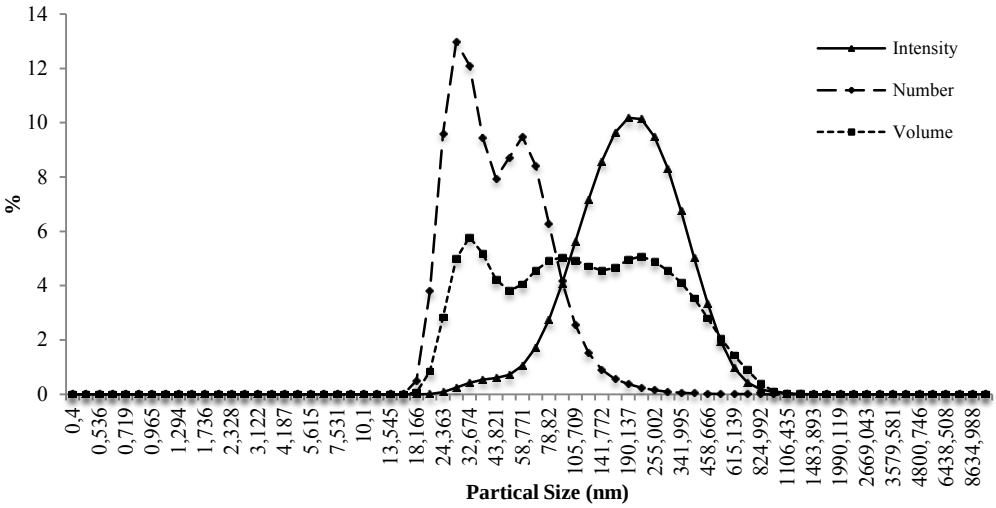

Figure 3.7. Intensity-, volume- and number-based average particle size distributions for 0.2% (w/v) sodium caseinate at pH 8.

All the other particle size distribution figures of chitosan and sodium caseinate solutions for different concentrations and pH values are given in Appendix A.

Based on the results obtained in this section, concentration values that will be used in layer deposition experiments of chitosan and sodium caseinate was determined as 0.2% (w / v) for both polyelectrolytes. The pH combinations are determined as both polyelectrolytes with the highest net effective charge density (chitosan pH 3 & sodium caseinate pH 8), both polyelectrolytes with an average net effective charge density (chitosan pH 5.5 & sodium caseinate to pH 5.5) and one of polyelectrolytes have a high net effective charge density and the other polyelectrolyte have average net effective charge density (chitosan pH 5.5 & casein pH 8).

3.1.3. Determination of the Multilayer Growth Follow-Up Wavelength Used in UV-Vis Spectroscopy Experiments

It was aimed to decide on the follow-up wavelength, which would be used to monitor the multilayer growth by UV-Vis spectroscopy. For this purpose, separate dilute solutions (0.1% w/v) of chitosan and sodium caseinate were prepared and analyzed with UV-Vis spectroscopy within the range, 200-400 nm. The absorption spectra obtained for each are shown in Figure 3.8. As anticipated, a characteristic peak of absorption for sodium caseinate was obtained at ~280 nm, which is the excitation wavelength of proteins. However, no characteristic peak was observed for chitosan. Since neither chitosan nor sodium caseinate contains a charecteristic chromophore that absorbs energy within the Visible range, it is not possible to differentiate the contribution of each polyelectrolyte in the formation of individual layers with this technique. However, it is still possible to monitor the multilayer formation by following the absorption at 280 nm. Therefore, 280 nm was chosen as the follow-up wavelength.

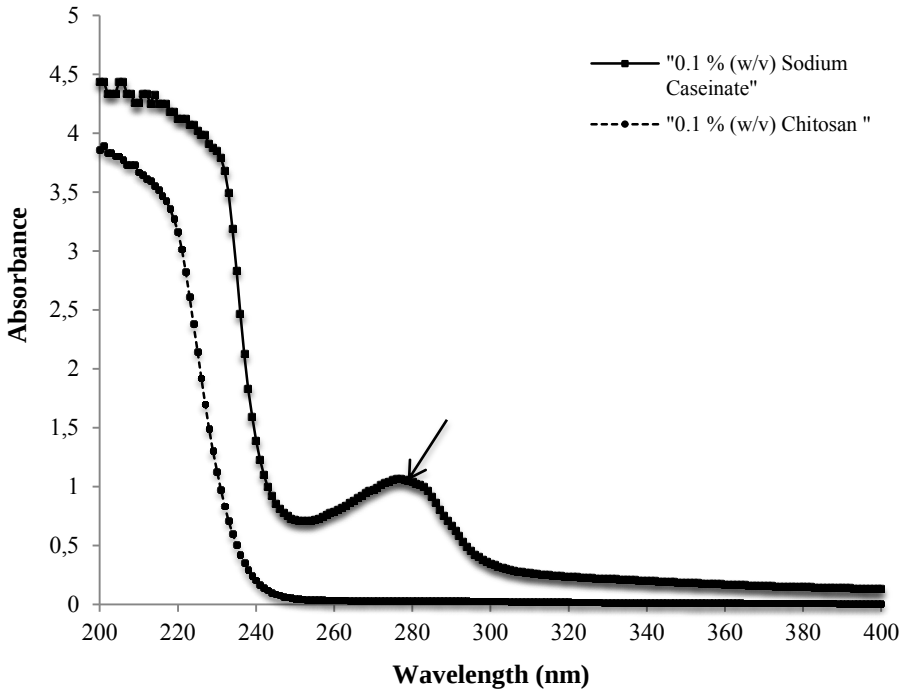

Figure 3.8.UV-Vis absorption spectra of 0.1% (w / v) chitosan and sodium caseinate solutions in the wavelength range of 200-400 nm.

3.1.4.Determination of the Spraying Distance for Spraying Experiments

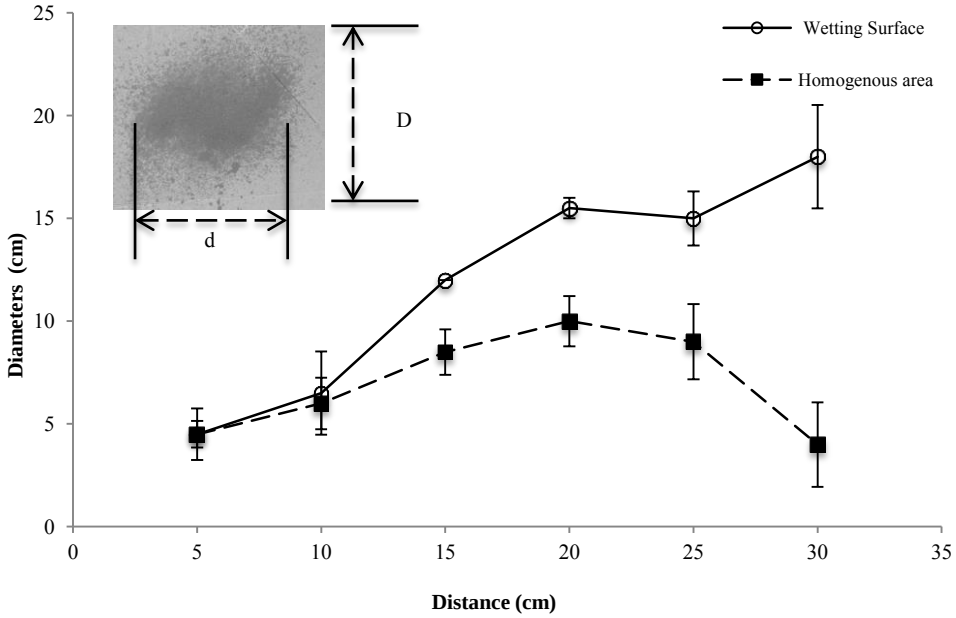

Figure 3.9. Effect of the spraying distance on the deposition of water on the receiving surface D: diameter of the incompletely wetted surface, d: diameter of the homogeneously wetted surface.

Spraying distance (distance between the nozzle and the substrate) was determined according to the method of Izquierdo et. al., (2005), which is described in Section 2.2.5. The resulting wetted diameter versus spraying distance curve (Figure.3.9) shows that the diameter of the homogeneously wetted area decreases beyond a spraying distance of 20 cm. Therefore, 20 cm was chosen as the spraying distance. The reason behind choosing the maximum possible distance is to avoid any possible damage on the formed layers due to the force applied by the sprayed particles.

3.2 Layer- by- Layer Assembly Experiments

3.2.1 UV-Visible Spectroscopy Results for Layer–by- Layer Assembly by Dipping

In this section, chitosan and sodium caseinate multilayer formation was performed by dipping method and followed by UV-Visible Spectroscopy. The factors examined were the pH value of the solution, the adsorption (dipping) time and the number of layers. In order to observe the effect of pH value of the solution, three combinations (specified for chitosan and casein, respectively) were chosen based on the zeta potential results; i.e. pH 3&8 ((the combination where each type of polyelectrolyte is highly charged) pH 5.5&5.5 (the combination where each type of polyelectrolyte is moderately charged)) and pH 5.5&8 (the combination where one type of polyelectrolyte is moderately charged while the other is highly charged)) . In order to observe the effect of adsorption time on LbL assembly, three dipping times were examined; i.e. 2 min (too short to reach the equilibrium), 10 min (approximate equilibrium time for adsorption) and 20 min (long after the equilibrium). The determination of the approximate equilibrium time for adsorption is explained in Section 3.2.2.1.

LbL film formation of the selected combinations of pH values and dipping times were followed up to 12 layers.

3.2.1.1. Effect of Solution pH

The development of layered deposition process depending on pH of solutions which was occurred in combinations of chitosan pH 3 & sodium caseinate pH 8, chitosan pH 5.5 & sodium caseinate pH 5.5 and chitosan pH 5.5& sodium casein pH 8 adsorption was depicted in Figure 3.10, 3.11 and 3.12, respectively.

As is seen, deposition process with chitosan and sodium caseinate was occurred only in condition of pH 5.5 which both polyelectrolytes had efficient average density of surface charge. Therefore, the results obtained here verify the thesis that the degree of ionization is appropriate for the formation of with weak polyelectrolyte multilayer film (Klitzing,2006). In the literature, there are multilayer film works where there is a significant peak in film thickness when the deposition process, with some weak polyelectrolytes, is carried out in the average degree of ionization (Yoo, 1998 ; Shiratori, & Rubner,2000). Film formation did not occur for combinations of chitosan pH 3 & sodium caseinate pH 8 and chitosan pH 5.5 & sodium caseinate pH 8. This situation can be explained as follows: The chitosan or sodium caseinate layer sticks on the substrate in acidic or alkaline aqueous solution depend on the positive or negative charge density. A sharp decline was observed in the degree of ionization in the basic or acidic sodium caseinate or chitosan solution. Therefore as the amount of surface “redundant” charge, necessary for the continuation of layered deposition, cannot be provided. The layered deposition process comes to a standstill.

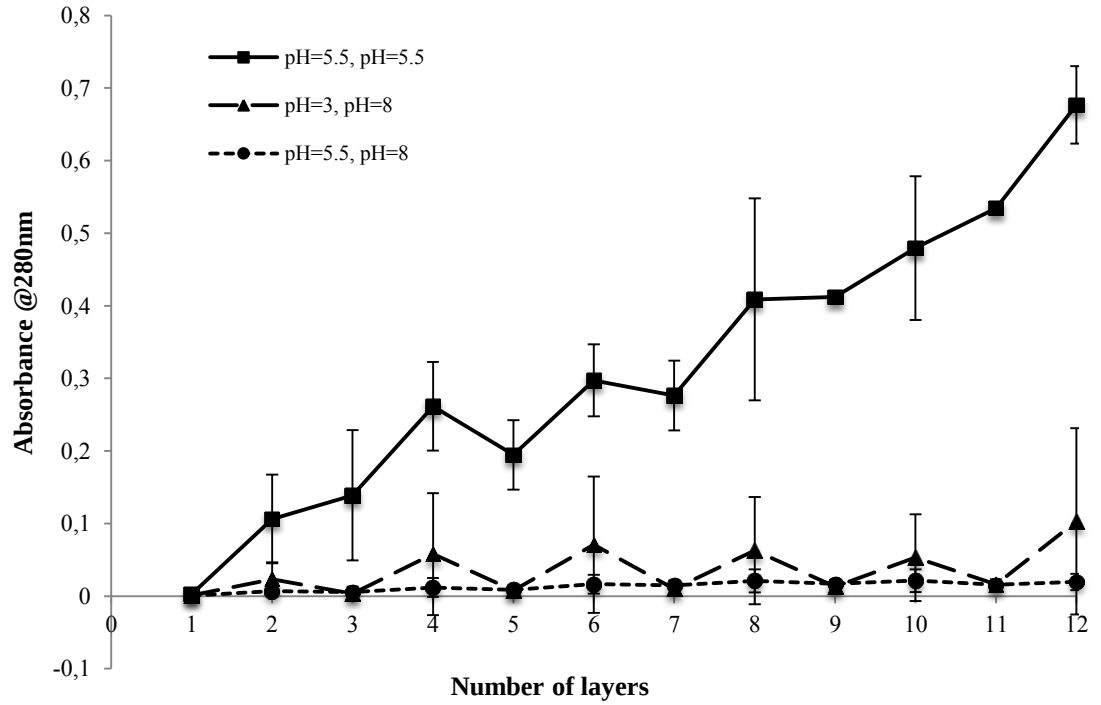

Figure 3.10.Multilayer formation obtained by dipping method at different pH combinations at 10 minutes. Error bars represent the standard deviations.

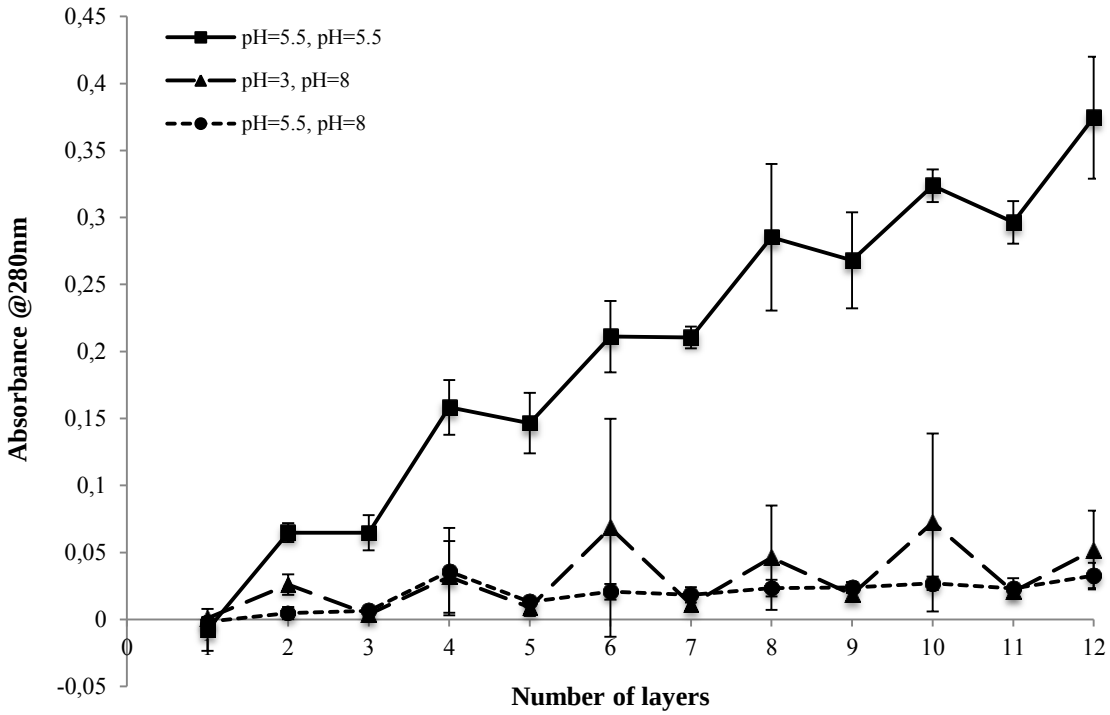

Figure 3.11.Multilayer formation obtained by dipping method at different pH combinations at 2 minutes. Error bars represent the standard deviations.

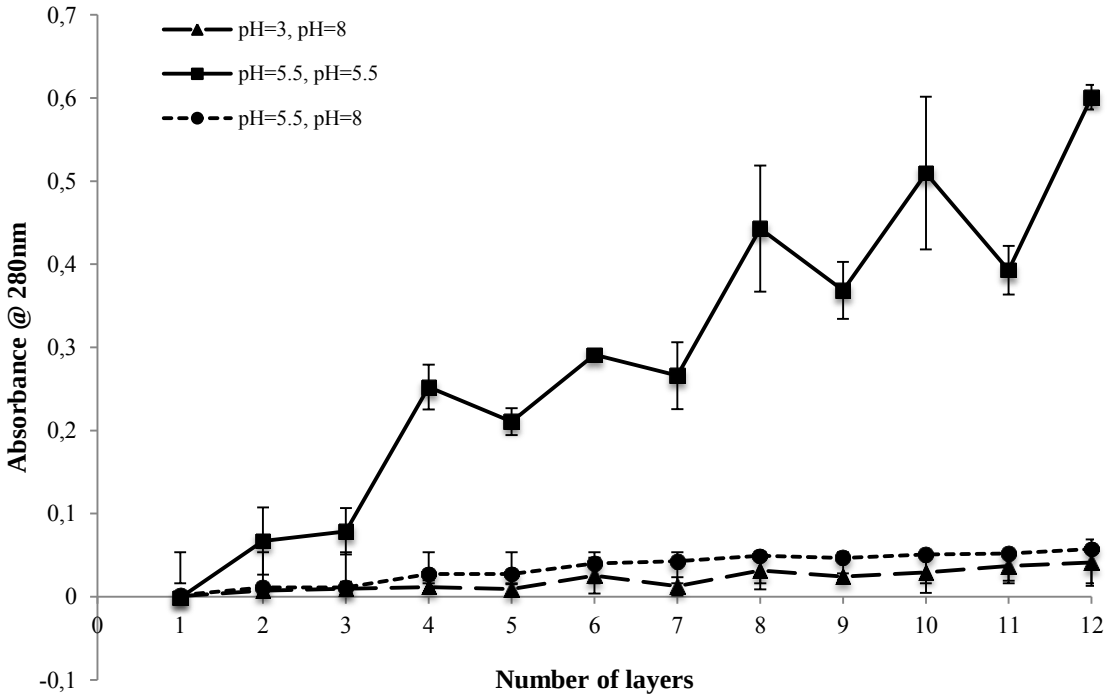

Figure 3.12. Multilayer formation obtained by dipping method at different pH combinations at 20 minutes. Error bars represent the standard deviations.

3.2.1.2. Effect of Adsorption (Dipping) Time

The development of layered deposition process depending on time of adsorption which was occurred in combinations of chitosan pH 3 & sodium caseinate pH 8, chitosan pH 5.5 & sodium caseinate pH 5.5 and chitosan pH 5.5& sodium caseinate pH 8 adsorption was depicted in Figure 3.13, 3.14 and 3.15, respectively.

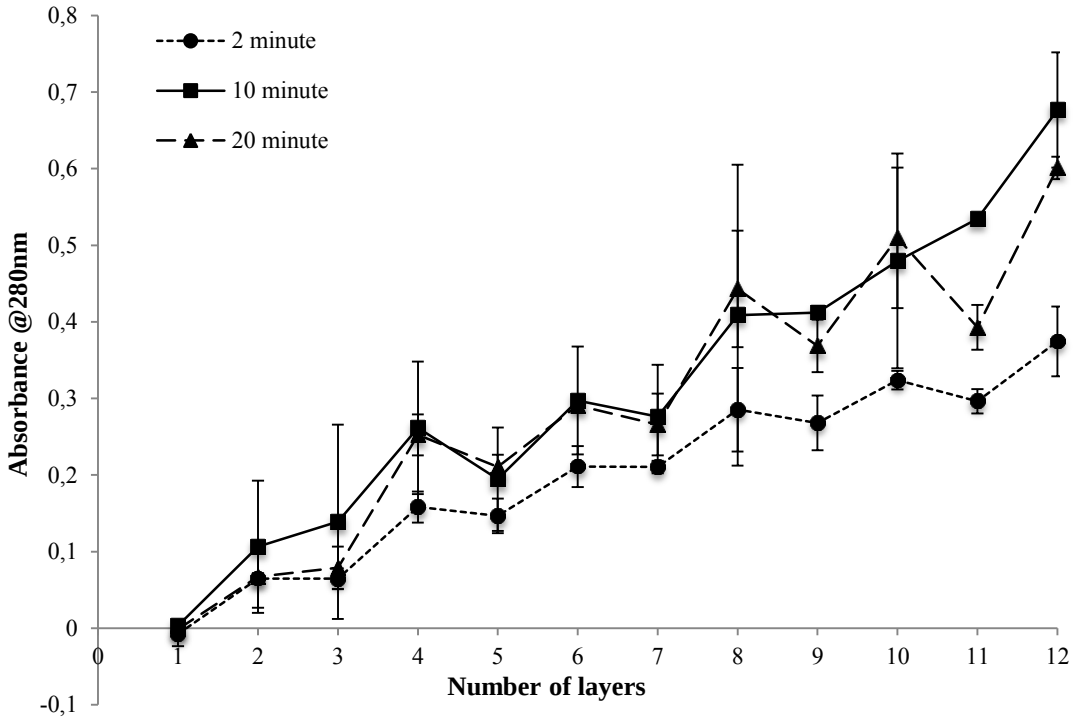

Figure 3.13. Effect of adsorption time on multilayer formation obtained by dipping method for pH 5.5&5.5 combination. Error bars represent the standard deviations.

The standard deviations of the results returned high as a balanced layered film formation was not occurred in the combination of pH 3& pH 8 where both polyelectrolyte having maximum density of charge due to the reason explained above (Figure 3.14).

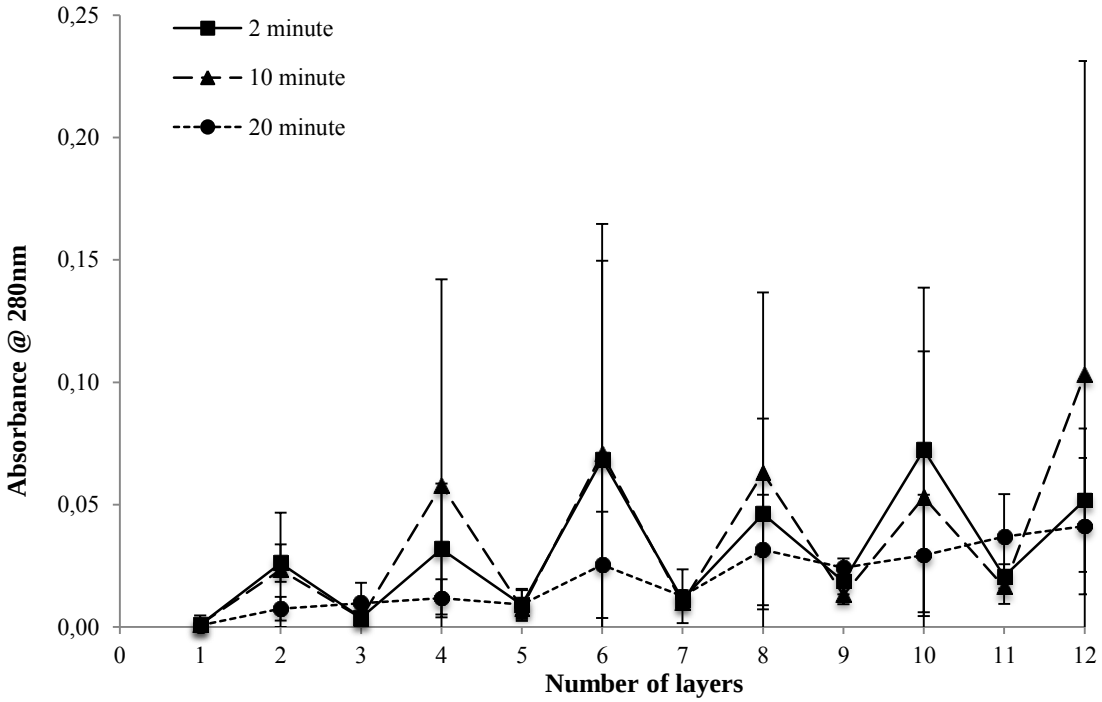

Figure 3.14. Effect of adsorption time on multilayer formation obtained by dipping method for pH 3&8 combination. Error bars represent the standard deviations.

In layered deposition studies based on electrostatic interaction, the general assumption is that the longer the duration of adsorption, the more successful a layered deposition is. The adsorption equilibrium time is considered to be 10-20 minutes (Kurth & Osterhout, 1999). Therefore adsorption time typically ranges from 5 to 20 minutes (Kim & Jung, 2005) (Nguyen et al., 2011). However, Xiang et al. (2013) argued that despite this assumption is considered to be valid for the layered deposition of strong polyelectrolytes, this assumption may not be valid for the deposition of multilayered weak polyelectrolytes. Indeed, during the layered deposition process carried out by conventional adsorption time, weak polyelectrolytes showed features changing the film formation tendency significantly such as drop off the surface (desorption), interdiffusion in film or forming an integrated structure which is soluble in solution with the oppositely charged polyelectrolyte, thereby leaving the film (Zacharia et al., 2007).

The chitosan and sodium caseinate used in this study are weak polyelectrolytes, it is seen highly likely that they may exhibit these kinds of behaviors. Thus, 3 different adsorption times was studied. As shown in Figure 3.13 to 3.15, the effect of adsorption

time gave different results at different pH combination. Both polyelectrolytes with a maximum charge density in the combination of pH 3& pH 8, regardless of the adsorption time, multilayer film formation is understood that sufficient residual charge amount cannot be achieved during subsequent deposition steps (Figure 3.14). Both polyelectrolytes with an average charge density in the combination of pH 5.5 & pH 5.5, 10 and 20 minutes immersion time did not make a difference in the formation of the film, but in 2 minute dipping time, decrease in the slope of formation of the multilayer film was seen.

In all adsorption times, up to 12 layers of a linear film formation is observed (Figure 3.14). Time- dependent SPR test results performed in this combination of pH shows that the film thickness obtained by 2-minute adsorption time were less than the film thickness obtained by 10-minute adsorption time. At the same time, as it was possible to observe the adsorption-desorption events in-situ, useful information regarding the film formation was obtained.

The combination of pH 5.5 & pH 8,where one type of polyelectrolyte is moderately charged while the other is highly charged, is shown in Figure 3.15. It is seen to exhibit a different situation from the combination of pH 5.5 & pH 5.5. Firstly, for all adsorption times, film formation curve is linear up to 6 layers. After 6^{th} layer, film formation did not show a liner increase. It was observed that film formation curve for 20 minutes of layer deposition process carried out by dipping time has a higher slope. However, this situation does not necessarily mean that the layer deposition process continued successfully.

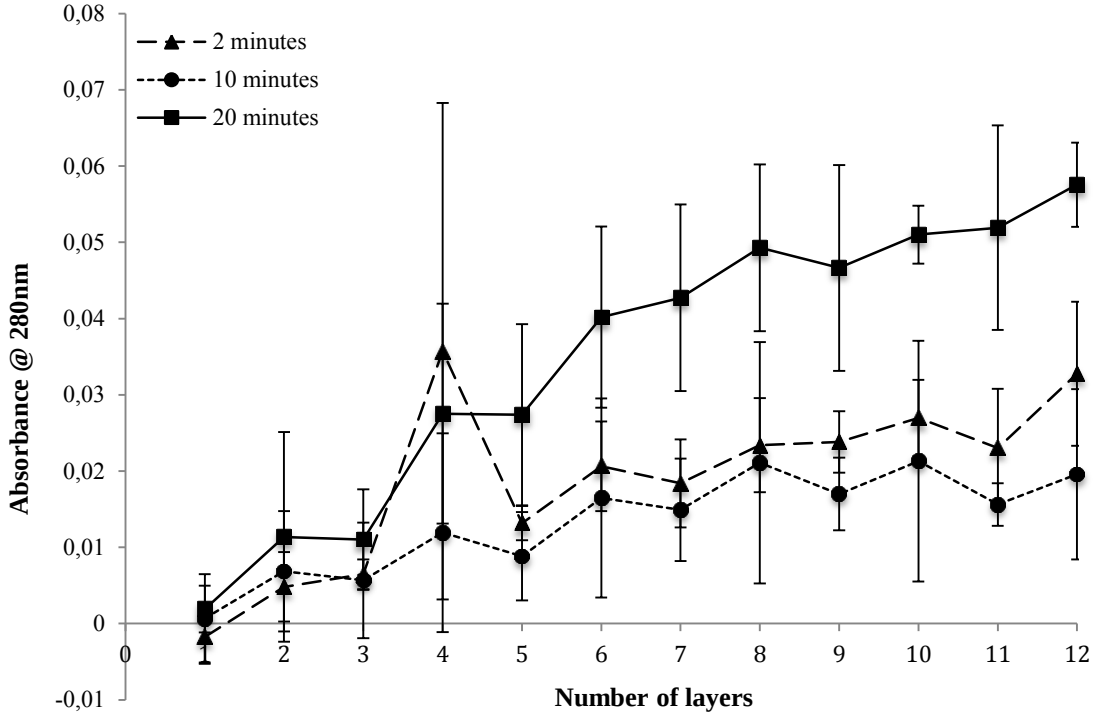

Figure 3.15. Effect of adsorption time on multilayer formation obtained by dipping method for pH 5.5&8 combination. Error bars represent the standard deviations.

3.2.1.3. Effect of Number of Layers

As is seen in all graphics, the absorbance in 280 nm increases with the number of layers. Although this situation is interpreted as a possible continuation of a layered film formation at first glance, timed SPR experiments carried out in pH 5.5 & pH 5.5 combination demonstrated that the fact is not in this way.

Thus, the increase in the absorbance associated with the number of layers is thought to be originated from the change in placement of layers or from the diffusion between the molecules in the layers occurring as a result of prolongation of processing time. A group of sodium caseinate molecules (or chitosan) might have come together to

form the integrated structures and caused localization, in this case an increase in concentration (parallel in an absorbance increase) might have been caused.

3.2.2 Surface Plasmon Resonance (SPR) Results

3.2.2.1 Determination of the Approximate Equilibrium Time of Adsorption

In this section, it was aimed to determine the equilibrium time of adsorption during LbL assembly of chitosan and casein via SPR, whic allows *in-situ* characterization of the self-assembly process. The pH 5.5 & 5.5 combination was chosen for this purpose. *In-situ* monitoring of the LbL assembly can be achieved by direct observation of the time dependent change in the reflection signal at fixed angle mode. The equilibrium time of adsorption will be the time where the SPR signal begins to form a plateau.

Firstly, to determine the angle at which surface plasmon resonance occurs at the Au-SiO_2 interface, an initial scan was taken in water (pH 5.5). The SPR angle was determined to be 71.3°. After this step, the instrument's scan motor was fixed at this SPR angle, and LbL assembly experiments were conducted. Due to the limitations in the configuration of the instrument (the necessity to work with a peristaltic pump to ensure flow and the limited capacity of the injection loop), the adsorption was continued for up to 10 minutes at each step. The resulting SPR signal versus time graph is shown in Figure 3.16. Red and black arrows indicate the injection time of dipping and washing solution, respectively. Vertical lines that observed after injection of the 1^{st} and 2^{nd} layers represent the adsorption equilibrium time. Visual inspection of the graph indicates that the time to reach the equilibrium of adsorption changes from 4 to 8 minutes. Noting that the LbL deposition experiments were conducted under mild flow (10 μL/min), the equilibration time of adsorption determined here is an underdetermined value. Considering the no-flow condition in LbL assembly by dipping experiments, the actual equilibration time is expected to be higher. On the other hand, because the flow in SPR experiments is minimal, a big difference is not expected. Therefore, it was concluded

that the equilibration of adsorption at each step in LbL deposition by dipping is approximately 10 minutes.

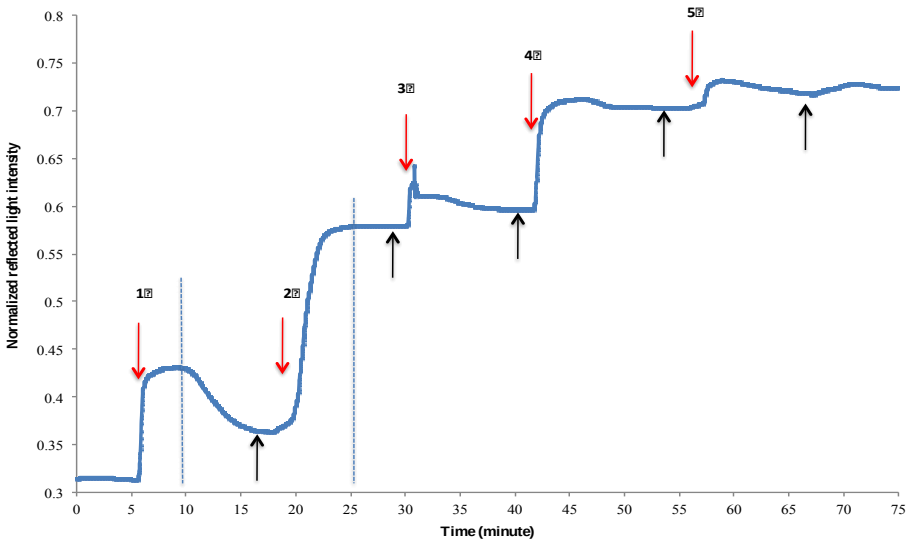

Figure 3.16. Reflected light intensity changes depending on time at fixed SPR angle (71.3 °) (0.2% (w/v) chitosan + 0.2% (w/v) sodium caseinate - pH 5.5). Red and black arrows indicate the injection time of dipping and washing solution, respectively. Vertical lines that observed after injection of the 1st and 2nd layers represent the adsorption equilibrium time.

3.2.2.2 *In-situ* Layer- by- Layer Deposition Process with Surface Plasmon Resonance (SPR)

Due to the limitations imposed by the current configuration of the instrument, LbL assembly of chitosan and sodium caseinate at pH 5.5 was performed exclusively. In order to examine the effect of adsorption time, 2 and 10 minutes were tried (Figure 3.17 and Figure 3.18).

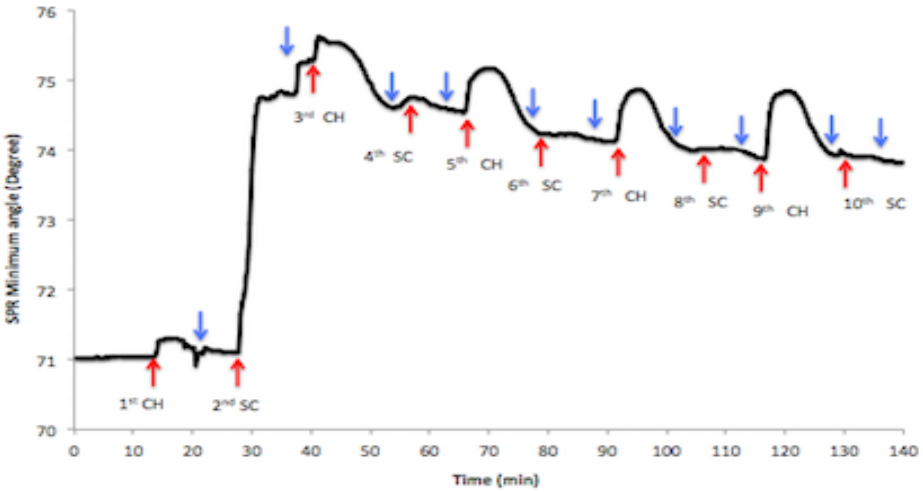

Figure 3.17. Sensogram of 0.2 % concentrations at pH=5.5 at 10 minute (CH: Chitosan SC: Sodium caseinate).

The following results concluded when Figure 3.17 is examined:

i. With first injection (arrow number 1) the adsorption of chitosan occurs rapidly on the sensor and weakly bound chitosan molecules released back from the surface with flow in time. A decrease was not observed in the SPR angle by the injection of the rinsing solution. Accordingly, it is understood that chitosan layer at bottom surface was bound tightly to the surface.

ii. In second step, by injection of sodium caseinate solution, a sudden increase is observed in the SPR angle (arrow number 2). This situation is evidence of the chitosan molecules that were bound tightly on surface at previous step reversed the surface charge oppositely. It is seen that the adsorption of sodium caseinate reaches equilibrium state by time and begins to form a plateau. After 10 minutes of injection the rinsing solution in flow cell, a surprising increase was observed at SPR angle. This situation can be explained by the swelling of the structures that are formed by casein, holding water molecules inside of them.

iii. In the third step by the injection of chitosan (3), again a slight increase was observed in SPR angle. However after short time, a decrease was seen in SPR angle. This decrease can be explained by the release of the complexes from surface that are formed by casein molecules which are bounded to each other weakly and positively charged chitosan molecules. In the literature it has been

reported that such events can occur in LBL deposition studies with weak polyelectrolytes (Bayramoglu & Stroeve, 2010).

iv. In next deposition step, by an increase in SPR angle with sample injection, adsorption reaches equilibrium state by time and begins to form a plateau. And releases of weakly bound excess material from the surface with surface flow were observed.

v. Contrary to the results of UV-Vis absorbance indicated, it is seen that the continuation of film formation after 5th and 6th layer was not continue. This indicates the inter-layer and inner layer mobility of chitosan and sodium caseinate molecules. Chitosan or sodium caseinate molecules diffuse each other in time required to obtain the first 4 or 5 layers, which causes surface saturation. This prevents the surface load changes that are necessary for layer deposition and deposition may have been interrupted. Interlayer diffusion studies have been reported in the literature (Klitzing, R., 2006).

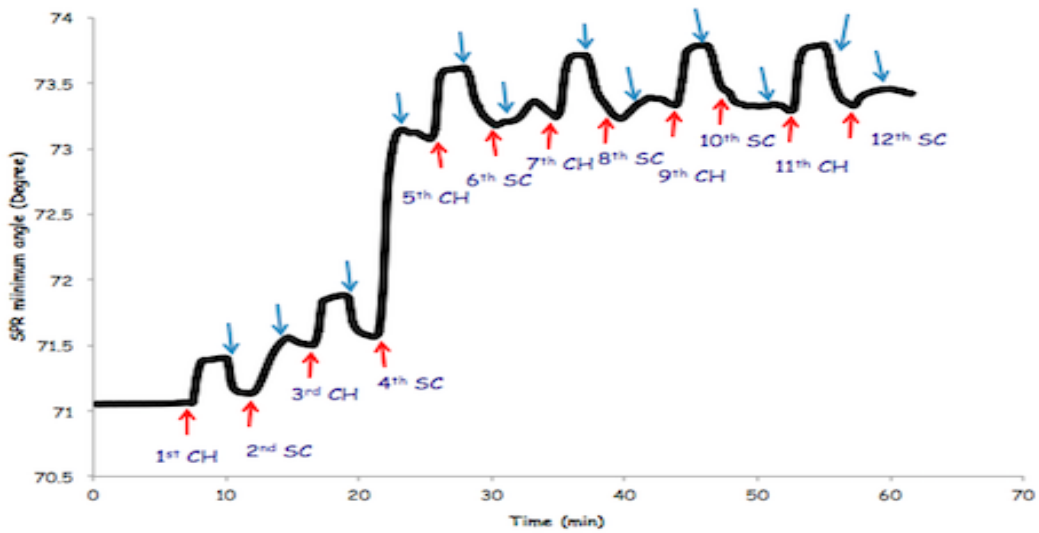

Figure 3.18. Sensogram of 0.2% concentrations at pH=5.5 at 2 minute (CH: Chitosan SC: Sodium caseinate).

The following results concluded when Figure 3.18 is examined:

i. By first injection of chitosan, the adsorption of occurs quickly on the sensor and weakly bound chitosan molecules released back from the surface with flow in

time. A decrease was not observed in the SPR angle by the injection of the rinsing solution.

ii. After injection of sodium caseinate (2^{nd} layer), a decrease was observed. However, an increasing was observed during adsorption time. The reason for this situation is that, 2 minute is not sufficient for adsorption equilibrium. It is supposed that the adsorption of chitosan molecules was not reach equilibrium in 2 minute.

iii. By injection of 4^{th} layer, a sudden increase was observed. Time required for obtain the 4^{th} layer is sufficient to reach the adsorption equilibrium. That's why, there is an increase observed. Chitosan and sodium caseinate molecules were bound tightly to the sensor surface.

iv. In next depositions step, decrease was observed in SPR angle with sample injection and then an increasing was seen. This is because the adsorption did not reach equilibrium state.

Striking point when compared 2 and 10 minutes experiments is that continuous decrease is observed after 2^{nd} layer in 10-minute experiment, whereas in 2 minutes experiment increase is observed. There are several possible reasons for this difference. Firstly, 2 minute is not sufficient to reach adsorption equilibrium. However, 10 minute cause more component deposition on surface. Secondly, it is supposed that soluble complexes release from the surface in 10-minute experiment.

The evolution of the actual SPR curves with each adsorption step for both 2 and 10 min- adsorption times is given Appendix B. A simpler demonstration revealing the shifts in SPR minimum angle with the adsorption of each layer are shown in Figure 3.13. Overall, it is understood that the film formation at 2 and 10 min-adsorption times are different from each other; i.e. it seems like 2 min adsorption time leads to incomplete coverage of the surface resulting in an incomplete film formation. Moreover, it is observed that the multilayer formation for both adsorption times continues up to 5-6 layers due to the reasons explained above.

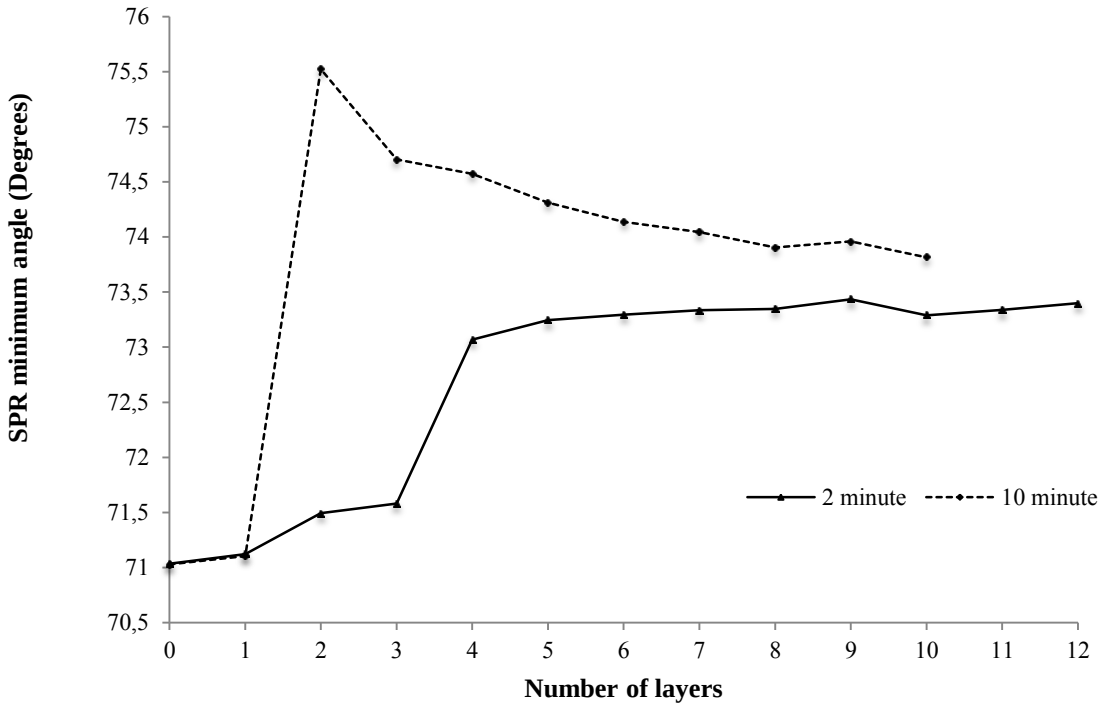

Figure 3.19. Shifts in SPR minimum angle during the adsorption of each layer in LbL assembly of 0.2% (w/v) chitosan and sodium caseinate at pH 5.5 for adsorption times 2 and 10 minutes.

3.2.3 UV-Visible Spectroscopy Results for Layer–by- Layer Assembly by Spraying

In this section, LbL deposition of chitosan and sodium caseinate was performed by spraying technique and the multilayer formation was followed by UV-Visible Spectroscopy.

As in dipping method, solution pH and spraying time were selected as factors to be examined. The same solution pH combinations (pH 3&8, pH 5.5&5.5, and pH 5.5&8) were experimented. In order to make an appropriate comparison wıth the dipping method, total spraying times of 2 and 10 minutes (for each adsorption step) were selected. The purpose of the spraying technique is to obtain suitable multilayer formation in less time. Therefore, 20 minutes adsorption time was removed from the spraying experiments.

As stated before in Section 2.2.5, different versions of the general procedure (varying in values of t_1, t_2, t_3 and t_4) were experimented in order to examine the importance and impact of spraying and rinsing steps. The modified versions of the procedure are shown in Table 3.3. According to the spraying procedure, spraying experiments were carried out both with rinsing and without rinsing steps for 2 and 10 minutes.

Table 3.3. Spraying procedures that were studied.

Spraying Procedure (for the formation of one layer only)	**t1+ t2 + t3 + t4**
2 minutes with rinsing	5 sec + 1min 55sec + 10 sec + 5 min
2 minutes in 4 sections with rinsing	(5 sec + 25 sec) x 4 + 20 sec + 5 min
2 minutes without rinsing	5 sec + 1 min 55 sec + 0 sec + 5 min
2 minutes in 4 sections without rinsing	(5 sec + 25 sec) x 4 + 0 sec + 5 min
10 minutes in 4 sections with rinsing	(5 sec + 2 min 25 sec) x 4 + 20 sec + 5 min
10 minutes in 4 sections without rinsing	(5 sec + 2 min 25 sec) x 4 + 0 sec + 5 min

(t1: the amount of time that the polyelectrolyte solution is sprayed onto the surface; t2: waiting time between the adsorption and the subsequent rinsing step; t3: the amount of time that the rinsing solution is sprayed onto the surface; t4: drying time between the rinsing and the subsequent adsorption step)

3.2.3.1 Effect of Solution pH

In Figure 3.20, selected pH combinations of LbL deposition by spraying technique at 2 minute adsorption time are given. First of all, it is clear that the rinsing step negatively affects the LbL deposition of chitosan and caseinate as the absorbances

are significantly lower compared to those obtained without rinsing step. This is probably because the molecules that are attached weakly to the substrate and/or on top of each other are cleaned from the surface with rinsing step. Furthermore, it is observed that LbL deposition by spraying at pH 5.5 & 5.5 combination looks similar to that at pH 5.5 & 8 combination. However, a closer inspection of the absorbance values (evaluated together with the standard deviations of the data) for each deposition step suggests that LbL deposition at pH 5.5 & 5.5 combination is more successful and therefore might be preferable, especially for the casein layers. On the other hand, LbL assembly at pH 3 & 8 combination is clearly not successful. The reason must be the interruption of the charge reversal process with each deposition step as discussed in Section 3.2.1.1 for the LbL by dipping results.

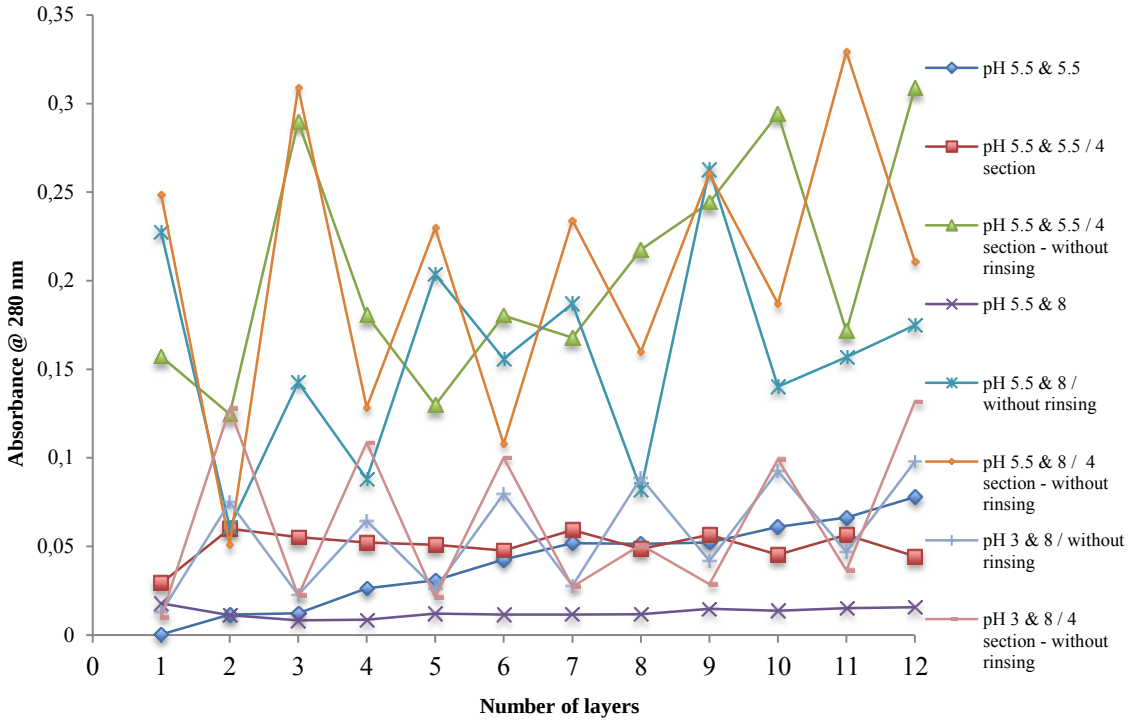

Figure 3.20. Multilayer formation by spraying method at different pH combinations with 2 min adsorption time. (Standard deviations for each data point are given in Tables C.1. - C.3.)

Similar to the case with 2 minute adsorption time, the highest absorbance values for 10 minutes adsorption time were obtained at pH 5.5&5.5 in 4 sections-without rinsing (Figure 3.21). It can be said that pH 3 &8 and pH 5.5&8 combinations did not

perform well in terms of multilayered coating formation compared to the pH 5.5 & 5.5 combination. The reason must be again the interruption of the charge reversal process with each deposition step.

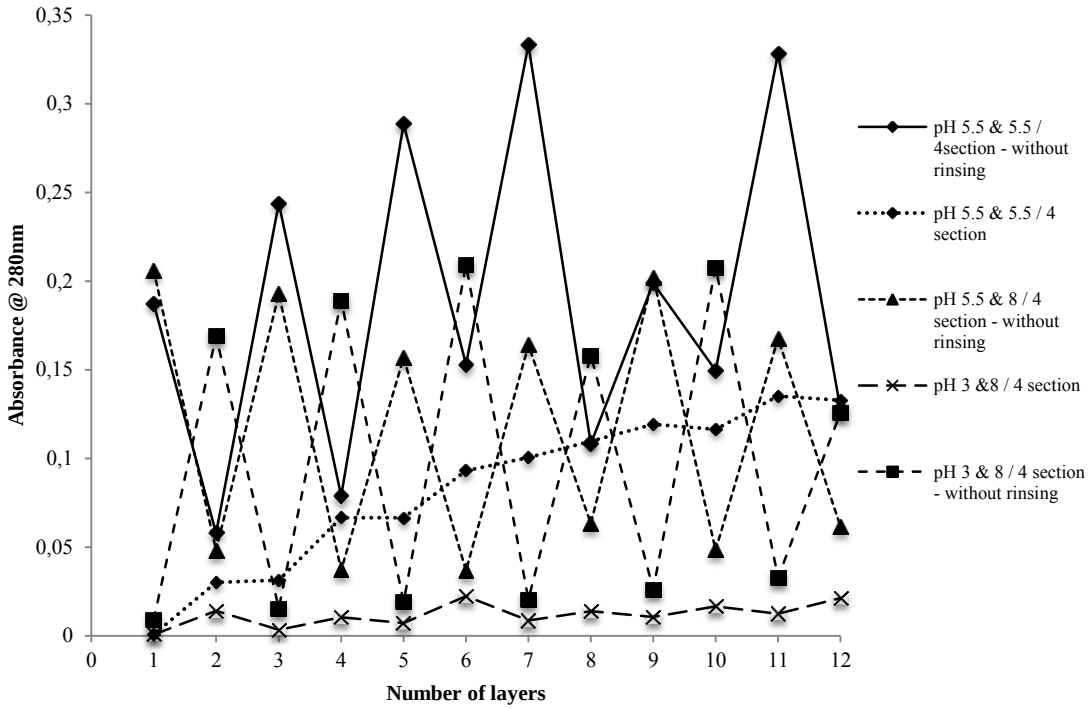

Figure 3.21. Multilayer formation by spraying method at different pH combinations with 10 min adsorption time. (Standard deviations for each data point are given in Table C.4. – C.6.)

3.2.3.2 Effect of Adsorption (Spraying) Time

In Figure 3.22, Figure 3.23 and Figure 3.24, comparison of the LbL assembly of chitosan and casein at pH 5.5 & 5.5, pH 5.5 & 8, and pH 3 & 8 combinations by spraying technique for different adsorption times are given, respectively. As it was shown in the previous section that rinsing affects the LbL deposition negatively, only the results obtained with the procedures excluding rinsing steps are given here.

One striking point in Figure 3.22 is that a regular trend in multilayer formation is observed with 10 min adsorption time at least up to 7 layers, while no such trend is observed with 2 min adsorption time. This is not surprising when one considers the fact that equilibrium of adsorption is not reached until ~10 min as revealed by SPR

experiments (Section 3.2.3.1). Speaking of the performance of both adsorption times in multilayer formation, it is hard to make a clear statement just based on the UV-Vis absorption results. However, one can still say that 10 minute adsorption time would be preferable considering the more regular trend in multilayer formation compared to that with 2 min adsorption time, and also considering the option to terminate the LbL assembly after the deposition of 5-7 layers (preferably right after the deposition of chitosan layers).

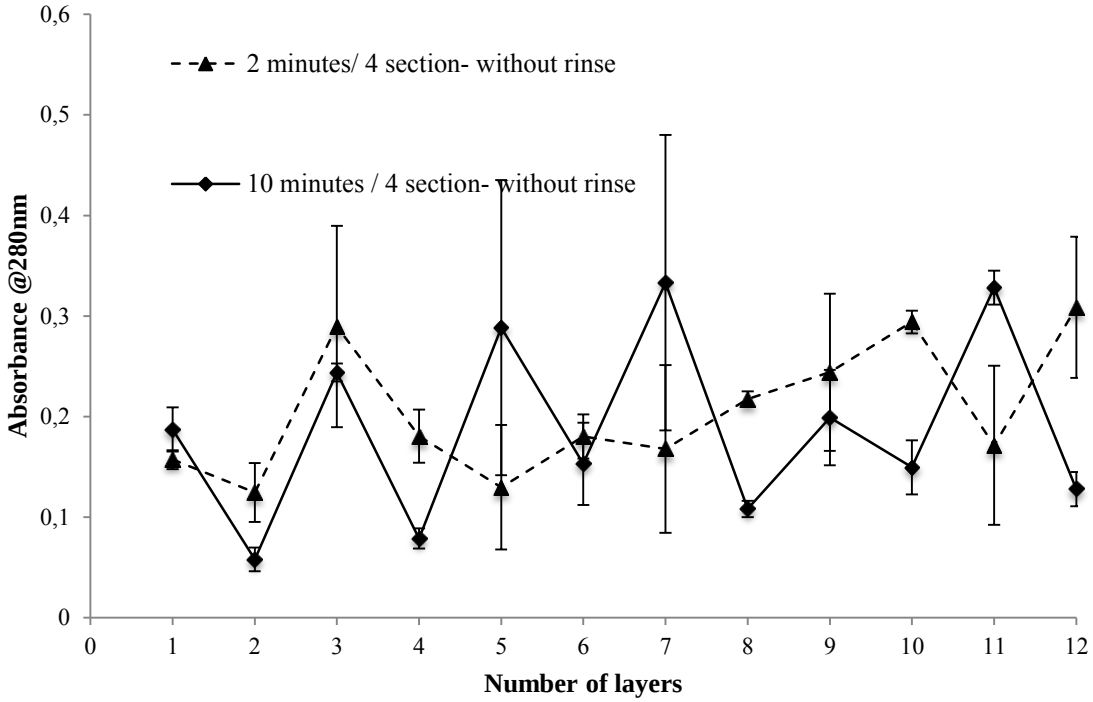

Figure 3.22. Multilayer formation by spraying method at pH 5.5&5.5 combination for different adsorption times (Standard deviations for each data point are given in Tables C.1. - C.6.).

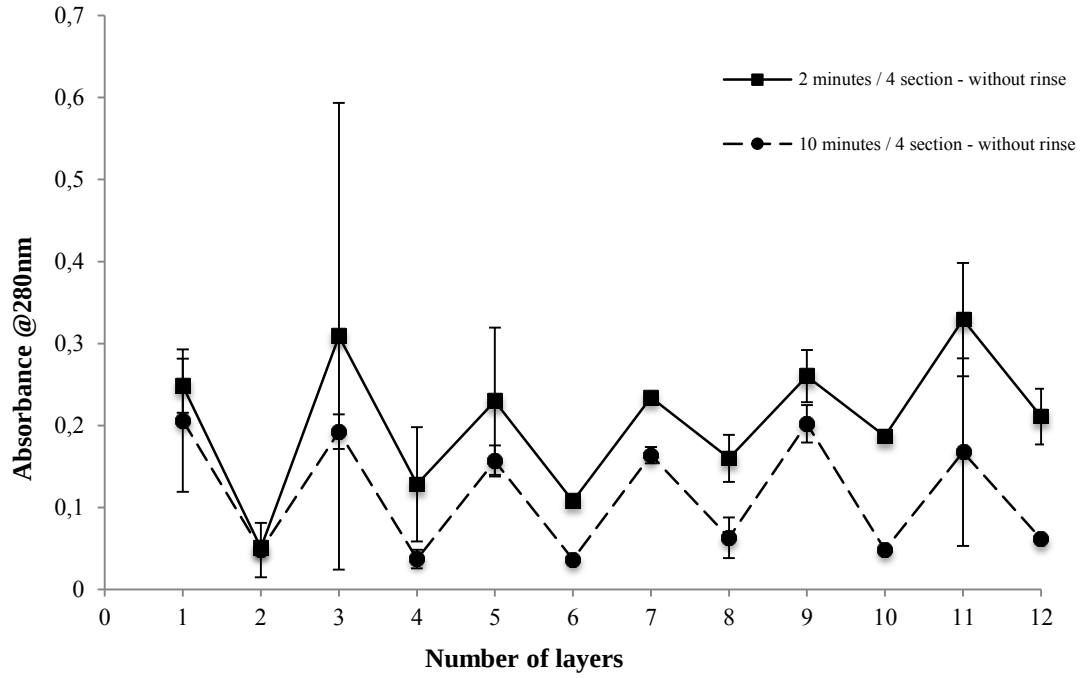

Figure 3.23. Multilayer formation by spraying method at the pH 5.5&8 combination for different adsorption times. (Standard deviations for each data point are given in Tables C.1. - C.2.).

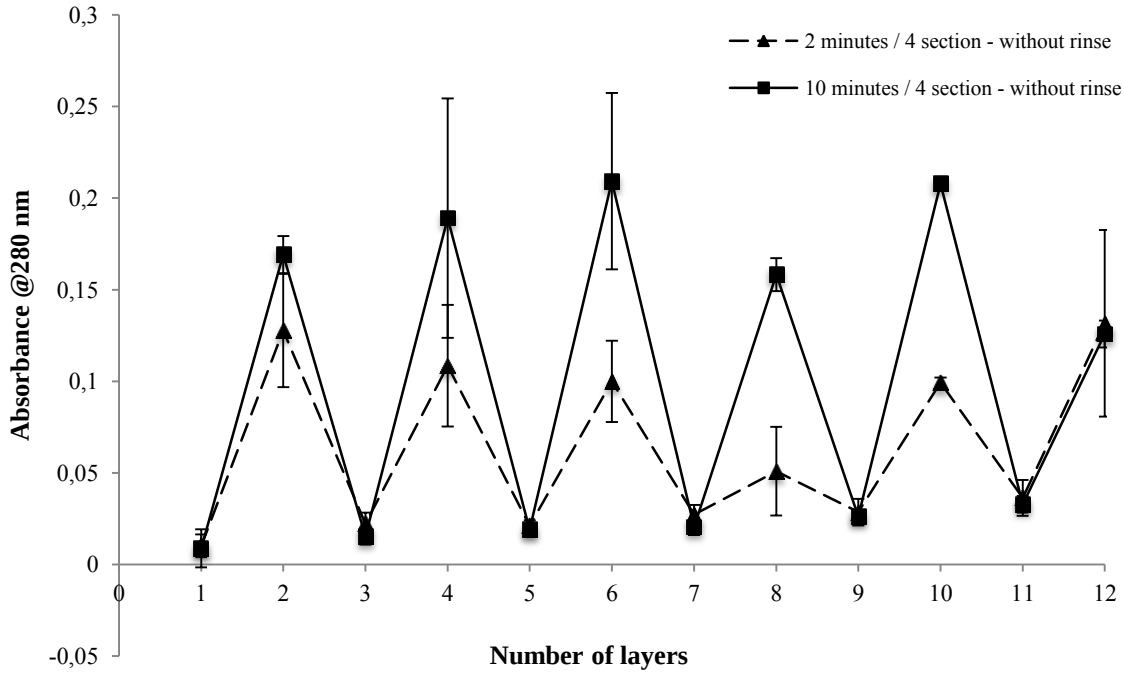

Figure 3.24. Multilayer formation by spraying method at the pH 3 & 8 combination for different adsorption times. (Standard deviations for each data point are given in Tables C.1. - C.6.).

3.2.4 Dipping versus Spraying Results

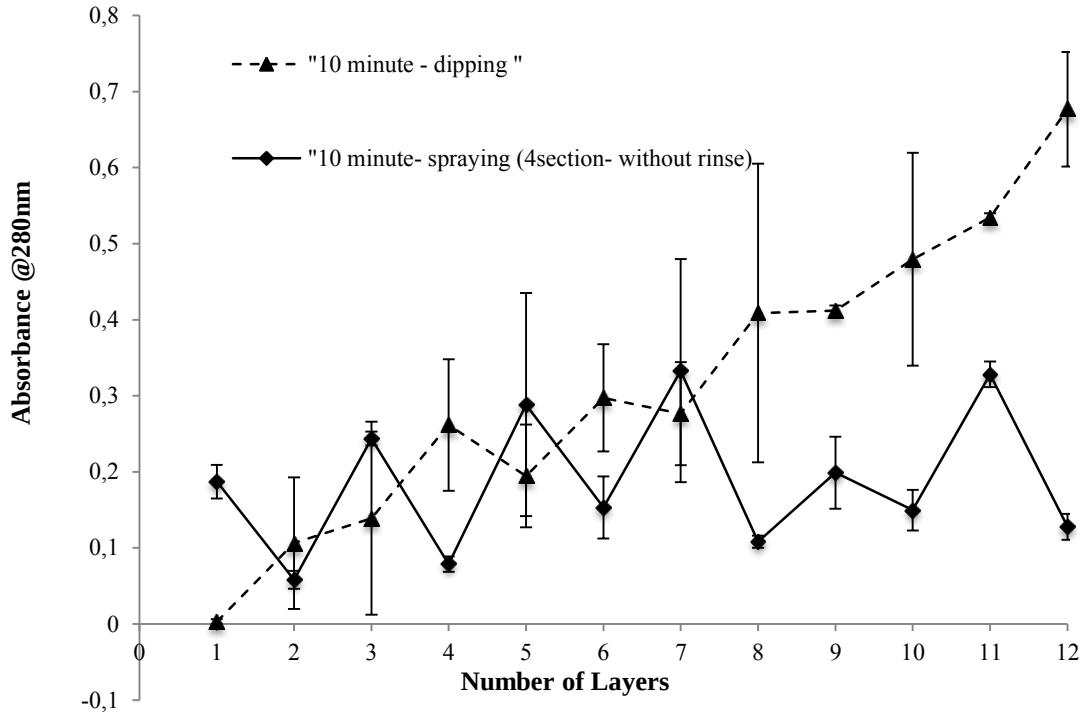

Figure 3.25.Comparison of multilayer formation obtained by dipping and spraying method with 0.2% (w/v) chitosan and sodium caseinate at pH 5.5. Adsorption time is 10 min.

Comparison of the dipping and spraying results for pH 5.5 & 5.5 combination at 10 min adsorption time (Figure 3.25) suggests that multilayer formation in the long run by dipping method was better than by spraying method. This is also confirmed by AFM thickness measurements, which are given in Section 3.3. However, if one considers terminating the LbL deposition after the 5th layer or so for the sake of reducing the total process time, the coating obtained by spraying would not be much different in thickness than that obtained by dipping (except that the surface would be smoother by spraying as suggested by the surface roughness values, which are given and discussed in Section 3.3.).

In contrast to the case in pH 5.5 & 5.5 combination, irrespectful of the deposition method, it is not possible to talk about a successful continuation of the LbL assembly of chitosan and casein for neither pH 3 & 8 combination nor the pH 5.5 & 8 combination. This is because no increase in the overall trend for the change of

absorbance values with respect to the layer number is observed for neither of the pH combinations (Figure.3.26 & 27). Furthermore, the absorbance values are very small compared to those in pH 5.5 & 5.5 combination. Nevertheless, the difference in absorbance values obtained by spraying compared to dipping in pH 5.5 & 8 combination (Figure.3.27), especially for the chitosan layers is significant enough to disregard. This is most probably due to the absence of rinsing step in spraying procedure compared to the dipping procedure. Higher deposition of chitosan at the first step obtained with spraying (and without rinsing) suggests that there are multiple layers of chitosan molecules weakly attached to each other through contribution of weaker forces such as van der Waals or H-bonding. These weakly attached molecules, then seem to dissociate with the application of the second deposition step by spraying casein solution (of pH 8) on the surface, which sort of acts like a rinsing step. It is clear that the same phenomenon is observed for the subsequent deposition steps.

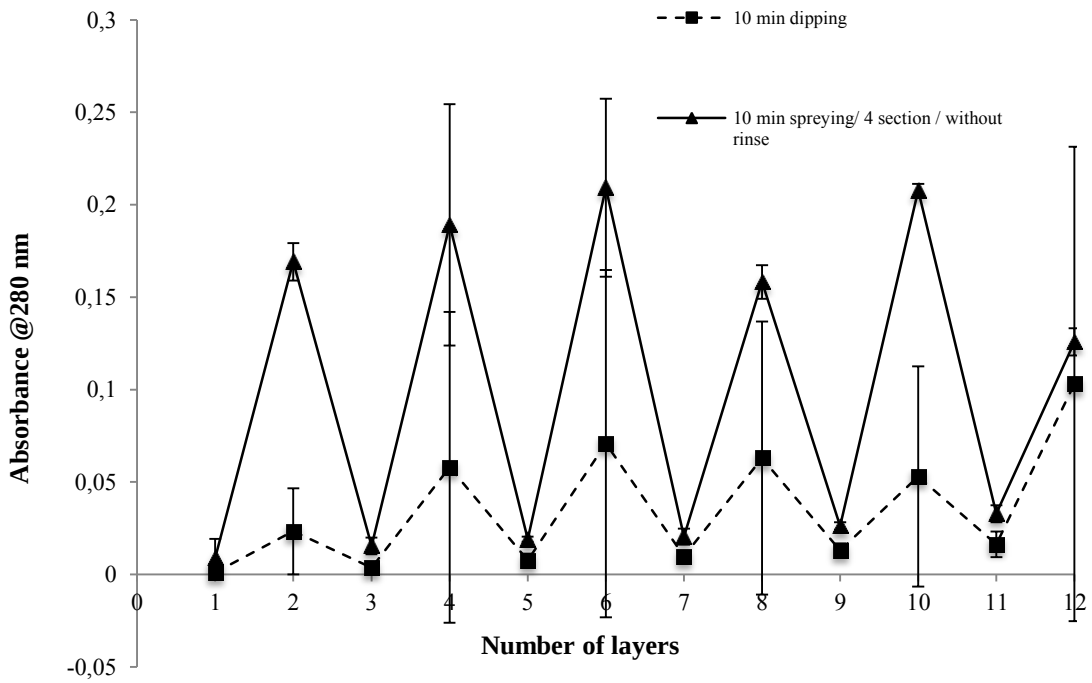

Figure 3.26. Comparison of multilayer formation obtained by dipping and spraying method for 0.2% (w/v) chitosan at pH 3 and 0.2% (w/v) sodium caseinate at pH 8**.** Adsorption time is 10 min.

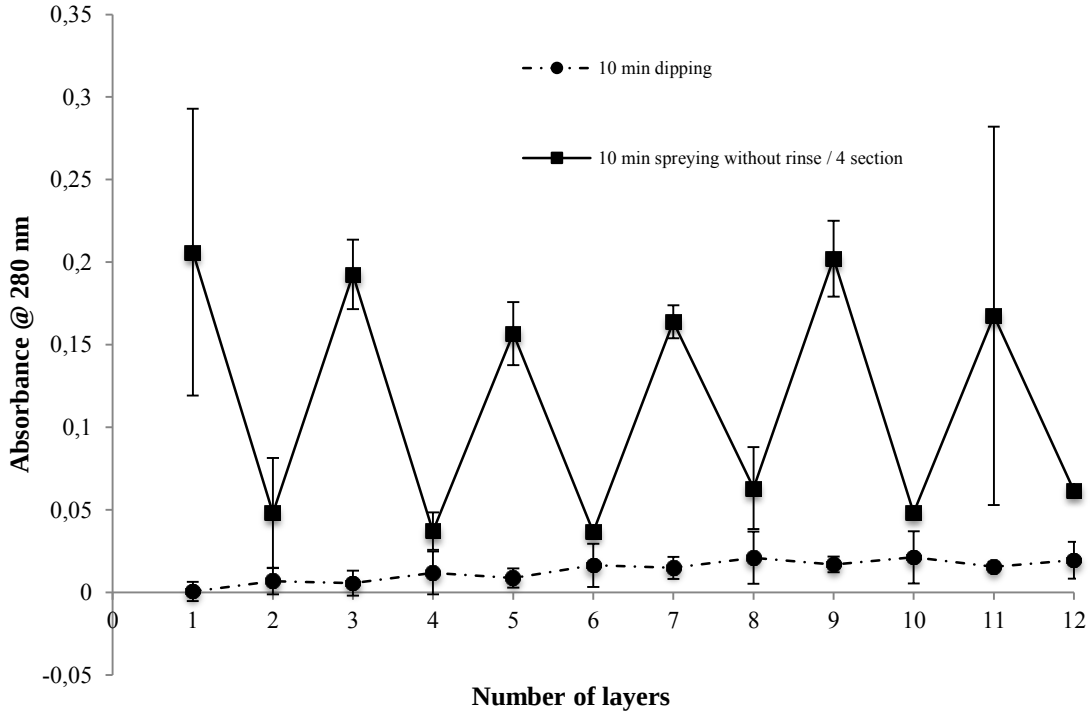

Figure 3.27. Comparison of multilayer formation obtained by dipping and spraying method for 0.2% (w/v) chitosan at pH 5.5 and 0.2% (w/v) sodium caseinate at pH 8**.** Adsorption time is 10 min.

In conclusion, according to the UV-Visible Spectroscopy results, multilayered coating formation was achieved at pH 5.5 & 5.5 combination best with 10 minutes adsorption time, but not at pH 5.5& 8 and pH 3 & 8 combinations.

Multilayered coatings obtained by chitosan pH 5.5 & sodium caseinate pH 5.5 with 10 minutes adsorption time were further characterized in terms of surface morphology, surface roughness, film thickness, oxygen permeability, water vapor permeability and antimicrobial activity.

3.3. Atomic Force Microscopy Results

As it was revealed by the UV-Vis spectroscopy and SPR experiments, the appropriate conditions to fabricate multilayered coatings from chitosan and sodium caseinate by both dipping and spraying methods are pH 5.5&5.5 combination with 10 min adsorption time. Therefore, the thickness measurements and surface characterization of the coatings fabricated at these experimental conditions were

performed using AFM. The thickness, surface morphology and roughness of the 1st, 2nd, 5th, 6th and 12th layers were determined separately in order to see the effect of number of layers.

Figure 3.28 shows the morphologies of chitosan and casein surfaces in ascending order of the number of layers, which were deposited *in situ* in the liquid cell of AFM. Morphological differences between the chitosan and casein layers are clearly apparent, which proves the assembly of disparate layers in each deposition step and therefore a layer-by-layer structure. It is also clearly observed that molecules at the surface tend to aggregate more with increasing number of layers. This appears in the images as larger forms of islets when going from the 1st to the 12th layer.

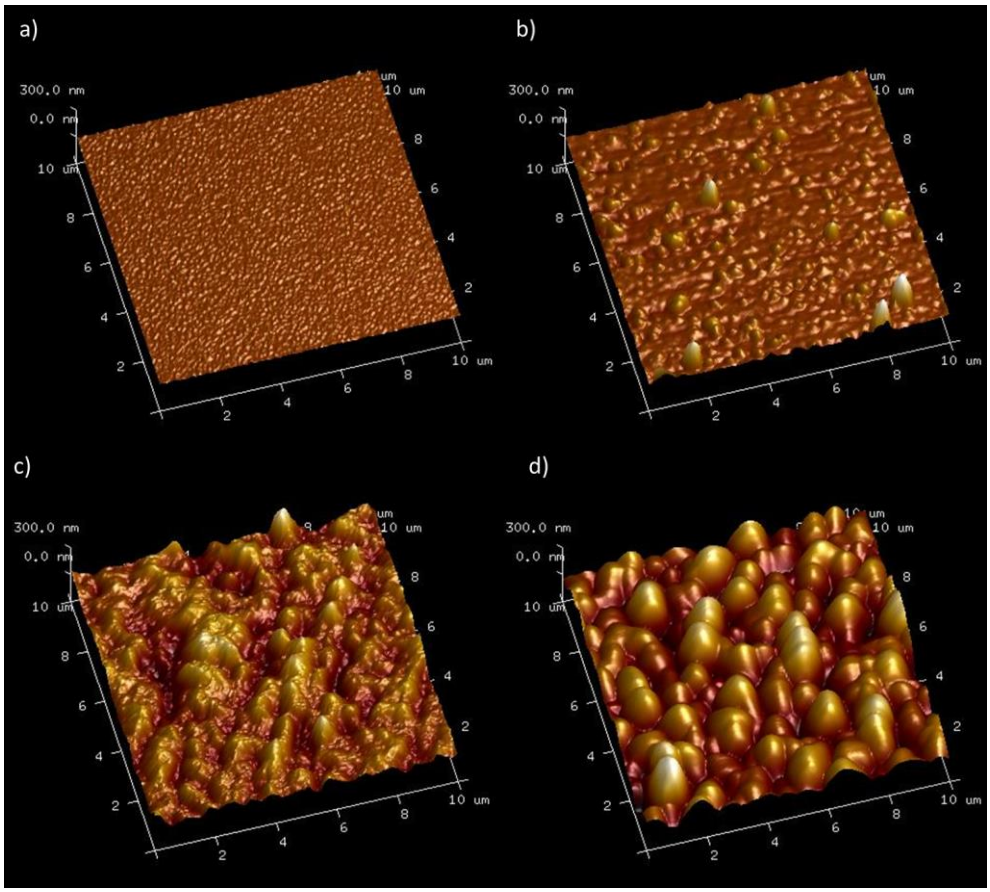

Figure 3.28. Surface morphology of different layers (deposited at pH 5.5& 5.5 combination with 10 min adsorption time) imaged by AFM *in situ* in liquid medium. Scan area is 10x10 μm^2 . Data scale of images were equalized. (a) 1st layer-chitosan, (b) 2nd layer- casein, (c) 5th layer- chitosan , (d) 6th layer – casein, (e) 11th layer- chitosan, f) 12th layer- casein.

(Cont. on next page)

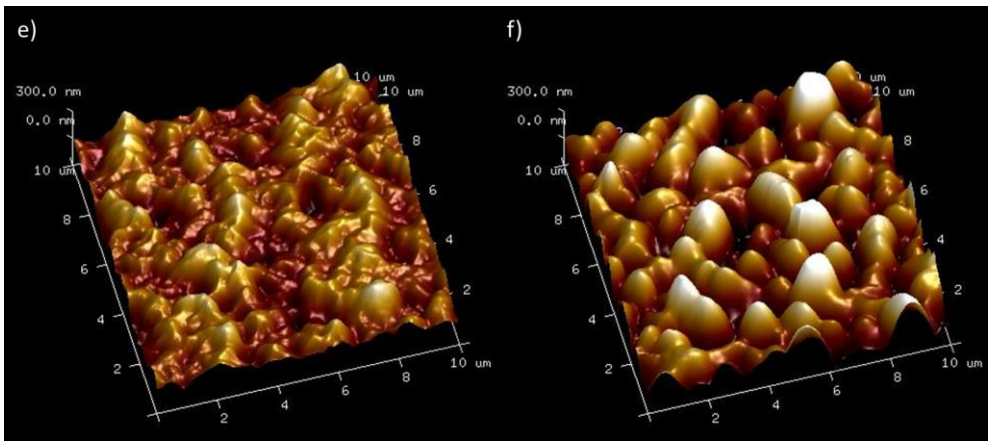

Figure 3.28. (cont)

In Figure 3.29, three-dimensional images of layers obtained by dipping method (imaged both in air and fluid medium) and spraying method are given. In order to compare the surface topography reliably, data scales were equalized.

When surface topography images, except for last layer, that obtained in air and liquid medium are compared, it is observed that more homogeneous surface structure was obtained in liquid medium. This statement is also supported by the results of surface roughness. However, this situation is associated with the time spend between the sample preparation and surface scanning. Screening in liquid medium was performed right after the film formation obtained in flow cell. However, the screening in air medium was performed after sample was prepared and dried in a desiccator. Therefore, screening in liquid medium allows for *in situ* examination of the surface topology of the layers while screening in air medium provide characterization of the surface structure after drying of the coating obtained by layer deposition.

In second condition, the reason of increasing surface roughness values, especially for low number of layers, may be due to the extra time that spend while samples were drying (water in the environment away from slowly), because of the continuation of the mobility of molecules. As a result both planar and cross-layer diffusion cluster structures occurred. In Figure 3.29 (e,h,k) presence of islets, in scanning of 2^{th} , 5^{th} and 6^{th} layers, indicate that. As mentioned before, deposition of chitosan and sodium caseinate at pH 5.5 with 10 minute adsorption time was continued up to 5-6th layers according to UV-Visible Spectroscopy and SPR results. This situation might be due to the surface saturation that is caused by the structures formed by the

inner and inter layer mobility of molecules. In literature, there are some studies that detected the diffusion between layers for weak polyelectrolytes. Thus, surface images obtained by atomic force microscopy supported the SPR results given in section 3.2.3.2.

Yin et. al.(2014) reported that, sodium caseinate films showed smooth surfaces without pores. However, when sodium caseinate interact with another material, clusters and pores were observed. As a result of interaction with chitosan, the surface structure of chitosan – sodium caseinate films were not homogeneous. In another study, chitosan - starch films were studied. Film surface was found smooth and continuous. They associated the smooth and continuous surface with chitosan structure (Mathew et.al., 2008).

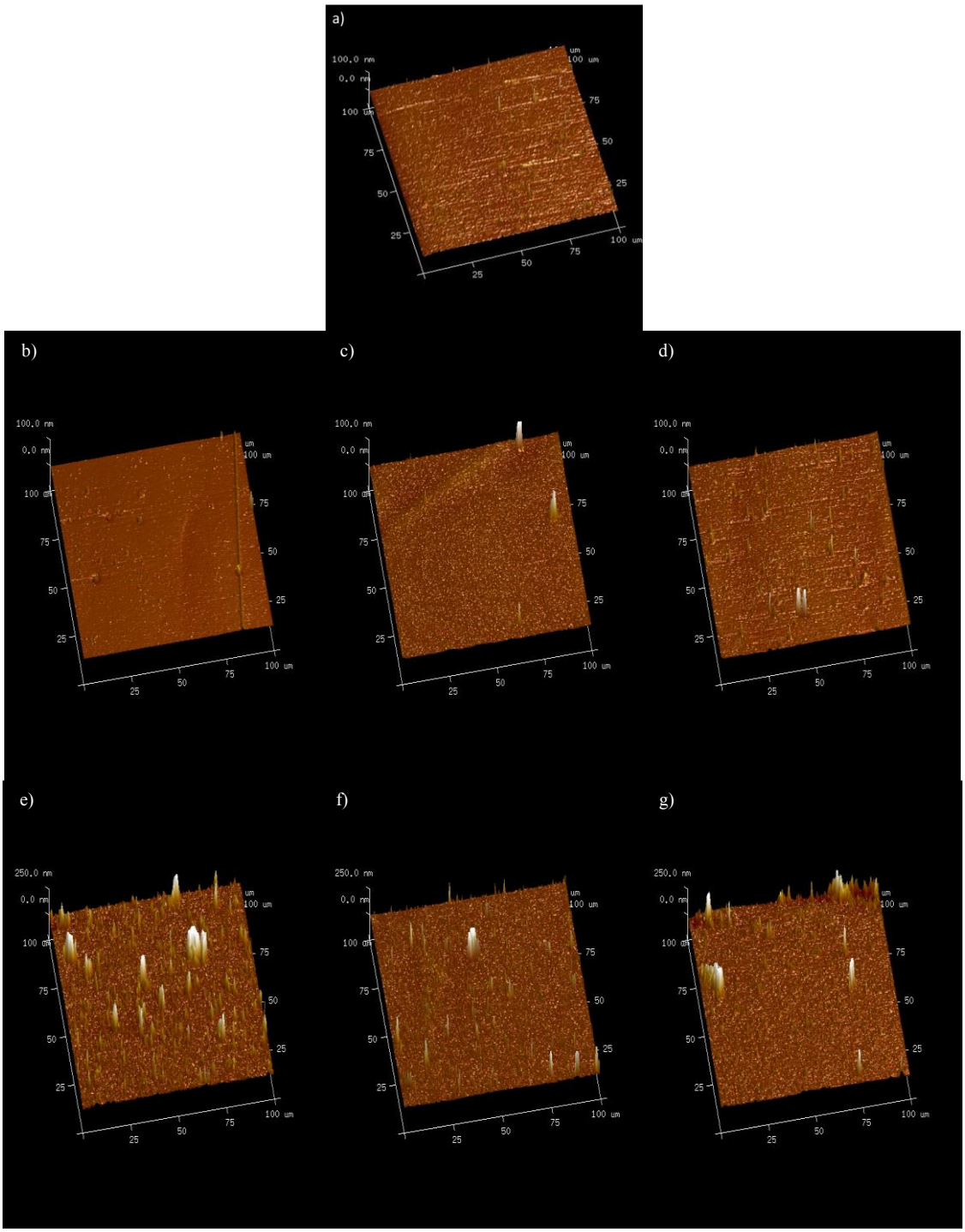

Figure 3.29. AFM images (in air and in fluid) of surface topography of the layers obtained by different methods (dipping or spraying) at pH 5.5& 5.5 combination with 10 min adsorption time. Scan area is 100x100 μm^2. Data scales of the images were equalized. (a) Plain glass, b) 1st layer (CH:chitosan)-air (c) 1st layer (CH)- liquid, (d) 1st layer (CH) -spray, (e) 2nd layer (CAS:casein)-air, (f) 2nd layer (CAS)-fluid, (g) 2nd layer (CAS)-spray, (h) 5th layer (CH)- air, (i) 5th layer (CH)- fluid, (j) 5th layer (CH)-spray, (k) 6th layer (CAS) – air, (l) 6th layer (CAS)- fluid, (m) 6th layer (CAS)- spray, (n) 12th layer (CAS)- air, (o) 12th layer (CAS)- fluid, (p) 12th layer (CAS)- spray.

(Cont. on next page)

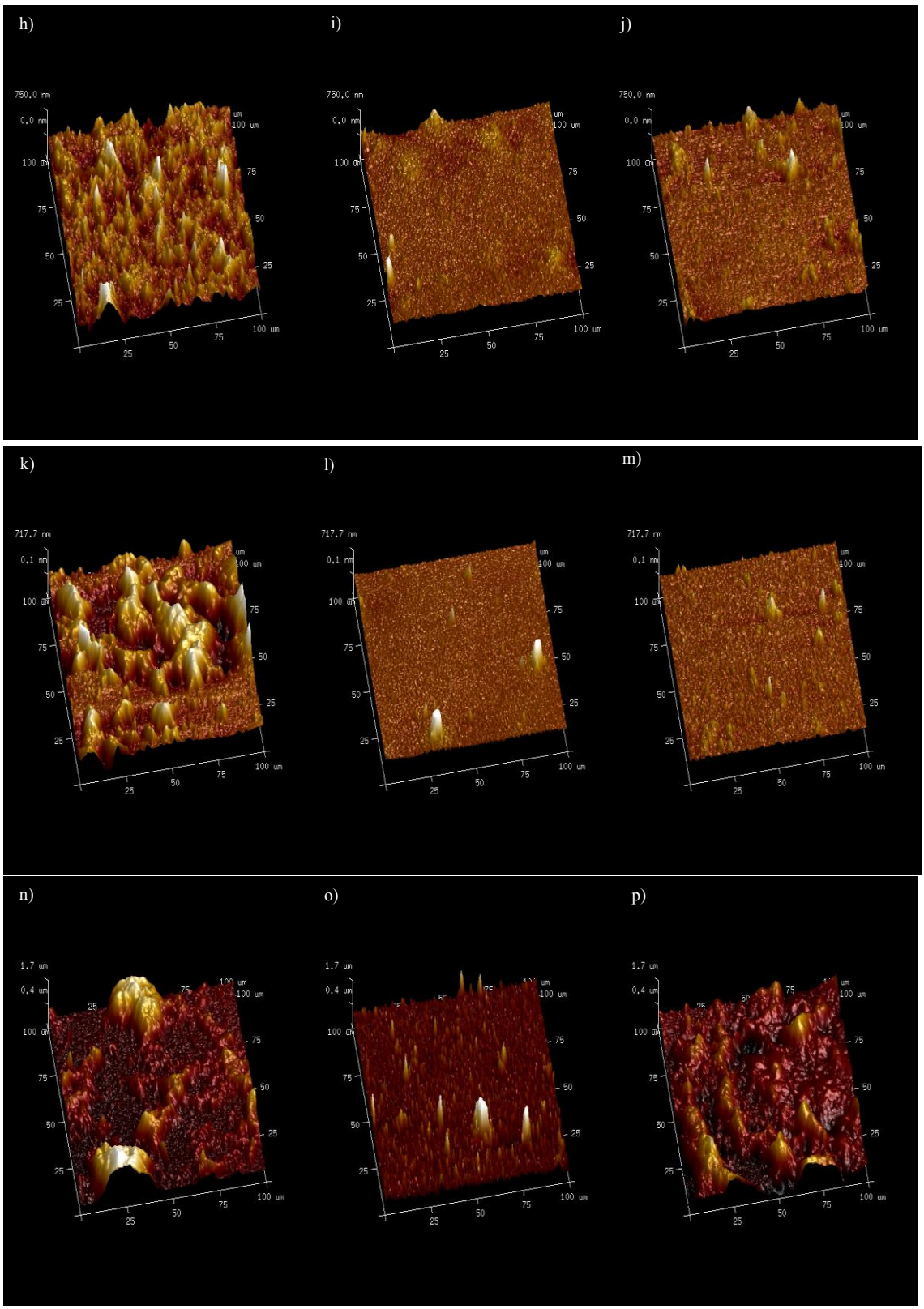

Figure 3.29. (cont)

Table 3.4. The surface roughness values obtained from 100x100 μm^2 scan areas. Statistically significant differences were tested with ANOVA and significant differences ($P < 0.05$) were determined by Tukey test. Values having different superscript letters within a column are a significantly different.

	R_a (nm) + SD	R_q (nm) + SD
Dipping -5th layer	203.33 ± 43.98^{A}	248.67 ± 45.35^{a}
Dipping -6th layer	178.67 ± 59.01^{A}	237.33 ± 48.42^{a}
Dipping -12th layer	181.40 ± 96.85^{A}	237.80 ± 119.84^{ab}
Fluid – 5th layer	26.70 ± 4.70^{B}	35.80 ± 3.52^{b}
Fluid – 6th layer	81.73 ± 25.62^{B}	99.80 ± 30.06^{b}
Fluid – 12th layer	237.67 ± 55.97^{A}	331.67 ± 82.51^{a}
Spray - 5th layer	60.33 ± 6.44^{B}	81.70 ± 8.01^{b}
Spray - 6th layer	56.80 ± 13.07^{B}	74.37 ± 14.30^{b}
Spray - 12th layer	77.42 ± 16.01^{B}	110.70 ± 19.24^{b}

Comparing the dipping and spraying methods in terms of surface morphology and roughness, it is clearly seen that the layers obtained by dipping method are rougher than the layers obtained by spraying method. As mentioned before in the spraying technique, surface filtration of substrate was possible due to gravity. However, it was not possible to flow in dipping method. It was assumed that the molecules were hold tighter in dipping method. So that, more rough film formation obtained by dipping technique.

Layer thickness were determined by using scratch method for air scanning for dipping and spraying technique.1^{st} , 2^{nd}, 5^{th}, 6^{th} , and 12^{th} layers thickness were examined both dipping and spraying methods. Scratch images and height profiles of 12^{th} layers were shown in Figure 3.30. Scratch images and height profiles of 1^{st}, 2^{nd}, 5^{th} and 6^{th} layers were shown in Appendix -C.

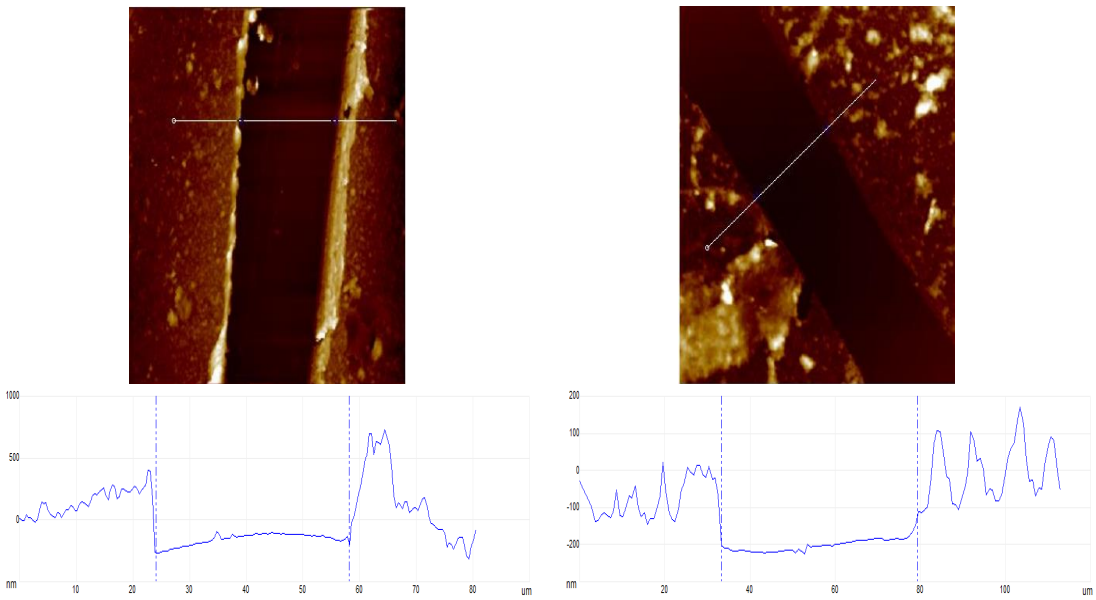

(a) (b)

Fig 3.30. Determination of 12th layer thickness by using scratches method by scanning atomic force microscopy. Scans were conducted in 100x100 μm^2 area. The height profiles of the white section lines are given in the bottom of each image in figure. (a) Dipping method (b) Spraying method.

The layer thickness values were given in Table 3.5. Both dipping and spraying methods, according to layer thickness values it was observed that film formation occurs. Between the layer thickness values, there were increases and decreases. This is because the solubility of chitosan and sodium caseinate. Soluble complexes were formed and these soluble complexes released from the surface during the deposition step.

According to layer thickness values, there was another striking point. 5th and 12th layers thickness did not show statistically significant difference in both spraying and dipping technique. Depending on this situation, it was understood that during the deposition between the chitosan and sodium caseinate molecules diffusion was comprised and integrated structures occur.

The resulting integrated structures cause the saturation to the surface. Resulting in saturation, changes in surface charges were blocked and thus deposition process was stopped. This situation supports the SPR results.

Table 3.5 Layer thickness values obtained by scratch method scanning by atomic force microscopy. Statistically significant differences tested with ANOVA and significant differences ($P < 0.05$) determined by the Tukey test. Exponential values with different letters were significantly different.

Number of layers	Thickness (nm)
Dipping – 1st layer	90.17 ± 20.69^{bc}
Dipping – 2nd layer	31.67 ± 14.26^{c}
Dipping – 5th layer	200.17 ± 113.68^{ab}
Dipping – 6th layer	98.50 ± 59.34^{bc}
Dipping – 12th layer	269.67 ± 98.25^{a}
Spray – 1st layer	113.0 ± 9.46^{abc}
Spray – 2nd layer	200.83 ± 176.54^{ab}
Spray – 5th layer	134.67 ± 79.23^{abc}
Spray – 6th layer	228.17 ± 86.71^{ab}
Spray – 12th layer	141.0 ± 23.79^{abc}

Film thicknesses obtained from dipping method were thicker than the film thickness obtained from spraying technique. It is understood that the multilayered film deposition with spraying technique and with weak polyelectrolyte such as chitosan and sodium caseinate cannot be shown same features as the films obtained with the dipping method. As mentioned above, surface filtration of substrates can also explain this situation.

3.4 Scanning Electron Microscopy Results

To obtained multilayered film formation of chitosan and sodium caseinate pH 5.5 – pH 5.5 and 10 minutes absorption time combination were used. Characterization of the surface structure and cross-sectional area were evaluated by using scanning electron microscope.

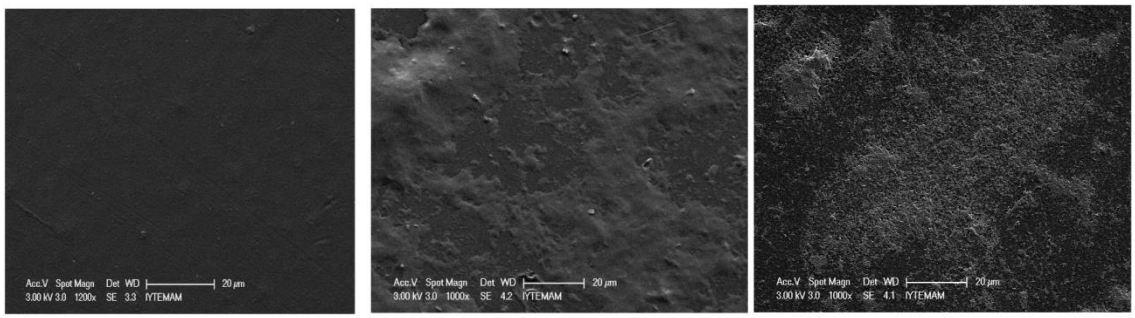

Figure 3.31. Coronal polypropylene film and multilayer deposition was prepared by 12-layer coating on the surface images obtained by scanning electron microscopy. (Left) coronal polypropylene film surface, (middle) 12 layer (casein) surface obtained by dipping method, (right) 12 layer (casein) surface obtained by spraying method.

In Figure 3.31, the surface of the corona treated blank PP film and 12 layered coating layer obtained by dipping and spraying deposition methods was shown. As in AFM results, in both methods it is clearly understood that there was a film formation. Based on SEM images, there was not a homogeneous film surface. In both techniques, clusters were observed. The surface topography of the film that was obtained by dipping technique, with clusters of chitosan and sodium caseinate molecules, seems more homogeneous compare to the surface topography of the film obtained by spraying technique.

Cross sectional area of the corona treated blank PP film and 12 layered coating layer obtained by dipping and spraying deposition methods was shown in Figure 3.32. The LBL coating was not distinguish significantly on the SEM images. However, compared with the cross-sectional image of blank PP film, LBL coating can be distinguished. When the cross- sectional surface of blank PP film was evaluated, top section seems to as a flat and sharp line. On the other hand, coated film top surfaces shown a wavy structure.

Acevedo-Fani et.al. studied the layer-by-layer assembly technique with chitosan and alginate. They concluded that SEM did not distinguish the nanolayered structure according to cross sectional image. However film surface characterized by small clusters because of the chitosan.

SEM does not provide much more information to compare about the cross-sectional surfaces and films surfaces obtained by dipping and spraying methods. In order to obtain the cross sectional images, films were exposed to vacuum process by

SEM. Vacuum process was not suitable for these type of films. Bending and breakage was observed in films because of the vacuum. Therefore, it has become difficult to take the cross-sectional image of films.

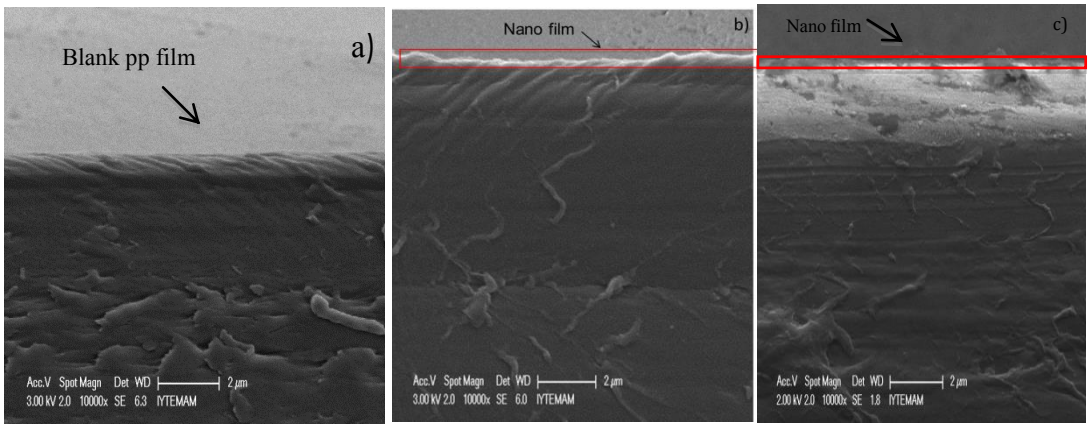

Figure 3.32. Compare the section surface of polypropylene film and coated films (a) cross sectional surface of polypropylene film, (b) cross sectional surface of 12 layer (casein) obtained by dipping method, (c) cross sectional surface of 12 layer (casein) obtained by spraying method.

3.5. Oxygen Permeability and Water Vapor Permeability Results

Oxygen permeability is an important factor to control the shelf life of packaged foods. If there is too much oxygen diffusion from the environment into the food, nutritional content of foods decreases. Depend on this, shelf life and food quality decreases (Wilhodo et al., 2013).

In this study, oxygen permeability was determined according to the ASTM D1434- 82 standard. According to AFM and SPR results, it was concluded that the after 5^{th} layer, film formation was not continued because of the surface saturation. Based on this, oxygen permeability was measured for 5^{th} and 12^{th} layers to examine the differences between 5^{th} and 12^{th} layers. Films were prepared by the combination pH 5.5 & pH 5.5 at 10 minutes for dipping method. In spraying method, pH 5.5& pH 5.5 combination at 10 minutes in 4-section protocole was used. Oxygen permeability results were given in Table 3.6.

Table 3.6. Oxygen permeability results for multilayered films obtained by chitosan and sodium caseinate at pH 5.5. Statistically significant differences tested with ANOVA and significant differences ($P < 0.05$) determined by the Tukey test. Exponential values with different letters were significantly different.

Samples	**OTR (ml/m^2 day atm) mm**
Blank PP	287.8 ± 0.0^{b}
5th layer – spraying	476.7 ± 32.2^{a}
5th layer – dipping	265.0 ± 39.7^{b}
12th layer – spraying	215.39 ± 0.0^{b}
12th layer – dipping	284.5 ± 12.0^{b}

According to Table 3.6, PP films coated with chitosan and sodium caseinate obtained by dipping method did not show significant difference between 5th and 12th layers' oxygen permeability. This situation confirmed that there was no difference about coating structure between the 5th and 12th layers obtained by dipping method. However, in spraying method results, oxygen permeability of 5th layers was different from the 12th layer. Important situation about the 5th layer was vacuum problem. In order to measure the oxygen permeability, samples remain in a vacuum environment. In 5th layer, there was a vacuum problem originating from the device. Device did not get coating into vacuum. Based on this vacuum problem, 5th layer oxygen permeability result were higher compare the other results.

Other important factor for food quality and shelf life is water vapor permeability. Water vapor permeability was measured according to ASTM F1249 standard. Same protocols were used to determine the water vapor permeability of coatings. Water vapor permeability results were given in Table 3.7.

Table 3.7. Water vapor permeability results for multilayered coatings obtained by chitosan and sodium caseinate at pH 5.5. Statistically significant differences tested with ANOVA and significant differences ($P < 0.05$) determined by the Tukey test. Exponential values with different letters were significantly different.

Samples	**WVTR (g/m^2 day mm Hg) mm**
Blank PP	6.57 ± 0.02^{a}
5^{th} layer – spraying	6.56 ± 0.03^{a}
5^{th} layer – dipping	6.24 ± 0.10^{a}
12^{th} layer – spraying	6.52 ± 0.03^{a}
12^{th} layer – dipping	5.95 ± 0.42^{a}

As expected, water vapor permeability of PP films coated with chitosan and sodium caseinate did not show any significant improvement because of layer thickness values.

3.6. Antimicrobial Activity of Chitosan and Sodium Caseinate Multilayered Coatings

Antimicrobial activity of 0.2% (w/v) chitosan and sodium caseinate multilayered coatings at pH 5.5&5.5 combination were determined by the classical zone inhibition method by using *Escherichia coli* (NRRL B-3008) as test microorganism. The results of antimicrobial tests are given in Figure 3.33. It is clear that the inhibition zones were not observed. However, since the growth of microorganisms was not observed under the films, it can be said that the coatings have a mild contact effect. In terms of number of layers or type of top layer, antimicrobial activity of coatings did not exhibit any significant difference.

Oi et al. (2004) studied the antibacterial activity of 0.5% (w/v) chitosan solution at pH 4.6 to 4.8 against *Escherichia coli* and they found that chitosan shows antibacterial activity. In our study, based on the antibacterial activity of chitosan and the

fact that the chitosan is positively charged and *E. coli* is a gram- negative bacteria, contact effect is expectable.

However, it is known that chitosan is dissolved in acetic acid solution and acetic acid also exhibits antimicrobial activity. Liu et al., (2006) studied the antibacterial activity of chitosan and acetic acid. They found that the antibacterial activity of acetic acid is based on the concentration of acetic acid and antibacterial activity of chitosan is changing according to the molecular weight of chitosan.

In summary, the multilayered coatings fabricated in this study by both dipping and spraying were found to exhibit mild contact antimicrobial effect against nonpathogenic *E. coli*. However, based on the findings of others reported in the literature, it would be erroneous to state that this effect is solely due to chitosan. Further research is definitely needed to differentiate the contributions of chitosan and acetic acid on this antimicrobial effect, which is not in the scope of this work.

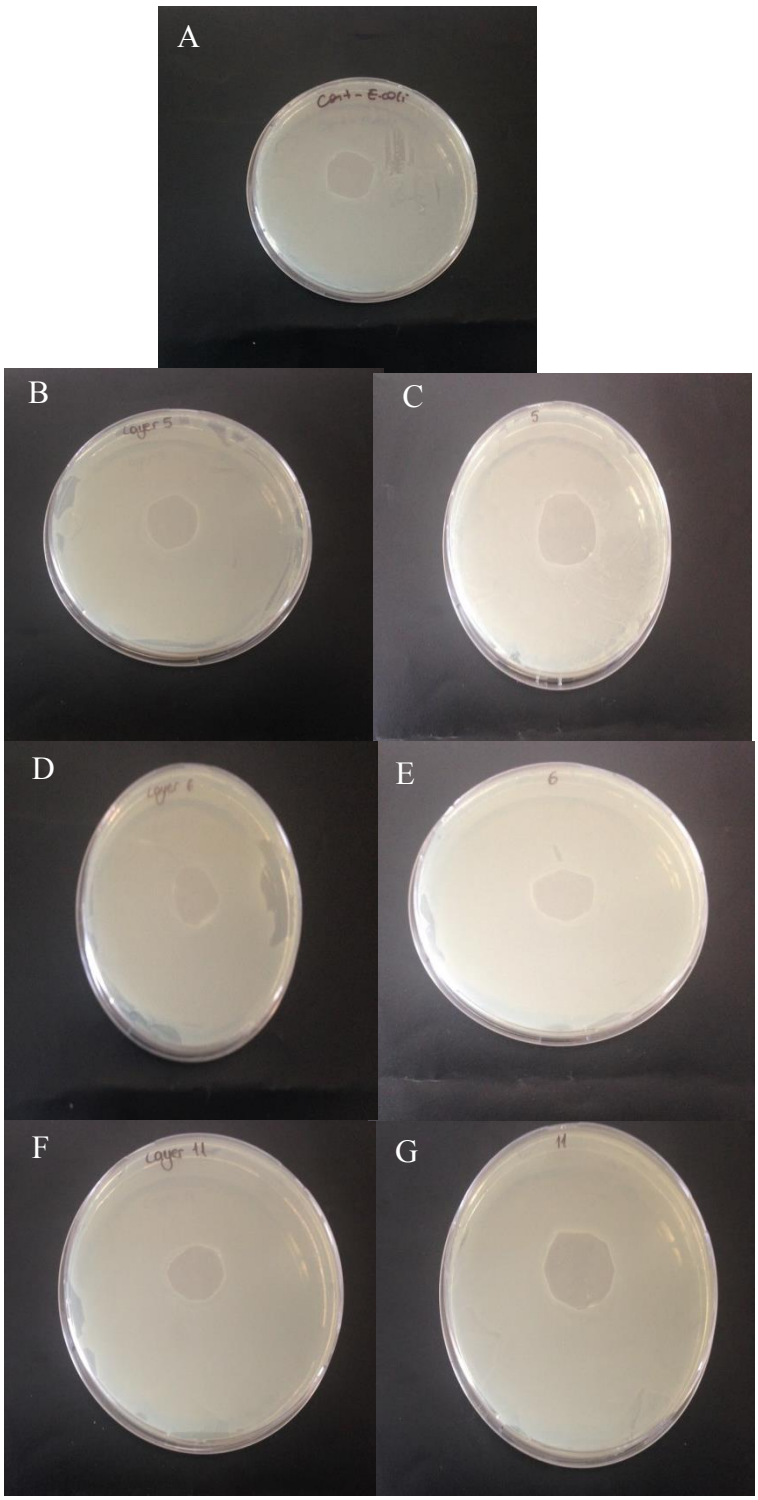

Figure 3.33. Antimicrobial activity of chitosan and sodium caseinate multilayered films (A: Control; B: 5th layer – dipping method; C: 5th layer – spraying method; D: 6th layer – dipping method; E: 6th layer – spraying method; F: 11th layer – dipping method; G: 11th layer – spraying method).

CHAPTER 4

CONCLUSION

In this study, multilayered coating formations obtained by chitosan and sodium caseinate by using dipping and spraying methods were studied to develop a novel, ultra thin, homogeneous edible coating with adequate gas barrier properties. To obtain the multilayered coating formation, physical properties (zeta potential and hydrodynamic diameter) of chitosan and sodium caseinate were investigated. Multilayer formation is possible with both polyelectrolytes at pH 5.5. According to SPR and AFM results film growth continues up to 5-6 layers, then the surface probably becomes saturated with both polyelectrolytes diffusing through the layers. Based on the electrostatic interactions, chitosan and sodium caseinate molecules diffused between each other and integrated structures occurred. For same reason, coating surface was not show homogeneous structure.

By comparing dipping and spraying methods, it was clearly understood that the coatings obtained by dipping method are thicker, but rougher than coatings obtained by spraying method. It was understood that the multilayered film deposition with spraying technique and with weak polyelectrolyte such as chitosan and sodium caseinate could not be show same properties as the films obtained with the dipping method. As barrier properties, multilayered film formation obtained by chitosan and sodium casinate did not show significant effect on polypropilen films. Chitosan and sodium caseinate films have mild contact antimicrobial effect against the *Escherichia coli*.

In conclusion, multilayered film formation and characterization obtained from chitosan and sodium caseinate by dipping and spraying methods was successfully characterized. Nanotechnology techniques (AFM and SPR) were found very effective in the characterization of multilayered nanofilms.

As a future study, different polyelectrolyte combinations for chitosan or sodium caseinate should be examined. Moreover, cross-linked method should be studied to obtain thicker, homogeneous and stable film formation. Gas barrier properties and antimicrobial activity of coatings may be improved by using cross linkers.

REFERENCES

Acevedo-Fani, A., Salvia-Trujillo, L., Soliva-Fortuny, R., & Martín-Belloso, O. (2015). Modulating Biopolymer Electrical Charge to Optimize the Assembly of Edible Multilayer Nanofilms by the Layer-by-Layer Technique. *Biomacromolecules*, 150902200730007. http://doi.org/10.1021/acs.biomac.5b00821

Alessio, P., Martin, C. S., De Saja, J. A., & Rodriguez-Mendez, M. L. (2016). Mimetic biosensors composed by layer-by-layer films of phospholipid, phthalocyanine and silver nanoparticles to polyphenol detection. *Sensors and Actuators, B: Chemical*, *233*, 654–666. http://doi.org/10.1016/j.snb.2016.04.139

Caleb, O. J., Mahajan, P. V., Al-Said, F. A.-J., & Opara, U. L. (2013). Modified Atmosphere Packaging Technology of Fresh and Fresh-cut Produce and the Microbial Consequences—A Review. *Food and Bioprocess Technology*, *6*(2), 303–329. http://doi.org/10.1007/s11947-012-0932-4

Carneiro-Da-Cunha, M. G., Cerqueira, M. A., Souza, B. W. S., Teixeira, J. A., & Vicente, A. A. (2011). Influence of concentration, ionic strength and pH on zeta potential and mean hydrodynamic diameter of edible polysaccharide solutions envisaged for multinanolayered films production. *Carbohydrate Polymers*, *85*(3), 522–528. http://doi.org/10.1016/j.carbpol.2011.03.001

Dhall, R. K. (2015). Advances in Edible Coatings for Fresh Fruits and Vegetables : A Review Advances in Edible Coatings for Fresh Fruits and Vegetables :, *8398*(November). http://doi.org/10.1080/10408398.2010.541568

Funami, T. (2010). Atomic Force Microscopy Imaging of Food Polysaccharides in Relation to Rheological Properties. *Food Science and Technology Research*, *16*(1), 13–22. http://doi.org/10.3136/fstr.16.13

Galgano, F., Condelli, N., Favati, F., Di Bianco, V., Perretti, G., & Caruso, M. (2014). Biodegradable Packaging and Edible Coating for Fresh-Cut Fruits and Vegetables. *Proquest*, *27*(March), 14–17. http://doi.org/http://dx.doi.org/10.1108/17506200710779521

Galus, S., & Kadzińska, J. (2015). Food applications of emulsion-based edible films and coatings. *Trends in Food Science & Technology*, *45*(2), 273–283. http://doi.org/10.1016/j.tifs.2015.07.011

Hu, M., Li, Y., Decker, E. A., Xiao, H., & McClements, D. J. (2011). Impact of Layer Structure on Physical Stability and Lipase Digestibility of Lipid Droplets Coated by Biopolymer Nanolaminated Coatings. *Food Biophysics*, *6*(1), 37–48. http://doi.org/10.1007/s11483-010-9173-0

Jokar, M., Rahman, R. A., & Ibrahim, N. A. (2012). Layer by Layer Deposition of Polyethylene Glycol Capped Silver Nanoparticles/Chitosan on Polyethylene Substrate. *International Journal of Polymeric Materials*, *61*(5), 371–383. http://doi.org/10.1080/00914037.2011.593055

Joseph, N., Ahmadiannamini, P., Hoogenboom, R., & Vankelecom, I. F. J. (2014). Layer-by-layer preparation of polyelectrolyte multilayer membranes for separation. *Polymer Chemistry*, *5*(6), 1817–1831. http://doi.org/10.1039/c3py01262j

Junthip, J., Tabary, N., Chai, F., Leclercq, L., Maton, M., Cazaux, F., … Martel, B. (2016). Layer-by-layer coating of textile with two oppositely charged cyclodextrin polyelectrolytes for extended drug delivery. *Journal of Biomedical Materials Research Part A*, *104*(6), 1408–1424. http://doi.org/10.1002/jbm.a.35674

Kim, E., & Jung, S. (2005). Layer-by-layer assembled electrochromic films for all-solid-state electrochromic devices. *Chemistry of Materials*, *17*(25), 6381–6387. http://doi.org/10.1021/cm051492n

Kurth, D. D. G., & Osterhout, R. (1999). In situ analysis of metallosupramolecular coordination polyelectrolyte films by surface plasmon resonance spectroscopy. *Langmuir*, *15*(12), 4842–4846. Retrieved from http://pubs.acs.org/doi/abs/10.1021/la981760e

Li, Y., Liu, X., & Lin, Z. (2012). Recent developments and applications of surface plasmon resonance biosensors for the detection of mycotoxins in foodstuffs. *Food Chemistry*, *132*(3), 1549–1554. http://doi.org/10.1016/j.foodchem.2011.10.109

Liang, H., Miranto, H., Granqvist, N., Sadowski, J. W., Viitala, T., Wang, B., & Yliperttula, M. (2010). Surface plasmon resonance instrument as a refractometer for liquids and ultrathin films. *Sensors and Actuators, B: Chemical*, *149*(1), 212–220. http://doi.org/10.1016/j.snb.2010.05.048

Lin, D., & Zhao, Y. (2007). Innovations in the development and application of edible coatings for fresh and minimally processed fruits and vegetables. *Comprehensive Reviews in Food Science and Food Safety*, *6*, 60–75. http://doi.org/10.1111/j.1541-4337.2007.00018.x

Liu, D., & Cheng, F. (2011). Advances in research on structural characterisation of agricultural products using atomic force microscopy. *Journal of the Science of Food and Agriculture*, *91*(5), 783–788. http://doi.org/10.1002/jsfa.4284

Liu, N., Chen, X. G., Park, H. J., Liu, C. G., Liu, C. S., Meng, X. H., & Yu, L. J. (2006). Effect of MW and concentration of chitosan on antibacterial activity of Escherichia coli. *Carbohydrate Polymers*, *64*(1), 60–65. http://doi.org/10.1016/j.carbpol.2005.10.028

Loveday, S. M., X.L. Wanga, M. A. R., Anema, S. G., & L.K. Creamera, H. S. (2010). Tuning the properties of β-lactoglobulin nanofibrils with pH, NaCl and CaCl2. *International Dairy Journal*, *20*(9), 571–579.

Mangaraj, S., Goswami, T. K., & Mahajan, P. V. (2009). Applications of Plastic Films for Modified Atmosphere Packaging of Fruits and Vegetables: A Review. *Food Engineering Reviews*, *1*(2), 133–158. http://doi.org/10.1007/s12393-009-9007-3

Mathew, S., & Abraham, T. E. (2008). Characterisation of ferulic acid incorporated starch-chitosan blend films. *Food Hydrocolloids*, *22*(5), 826–835. http://doi.org/10.1016/j.foodhyd.2007.03.012

Mellinas, C., Valdes, A., Ramos, M., Burgos, N., Garrigos, M. del C., & Jİmenez, A. (2015). Active edible films. *Journal of Applied Polymer Science*, *133*(2). http://doi.org/10.1002/app.42971

MEZDOUR, S., BRULÉ, G., & KOROLCZUK, J. (2006). Physicochemical analysis of casein solubility in water-ethanol solutions. *EDP Sciences*, *83*(10), 435–452. http://doi.org/10.1051/lait

Morris, V. J., Woodward, N. C., & Gunning, A. P. (2011). Atomic force microscopy as a nanoscience tool in rational food design. *Journal of the Science of Food and Agriculture*, (July), n/a–n/a. http://doi.org/10.1002/jsfa.4501

Nanocomposix. 2007. Zeta Potential. http://nanocomposix.com/pages/characterization-techniques#zeta-potential (accessed June 15,2016).

Nguyen, C. A., Argun, A. A., Hammond, P. T., Lu, X., & Lee, P. S. (2011). Layer-by-layer assembled solid polymer electrolyte for electrochromic devices. *Chemistry of Materials*, *23*(8), 2142–2149. http://doi.org/10.1021/cm103572q

Olaru, A., Bala, C., Jaffrezic-Renault, N., & Aboul-Enein, H. Y. (2015). Surface plasmon resonance (SPR) biosensors in pharmaceutical analysis. *Critical Reviews in Analytical Chemistry / CRC*, *45*(2), 97–105. http://doi.org/10.1080/10408347.2014.881250

Oliveira, M., Abadias, M., Usall, J., Torres, R., Teixidó, N., & Viñas, I. (2015). Application of modified atmosphere packaging as a safety approach to fresh-cut fruits and vegetables – A review. *Trends in Food Science & Technology*, *46*(1), 13–26. http://doi.org/10.1016/j.tifs.2015.07.017

Qi, L., Xu, Z., Jiang, X., Hu, C., & Zou, X. (2004). Preparation and antibacterial activity of chitosan nanoparticles. *Carbohydrate Research*, *339*(16), 2693–2700. http://doi.org/10.1016/j.carres.2004.09.007

Ramos, B., Miller, F. A., Brandão, T. R. S., Teixeira, P., & Silva, C. L. M. (2013). Fresh fruits and vegetables—An overview on applied methodologies to improve its quality and safety. *Innovative Food Science & Emerging Technologies*, *20*, 1–15. http://doi.org/10.1016/j.ifset.2013.07.002

Rials, M., & Ods, M. E. T. H. (2000). Ox y g e n P e rm e a bility a n d Me c h a n ic a l P ro p e rtie s o f F ilm s fro m Hy d ro ly ze d Wh e y P ro te in, 3913–3916.

Rojas-Graü, M. A., Oms-Oliu, G., Soliva-Fortuny, R., & Martín-Belloso, O. (2009). The use of packaging techniques to maintain freshness in fresh-cut fruits and vegetables: A review. *International Journal of Food Science and Technology*, *44*(5), 875–889. http://doi.org/10.1111/j.1365-2621.2009.01911.x

Sandhya. (2010). Modified atmosphere packaging of fresh produce: Current status and future needs. *LWT - Food Science and Technology*, *43*(3), 381–392. http://doi.org/10.1016/j.lwt.2009.05.018

Sipahi, R. E., Castell-Perez, M. E., Moreira, R. G., Gomes, C., & Castillo, A. (2013). Improved multilayered antimicrobial alginate-based edible coating extends the shelf life of fresh-cut watermelon (Citrullus lanatus). *LWT - Food Science and Technology*, *51*(1), 9–15. http://doi.org/10.1016/j.lwt.2012.11.013

Tyowua, A. T., Yiase, S. G., & Wuanna, R. A. (2012). Manipulation of Concentration-Conductivity Data of Sodium Dodecyl Sulphate and Sodium Dodecylbenzene Sulphonate in KCl Solution in Relation to Micellisation Parameters Dodecyl Sulphate and Sodium Dodecylbenzene Sulphonate in KCl Solution in Relation to M, *2012*.

V Klitzing, R. (2006). Internal structure of polyelectrolyte multilayer assemblies. *Physical Chemistry Chemical Physics*, *8*(43), 5012–33. http://doi.org/10.1039/b607760a

Vargas, M., Pastor, C., Chiralt, A., McClements, D. J., & González-Martínez, C. (2008). Recent Advances in Edible Coatings for Fresh and Minimally Processed Fruits. *Critical Reviews in Food Science and Nutrition*, *48*(6), 496–511. http://doi.org/10.1080/10408390701537344

Yin, Y. C., Yin, S. W., Yang, X. Q., Tang, C. H., Wen, S. H., Chen, Z., … Wu, L. Y. (2014). Surface modification of sodium caseinate films by zein coatings. *Food Hydrocolloids*, *36*, 1–8. http://doi.org/10.1016/j.foodhyd.2013.08.027

Yoo, D., Shiratori, S. S., & Rubner, M. F. (1998). Controlling bilayer composition and surface wettability of sequentially adsorbed multilayers of weak polyelectrolytes. *Macromolecules*, *31*(13), 4309–4318. http://doi.org/10.1021/ma9800360

Zacharia, N. S., Modestino, M., & Hammond, P. T. (2007). Factors influencing the interdiffusion of weak polycations in multilayers. *Macromolecules*, *40*(26), 9523–9528. http://doi.org/10.1021/ma071828

APPENDIX A

PARTICLE SIZE DISTRIBUTON GRAPHS FOR CHITOSAN AND SODIUM CASEINATE FOR EACH CONCENTRATION AND PH VALUES

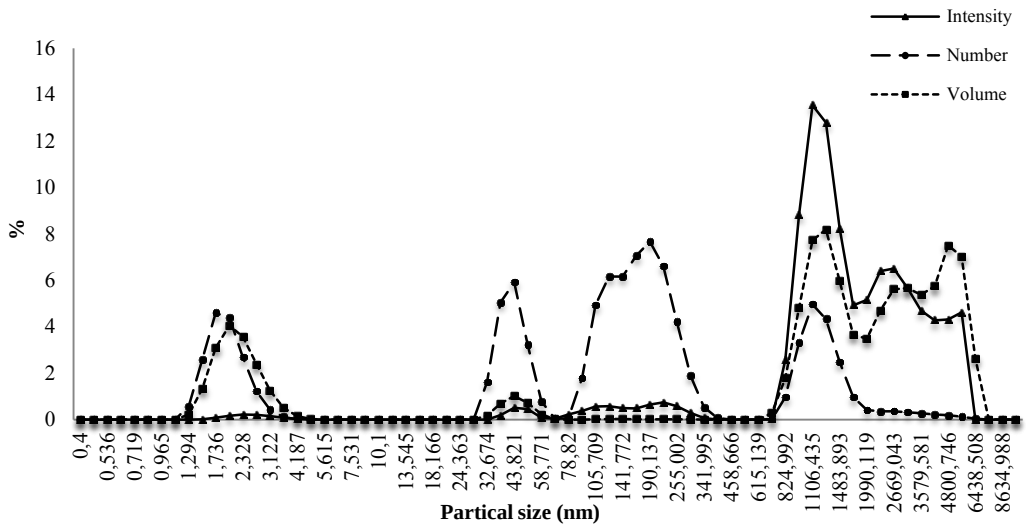

Figure A.1. Average particle size distribution for 0.2% chitosan at pH 3.5 based on intensity, volume and number distributions.

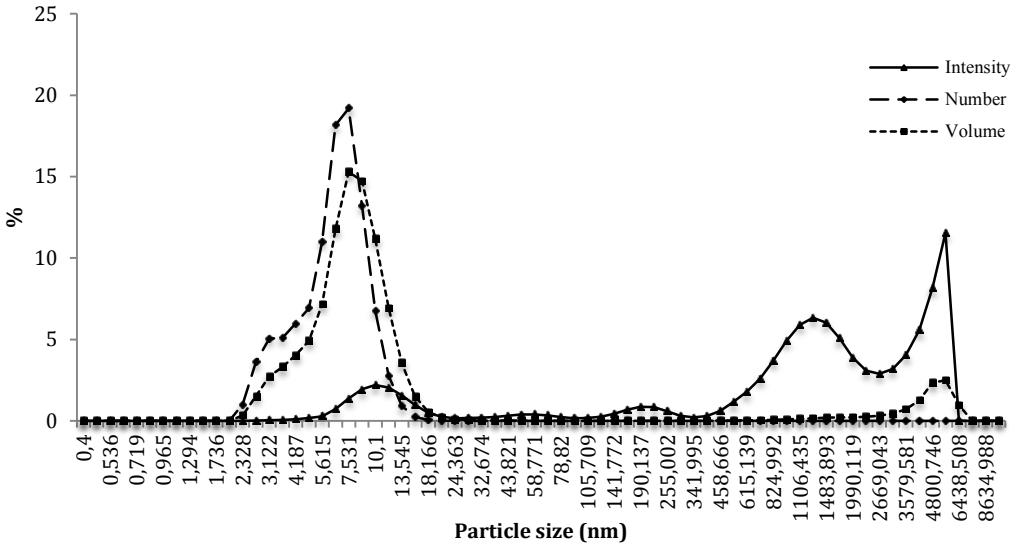

Figure A.2. Average particle size distribution for 0.2% chitosan at pH 4 based on intensity, volume and number distributions.

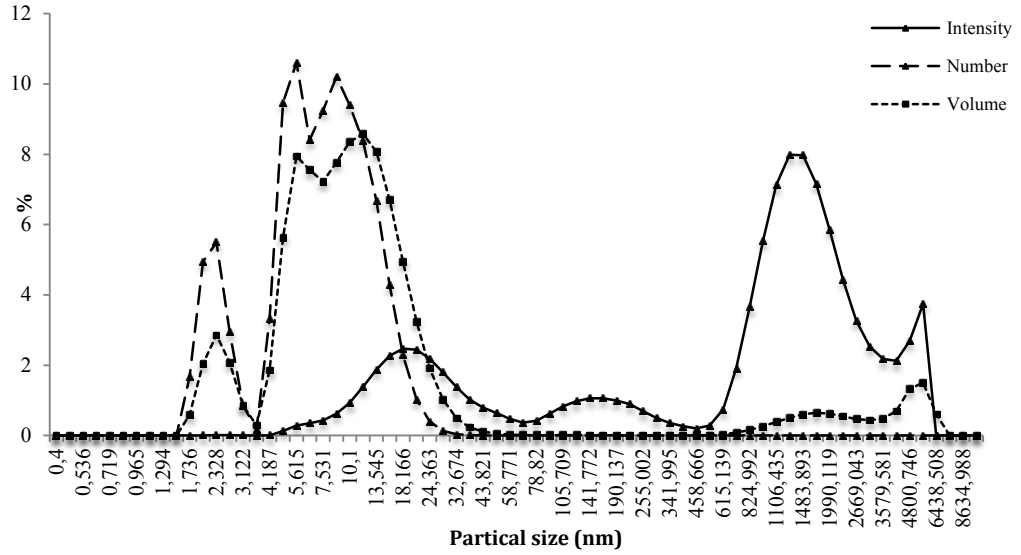

Figure A.3. Average particle size distribution for 0.2% chitosan at pH 4.5 based on intensity, volume and number distributions.

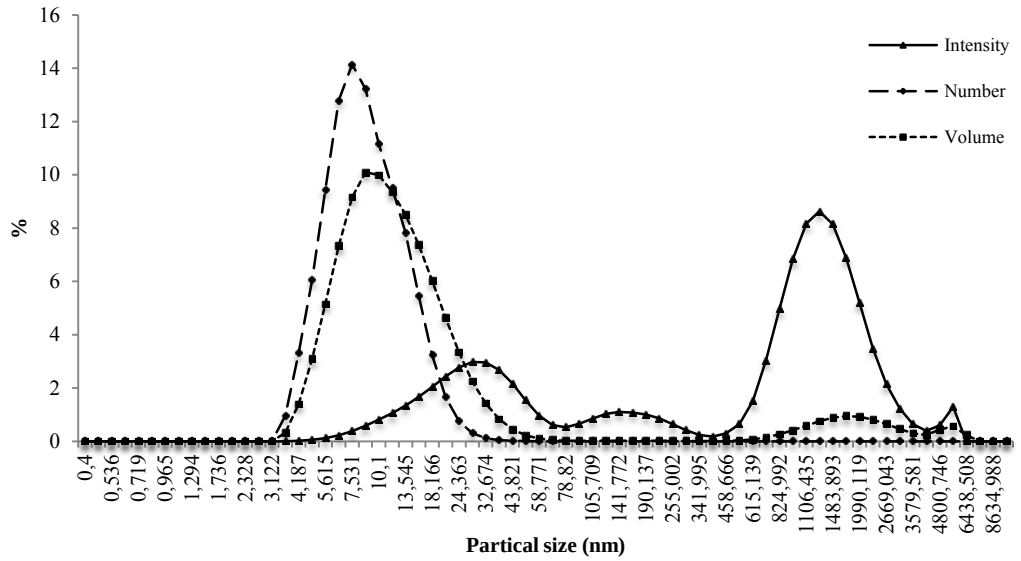

Figure A.4. Average particle size distribution for 0.2% chitosan at pH 5 based on intensity, volume and number distributions.

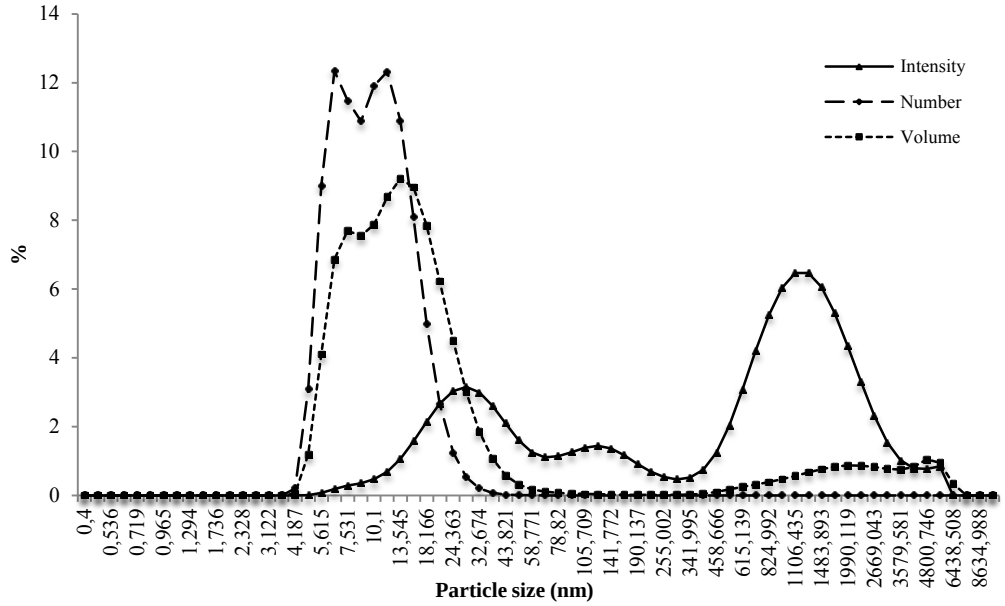

Figure A.5. Average particle size distribution for 0.2% chitosan at pH 5.5 based on intensity, volume and number distributions.

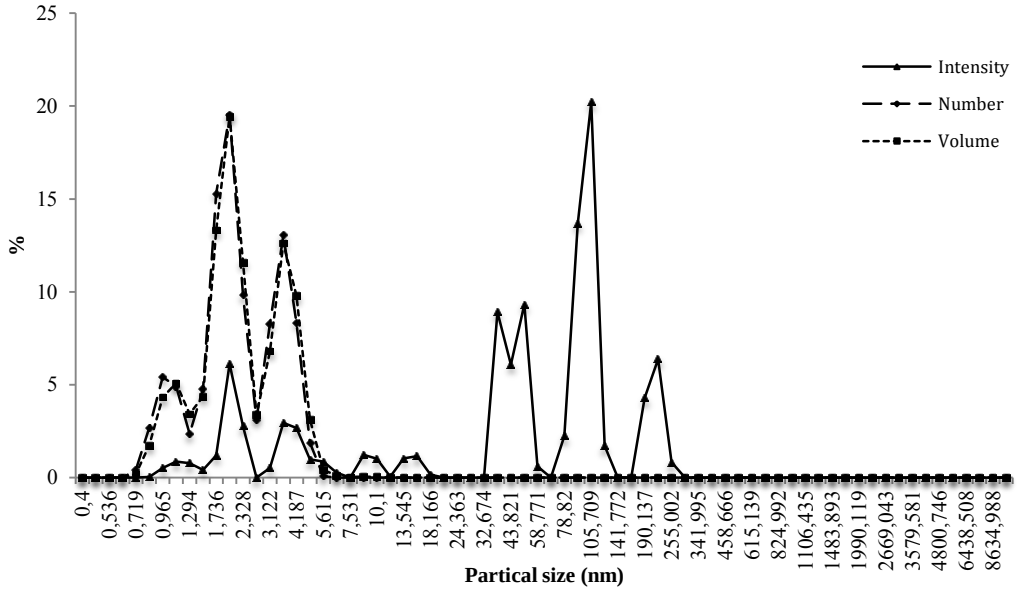

Figure A.6. Average particle size distribution for 0.5% chitosan at pH 3 based on intensity, volume and number distributions.

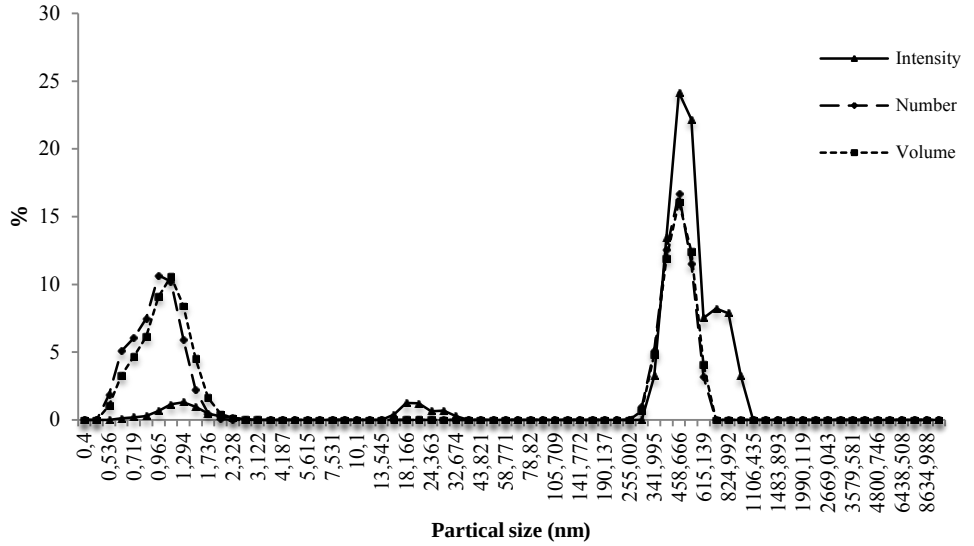

Figure A.7. Average particle size distribution for 0.5% chitosan at pH 3.5 based on intensity, volume and number distributions.

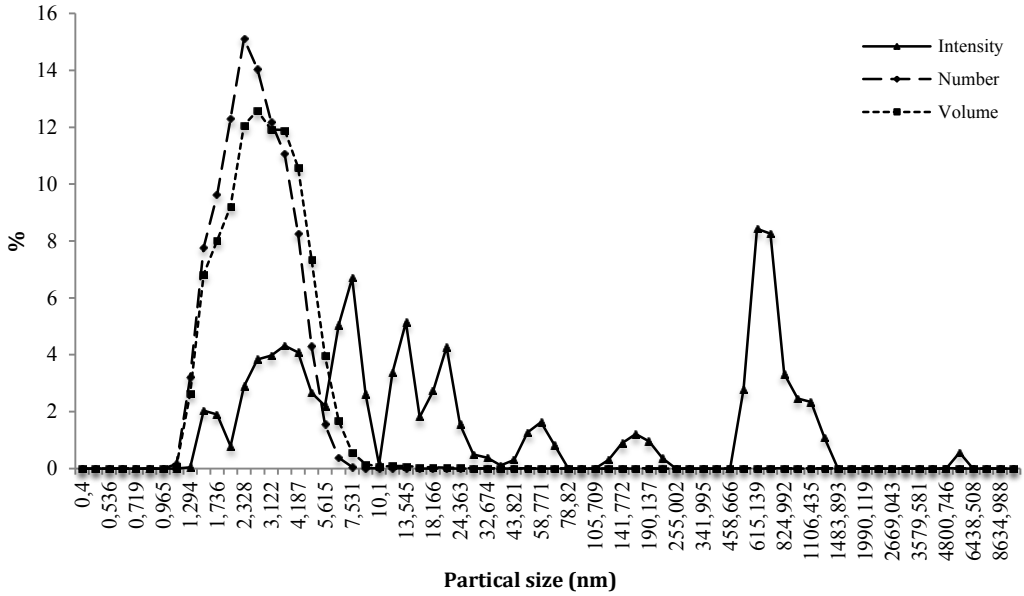

Figure A.8. Average particle size distribution for 0.5% chitosan at pH 4 based on intensity, volume and number distributions.

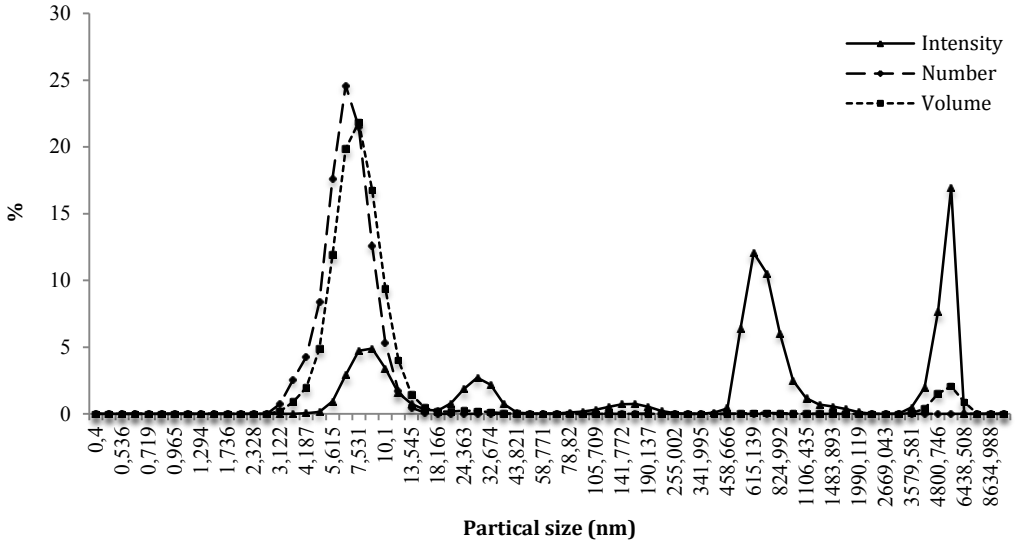

Figure A.9. Average particle size distribution for 0.5% chitosan at pH 4.5 based on intensity, volume and number distributions.

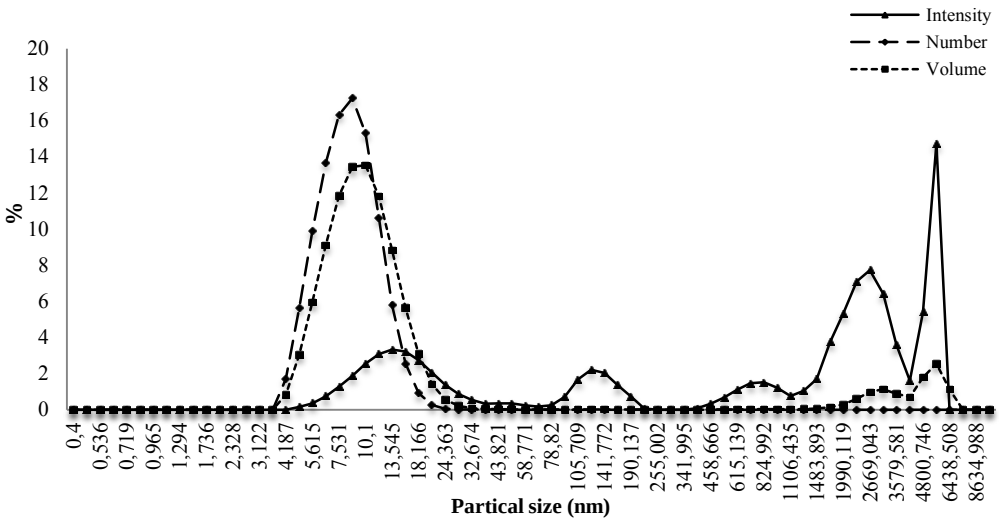

Figure A.10. Average particle size distribution for 0.5% chitosan at pH 5 based on intensity, volume and number distributions.

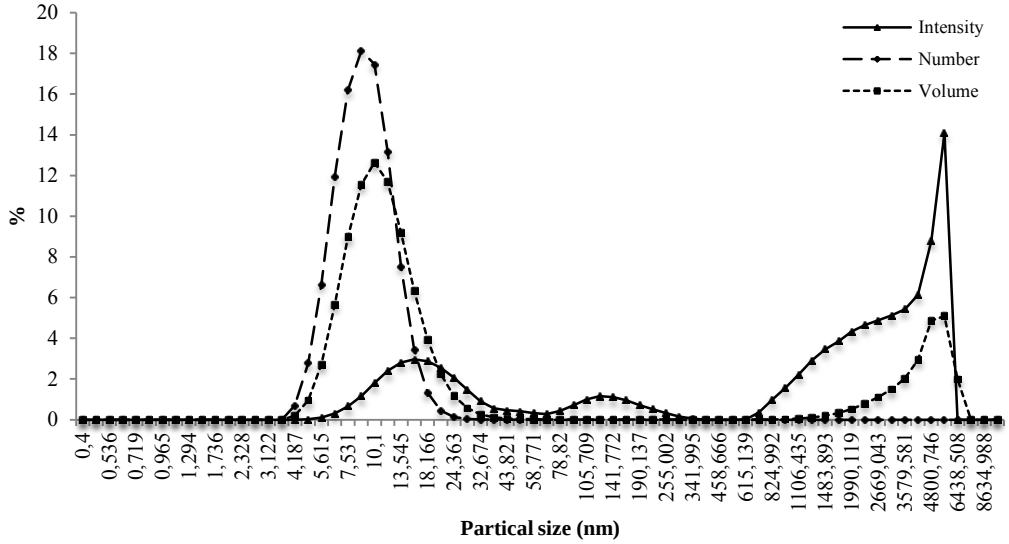

Figure A.11. Average particle size distribution for 0.5% chitosan at pH 5.5 based on intensity, volume and number distributions.

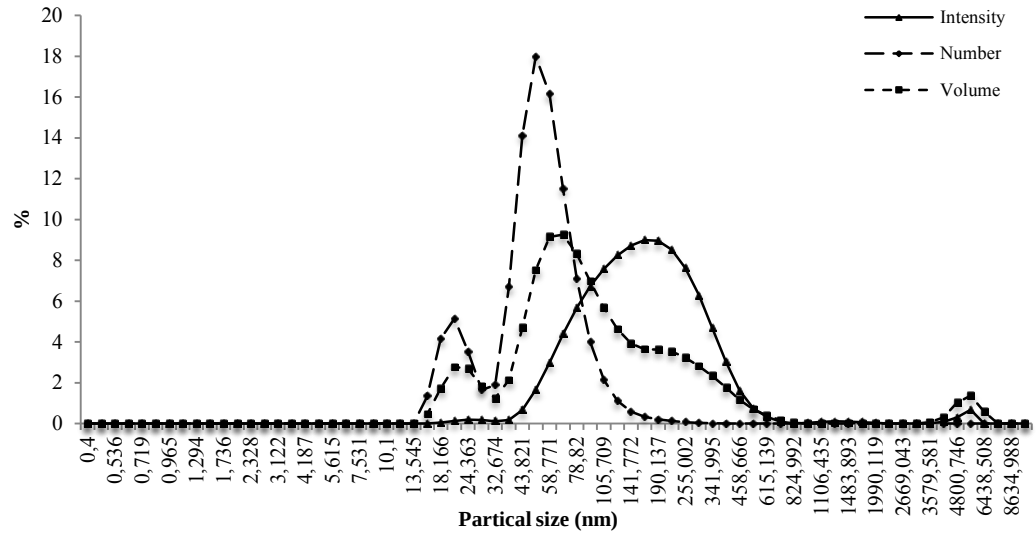

Figure A.12. Average particle size distribution for 0.2% sodium caseinate at pH 6 based on intensity, volume and number distributions.

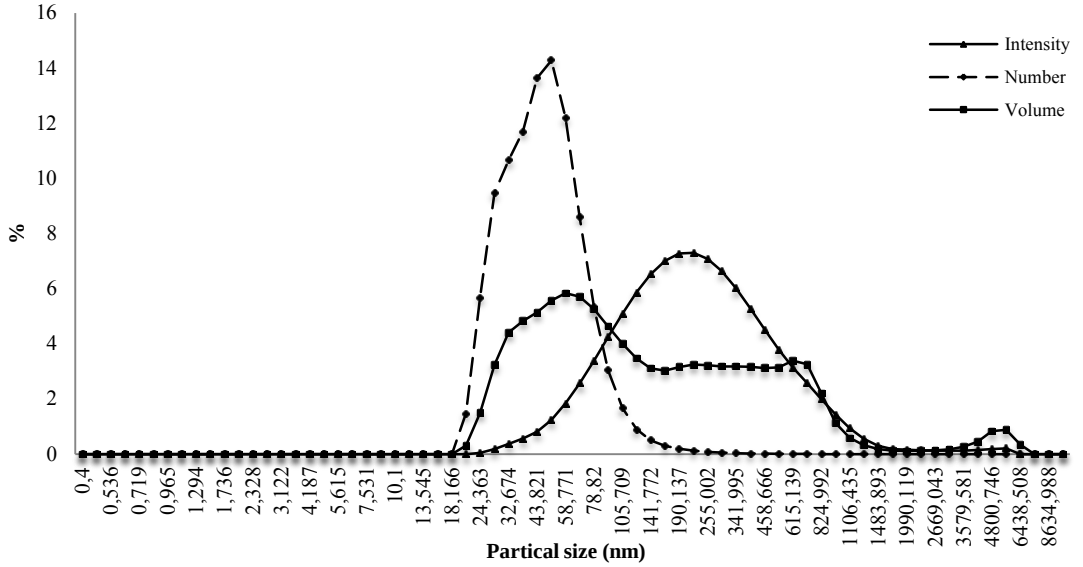

Figure A.13. Average particle size distribution for 0.2% sodium caseinate at pH 7 based on intensity, volume and number distributions.

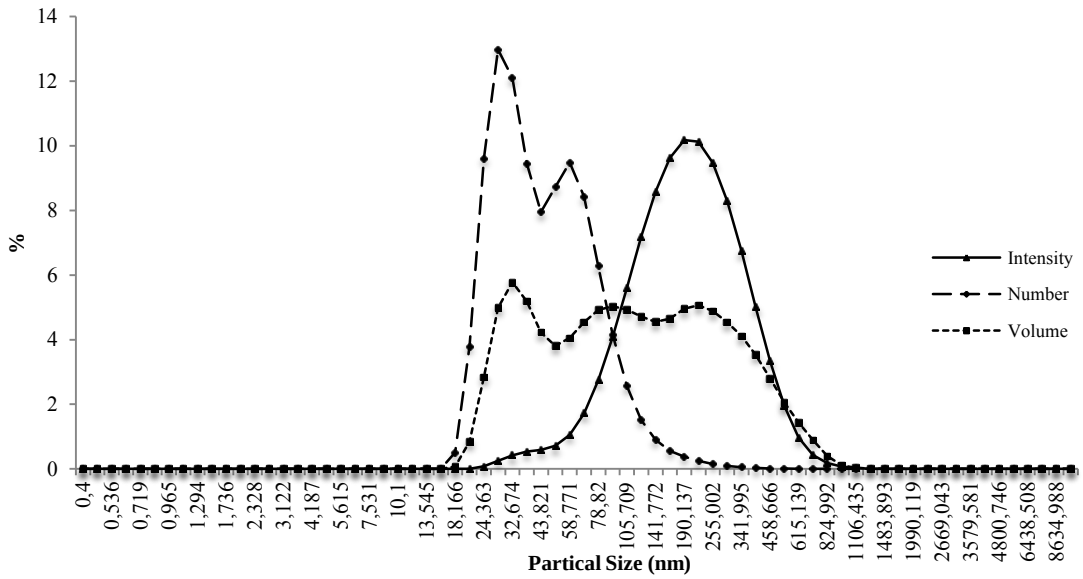

Figure A.14. Average particle size distribution for 0.2% sodium caseinate at pH 8 based on intensity, volume and number distributions.

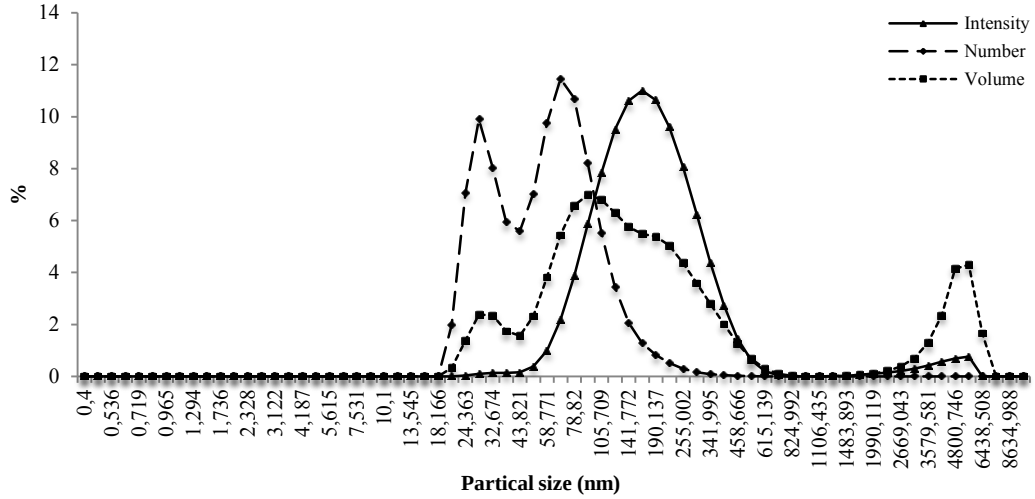

Figure A.15. Average particle size distribution for 0.5% sodium caseinate at pH 5.5 based on intensity, volume and number distributions.

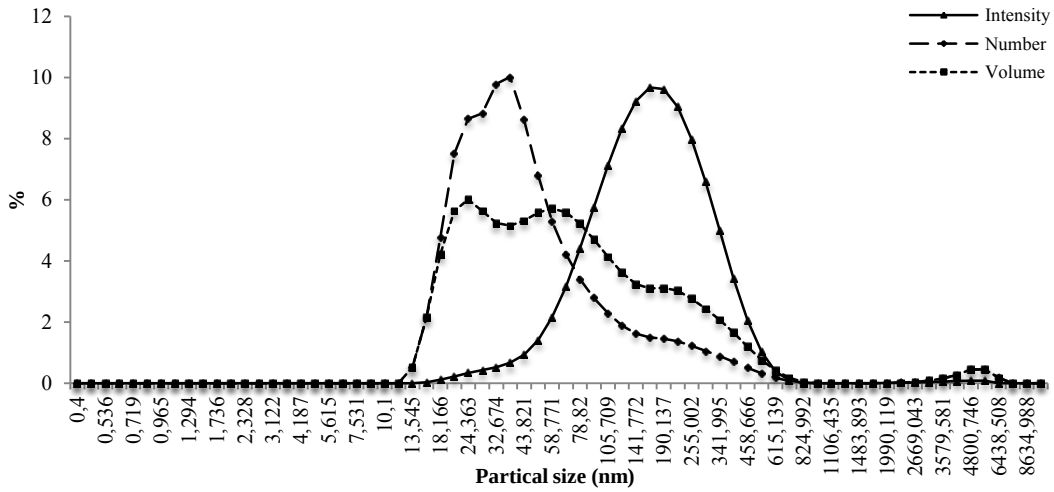

Figure A.16. Average particle size distribution for 0.5% sodium caseinate at pH 6 based on intensity, volume and number distributions.

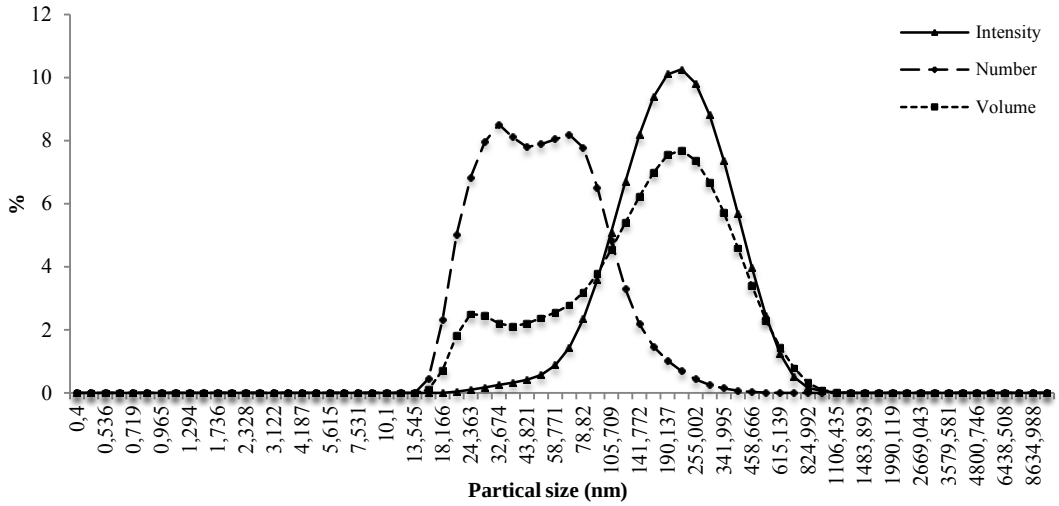

Figure A.17. Average particle size distribution for 0.5% sodium caseinate at pH 7 based on intensity, volume and number distributions.

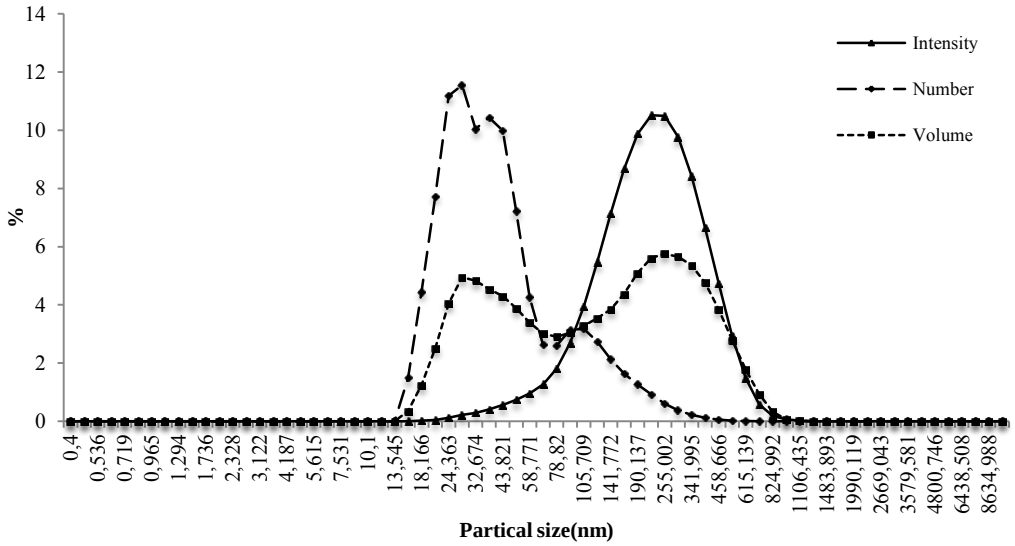

Figure A.18. Average particle size distribution for 0.5% sodium caseinate at pH 8 based on intensity, volume and number distributions.

APPENDIX B

SPR CURVES

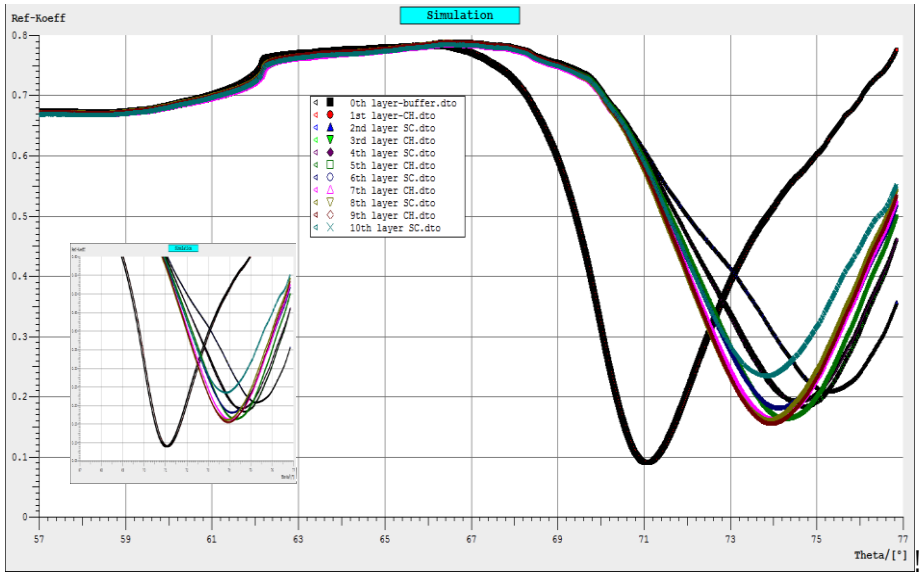

Figure B.1. SPR curve of 6 layer pair of chitosan/sodium caseinate at 10 minute.

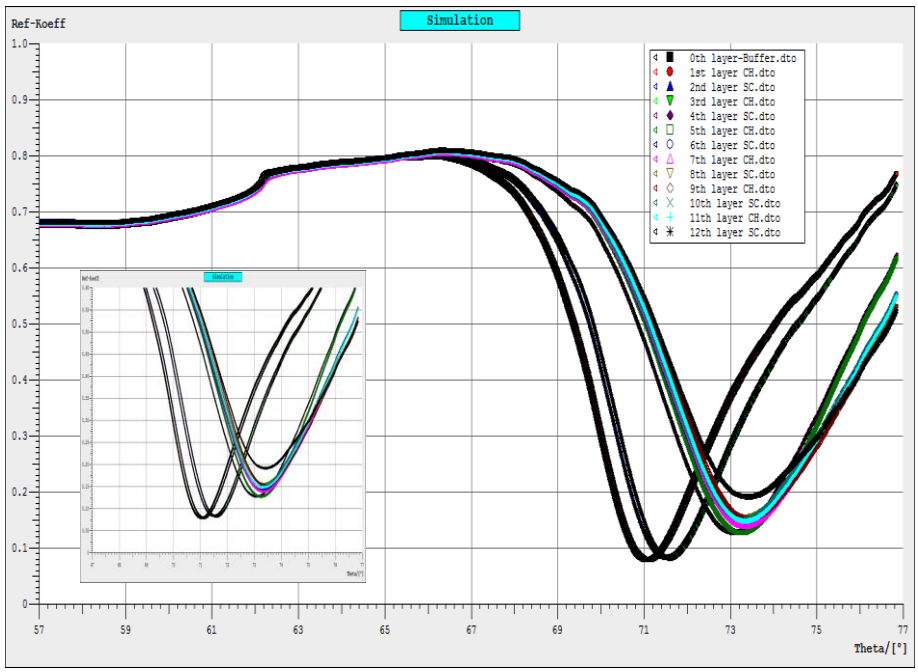

Figure B.1. SPR curve of 6 layer pair of chitosan/sodium caseinate at 2 minute.

APPENDIX C

STANDARD DEVIATION TABLES FOR SPRAYING GRAPHS

Table C.1. Standard deviations for 0.2% concentrations at pH 5.5 & 5.5 at 2 minutes multilayered formation obtained by spraying method.

Number of Layers	With rinse	With rinse - 4 section	Without rinse - 4 section
1	0,002	0.043	0.029
2	0.005	0.033	0.020
3	0.004	0.051	0.033
4	0.003	0.014	0.007
5	0.006	0.017	0.008
6	0.005	0.014	0.006
7	0.009	0.028	0.013
8	0.000	0.014	0.009
9	0.001	0.024	0.016
10	0.006	0.008	0.002
11	0.010	0.020	0.007
12	0.025	0.008	0.012

Table C.2. Standard deviations for 0.2% concentrations at pH 5.5 & 8 at 2 minutes multilayered formation obtained by spraying method.

Number of Layers	With rinse	Without rinse	Without rinse - 4 section
1	0.014	0.091	0.033
2	0.004	0.024	0.003
3	0.001	0.038	0.285
4	0.000	0.041	0.070
5	0.002	0.166	0.090
6	0.001	0.037	0.001
7	0.001	0.098	0.006
8	0.001	0.029	0.029
9	0.001	0.088	0.032
10	0.000	0.065	0.004
11	0.001	0.080	0.069
12	0.002	0.006	0.034

Table C.3. Standard deviations for 0.2% concentrations at pH 3 & 8 at 2 minutes multilayered formation obtained by spraying method.

Number of Layers	Without rinse	Without rinse - 4 section
1	0.010	0.006
2	0.004	0.031
3	0.003	0.006
4	0.005	0.033
5	0.001	0.003
6	0.035	0.022
7	0.002	0.005
8	0.006	0.024
9	0.003	0.007
10	0.024	0.003
11	0.014	0.010
12	0.014	0.051

Table C.4. Standard deviations for 0.2% concentrations at pH 5.5 & 5.5 at 10 minutes multilayered formation obtained by spraying method.

Number of Layers	With rinse- 4 section	Without rinse - 4 section
1	0.000	0.022
2	0.017	0.012
3	0.012	0.009
4	0.024	0.010
5	0.026	0.147
6	0.052	0.041
7	0.057	0.147
8	0.062	0.008
9	0.062	0.047
10	0.048	0.027
11	0.045	0.017
12	0.044	0.017

Table C.5. Standard deviations for 0.2% concentrations at pH 5.5 & 8 at 10 minutes multilayered formation obtained by spraying method.

Number of Layers	Without rinse - 4 section
1	0.087
2	0.033
3	0.021
4	0.011
5	0.019
6	0.003
7	0.010
8	0.025
9	0.023
10	0.001
11	0.115

Table C.6. Standard deviations for 0.2% concentrations at pH 3 & 8 at 10 minutes multilayered formation obtained by spraying method.

Number of Layers	With rinse- 4 section	Without rinse - 4 section
1	0.001	0.010
2	0.015	0.010
3	0.002	0.005
4	0.008	0.065
5	0.001	0.001
6	0.008	0.048
7	0.000	0.004
8	0.003	0.009
9	0.001	0.002
10	0.000	0.004
11	0.000	0.005
12	0.008	0.007

APPENDIX D

SCRATCH IMAGES OF MULTILAYERED FILM FORMATION

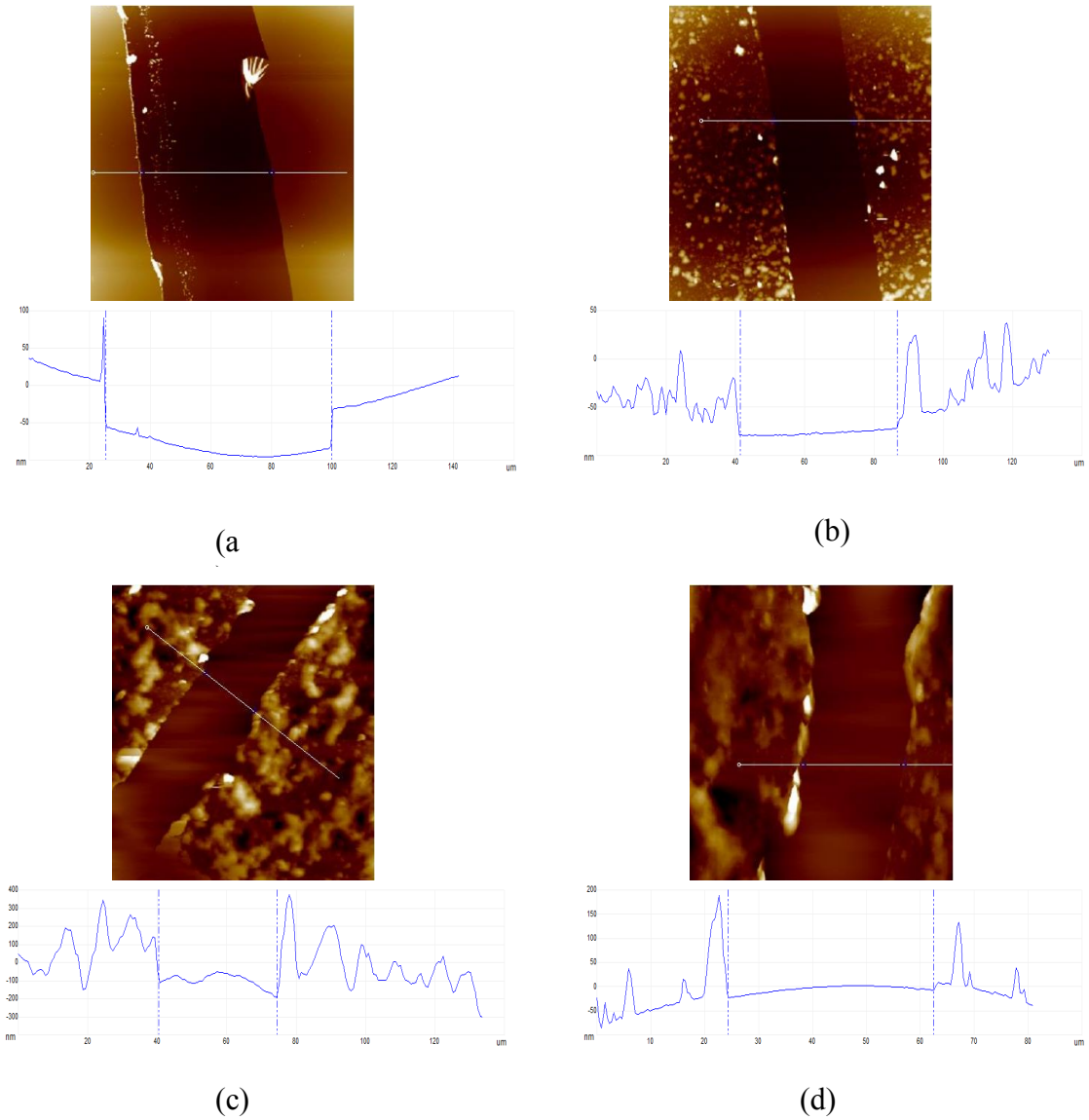

(a) (b)

(c) (d)

Figure D.1. Scratch images of multilayered films obtained by dipping method (a)1st layer (b)2nd layer (c) 5th layer (d) 6th layer.

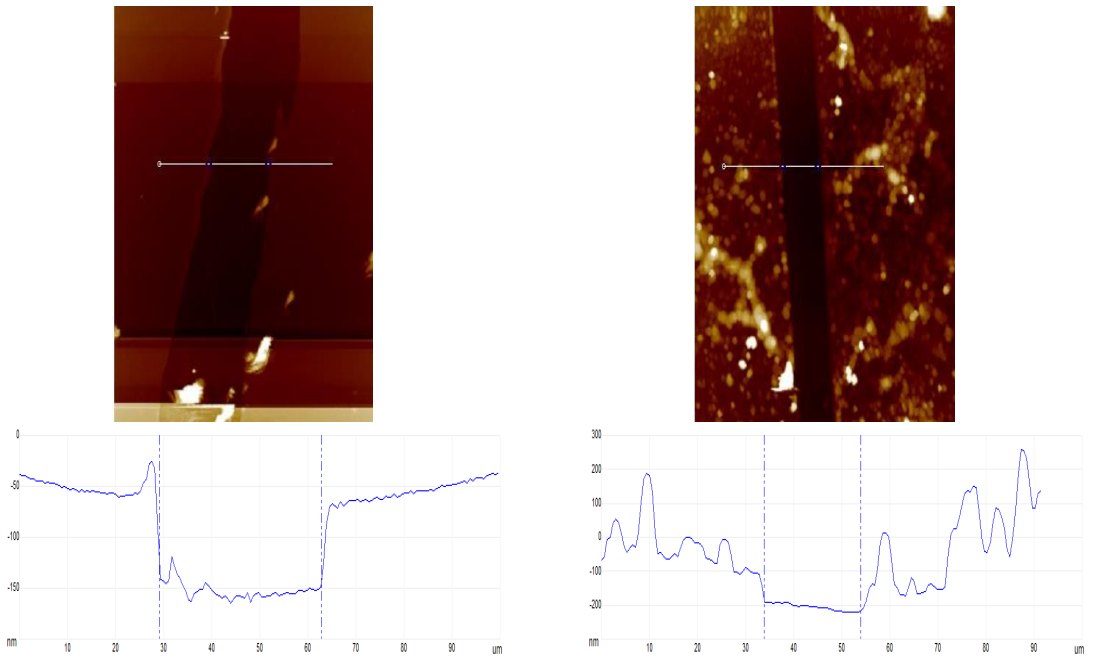

(a) (b)

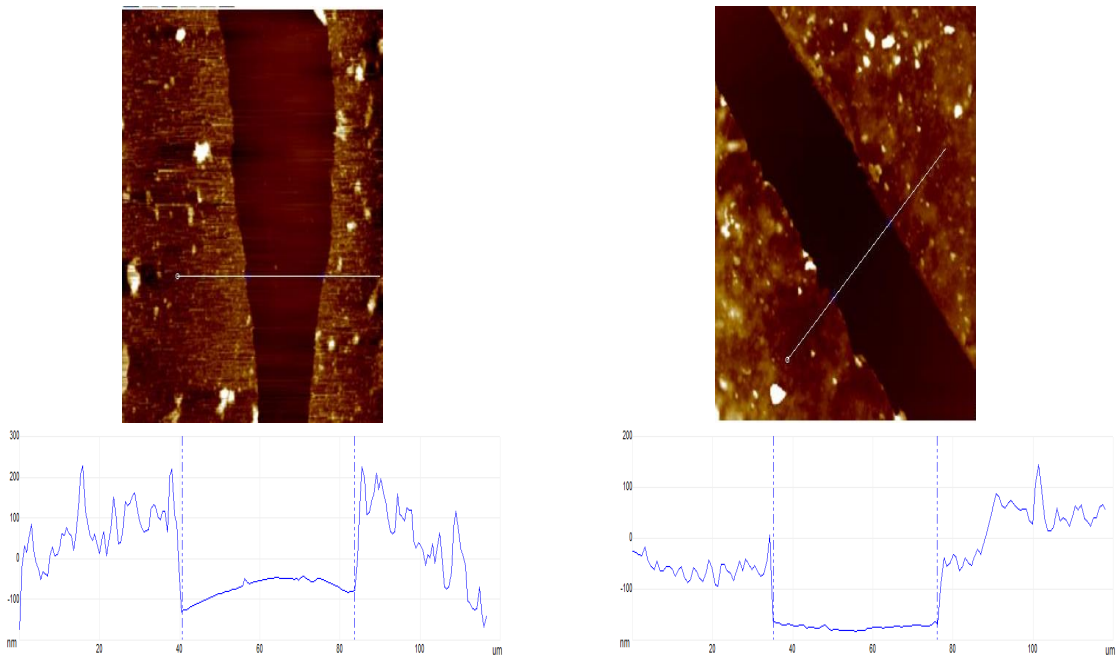

(c) (d)

Figure D.2. Scratch images of multilayered films obtained by spraying method (a)1st layer (b)2nd layer (c) 5th layer (d) 6th layer.

APPENDIX E

ANOVA TABLES

Table E.1. Analyses of Variance table for critical micelle concentration for different pH values.

Source	DF	Adj SS	Adj MS	F-Value	P-Value
ph	3	0,111648	0,0372161	7,65	0,0392
Error	4	0,019460	0,0048649		
Total	7	0,131108			

Table E.2. Grouping information for critical micelle concentration for different pH values using the Tukey method and 95% confidence.

ph	N	Mean	Grouping	
7	2	1,15000	A	
8	2	1,10850	A	B
5	2	1,08750	A	B
6	2	0,847500		B

Table E.3. Analyses of Variance table for zeta potential of 0.2% sodium caseinate and 0.5% sodium caseinate at different pH values.

Source	DF	SS	MS	F	P
Kazein - ph	7	133,9	19,1	0,50	0,812
Error	9	343,0	38,1		
Total	16	477,0			

S = 6,174 R-Sq = 28,08% R-Sq(adj) = 0,00%

Table E.4. Grouping information for zeta potential of 0.2% sodium caseinate and 0.5% sodium caseinate at different pH values using the Tukey method and 95% confidence (01: 0.5%sodium caseinate, 02: 0.2% sodium caseinate).

- ph	N	Mean	Grouping
5,52	3	-16,285	A
5,51	2	-19,000	A
6,01	2	-20,283	A
6,02	2	-20,715	A
8,01	2	-21,166	A
7,02	2	-22,180	A
7,01	2	-23,450	A
8,02	2	-25,680	A

Table E.5. Analyses of Variance table for zeta potential of 0.2% chitosan and 0.5% chitosan at different pH values.

Source	DF	SS	MS	F	P
Kitozan ph	11	2571,0	233,7	4,87	0,006
Error	12	576,0	48,0		
Total	23	3147,0			

S = 6,928 R-Sq = 81,70% R-Sq(adj) = 64,92%

Table E.6. Grouping information for zeta potential of 0.2% chitosan and 0.5% chitosan at different pH values using the Tukey method and 95% confidence (01: 0.5%chitosan, 02: 0.2% chitosan).

ph	N	Mean	Grouping
3,02	2	45,945	A
4,01	2	43,600	A B
4,51	2	30,900	A B C
3,52	2	30,630	A B C
3,01	2	27,850	A B C
4,52	2	25,830	A B C
4,02	2	22,880	A B C
5,01	2	21,200	A B C
5,02	2	17,380	B C
5,52	2	15,465	C
3,51	2	13,750	C
5,51	2	13,280	C

Table E.7. Analyses of Variance table of dipping vs spraying methods for thickness of multilayered film formation obtained by 0.2% chitosan and 0.2% sodium caseinate at pH 5.5.

Source	DF	SS	MS	F	P
Number of layers	9	283218	31469	4,26	0,000
Error	49	361635	7380		
Total	58	644852			

S = 85,91 R-Sq = 43,92% R-Sq(adj) = 33,62%

Table E.8.Grouping information of dipping vs spraying methods for thickness of multilayered film formation obtained by 0.2 % chitosan and 0.2% sodium caseinate at pH 5.5 using the Tukey method and 95% confidence.

Number of layers	N	Mean	Grouping
120	6	269,67	A
61	6	228,17	A B
21	6	200,83	A B
50	6	200,17	A B
121	6	141,00	A B C
51	6	134,67	A B C
11	5	113,00	A B C
60	6	98,50	B C
10	6	90,17	B C
20	6	31,67	C

Table E.9. Analyses of Variance table of dipping vs spraying methods for roughness (Ra (nm)) of multilayered film formation obtained by 0.2% chitosan and 0.2% sodium caseinate at pH 5.5.

Source	DF	SS	MS	F	P
Number of layers	8	149453	18682	6,99	0,000
Error	21	56131	2673		
Total	29	205583			

S = 51,70 R-Sq = 72,70% R-Sq(adj) = 62,30%

Table E.10. Grouping information of dipping vs spraying methods for roughness (Ra (nm)) of multilayered film formation obtained by 0.2% chitosan and 0.2% sodium caseinate at pH 5.5 using the Tukey method and 95% confidence (50:5th layer-dipping method, 51:5th layer-spraying method, 52:5th layer-fluid method).

Number of layers	N	Mean	Grouping
122	3	237,67	A
50	3	203,33	A B
120	5	181,40	A B C
60	3	178,67	A B C
62	2	96,40	A B C D
121	5	77,42	B C D
51	3	60,33	B C D
61	3	56,80	C D
52	3	26,70	D

Table E.11. Analyses of Variance table of dipping vs spraying methods for roughness (Rq (nm)) of multilayered film formation obtained by 0.2% chitosan and 0.2% sodium caseinate at pH 5.5.

Source	DF	SS	MS	F	P
Number of layers	8	261316	32665	8,37	0,000
Error	21	81935	3902		
Total	29	343252			

S = 62,46 R-Sq = 76,13% R-Sq(adj) = 67,04%

Table E.12. Grouping information of dipping vs spraying methods for roughness (Ra (nm)) of multilayered film formation obtained by 0.2% chitosan and 0.2% sodium caseinate at pH 5.5 using the Tukey method and 95% confidence (50:5th layer-dipping method, 51:5th layer-spraying method, 52:5th layer-fluid method).

Number of layers	N	Mean	Grouping
122	3	331,67	A
50	3	248,67	A B C
120	5	237,80	A B
60	3	237,33	A B C
62	2	117,00	B C D
121	5	110,70	B C D
51	3	81,70	B C D
61	3	74,37	C D
52	3	35,80	D

Table E.13. Analyses of Variance table of dipping vs spraying methods for oxygen permeability of multilayered film formation obtained by 0.2% chitosan and 0.2% sodium caseinate at pH 5.5.

Source	DF	SS	MS	F	P
C1	4	79636	19909	36,06	0,001
Error	5	2760	552		
Total	9	82397			

S = 23,50 R-Sq = 96,65% R-Sq(adj) = 93,97%

Table E.14.Grouping information of dipping vs spraying methods for oxygen permeability of multilayered film formation obtained by 0.2% chitosan and 0.2% sodium caseinate at pH 5.5 using the Tukey method and 95% confidence (0:blank film, 51:5th layer- dipping method, 52:5th layer-spraying method, 121:12th layer- dipping method, 122:12th layer- spraying method).

C1	N	Mean	Grouping
52	2	476,67	A
0	2	287,80	B
121	2	284,50	B
51	2	264,96	B
122	2	215,39	B

Table E.15. Analyses of Variance table of dipping vs spraying methods for water vapor permeability of multilayered film formation obtained by 0.2 % chitosan and 0.2% sodium caseinate at pH 5.5.

Source	DF	SS	MS	F	P
C1	4	0,5798	0,1449	3,78	0,089
Error	5	0,1918	0,0384		
Total	9	0,7716			

S = 0,1959 R-Sq = 75,14% R-Sq(adj) = 55,25%

Table E.16. Grouping information of dipping vs spraying methods for water vapor permeability of multilayered film formation obtained by 0.2 % chitosan and 0.2% sodium caseinate at pH 5.5 using the Tukey method and 95% confidence (0:blank film, 51:5th layer- dipping method, 52:5th layer- spraying method, 121:12th layer- dipping method, 122:12th layer- spraying method).

C1	N	Mean	Grouping
0	2	6,5650	A
52	2	6,5600	A
122	2	6,5200	A
51	2	6,2400	A
121	2	5,9500	A